# Handheld synthetic array – Final report, Part B

Prepared by:
Department of Electrical and Computer Engineering
The University of Calgary
2500 University Dr, N.W.
Calgary, T2N 1N4

# Defence Research and Development Canada

Contract Report
DRDC-RDDC-2014-C309
December 2014

# FINAL REPORT PART B

## MARCH 31, 2014

**for**

**Department of National Defence**

**DRDC-Ottawa**

**contract number  w7714-115195/A**

**Department of Electrical and Computer Engineering**

**The University of Calgary**

**2500 University Dr, N.W.**

**Calgary, T2N 1N4**

# Executive Summary

This document is the summary of the final outcome of the research contract  w7714-115195/A entitled  Research & development for Long Term Evolution (LTE) wireless location based on synthetic array.  The report is a compilation of the research activities and outcomes for the period of January 2012 to March 31 2014.

The final report consists of two parts whereas this is part B.  This document is primarily based on the PhD dissertation of Dr. Neda Moazen who did her doctoral research as part of this contract.

## Acronyms

| | |
|---|---|
| AN | Access node (eNodeB) |
| AP | Anchor point |
| ANan | Access node that is an anchor node |
| ANfp | Access node that is feature point |
| AWGN | Additive White Gaussian Noise |
| AOA | Angle of Arrival |
| BCRLB | Bayesian Cramer-Rao Lower Bound |
| BF | Bayesian Filter |
| BFI | Bayesian Fisher Information |
| BFIM | Bayesian Fisher Information Matrix |
| CDMA | Code Division Multiple Access |
| CML | Concurrent Mapping and Localization |
| CRLB | Cramer-Rao Lower Bound |
| CV | Computer Vision |
| EKF | Extended Kalman Filter |
| FastSLAM | Factorized Solution for Simultaneous Localization and Mapping |
| FI | Fisher Information |
| FIM | Fisher Information Matrix |
| FP | Feature Point |
| GNSS | Global Navigation Satellite Systems |
| GPS | Global Positioning System |
| i.i.d | Independent and Identically Distributed |
| IMM | Interacting Multiple Model |
| IMU | Inertial Measurement Unit |

| IEEE | Institute of Electrical and Electronics Engineers |
|------|---------------------------------------------------|
| KF | Kalman Filter |
| KL | Kullback-Leibler |
| LAMBDA | Least-squares Ambiguity Decorrelation Adjustment |
| LJG | Linear and Jointly Gaussian |
| LML | Local Maximum Likelihood |
| LOS | Line of Sight |
| LTE | Long Term Evolution |
| MAP | Maximum A Posterior |
| MC | Monte Carlo |
| M-CRLB | Modified Cramer-Rao Lower Bound |
| MEMS | Micro Electro-Mechanical Systems |
| MI | Mutual Information |
| MLE | Maximum Likelihood Estimator |
| MM | Multiple Model |
| MMSE | Minimum Mean Square Error |
| MN | Mobile Node |
| NEES | Normalized Estimation Error Squared |
| OCXO | Oven-Controlled Crystal Oscillator |
| OWLS | Opportunistic Wireless Localization System |
| PDF | Probability Density Function |
| PDOA | Phase Difference of Arrival |
| PEB | Position Error Bound |
| PF | Particle Filter |
| PRN | Pseudo-Random Noise |

| POA | Phase of Arrival |
|-----|------------------|
| RB | Rao-Blackwellized |
| RBPF | Rao-Blackwellized Particle Filter |
| RFID | Radio Frequency Identification |
| RIM | Research in Motion |
| RTOF | Round-trip Time of Flight |
| SLAM | Simultaneous Localization and Mapping |
| SNR | Signal-to-Noise Ratio |
| SS | Signal Strength |
| TCXO | Temperature Compensated Crystal Oscillator |
| TDOA | Time Difference of Arrival |
| TOA | Time of Arrival |
| UWB | Ultra Wideband |
| WiFi | Wireless Fidelity |
| WLAN | Wireless Local Access Network |

## Variables used

| variable | description |
|----------|-------------|
| $bel\left(x_{0:t}\right)$ | Posterior pdf of the particles over the complete time interval from 0 to $tT_s$ |
| $b_t$ | range offset |
| $B_s$ | signal bandwidth |
| $c$ | propagation velocity |
| $e_{1\times m}^{i}$ | $1\times m$ row vector whose elements are zero, except the $i$-th element which is equal to one. |

| $f$ | carrier frequency |
|---|---|
| $f_b$ | clock frequency bias |
| $\overline{f}$ | clock frequency drift |
| $f_r(t)$ | clock random frequency error |
| $I(X,Y)$ | mutual information between Y and $X$ |
| $J$ | Fisher information matrix in general |
| $J_{tot}$ | total Bayesian Fisher information matrix |
| $J_Z$ | measurement information matrix |
| $J_P$ | apriori information matrix |
| $\mathbf{K}_{AN}$ | vector of direction |
| $\mathbf{m}$ | stacked vector of AN locations |
| $\mathbf{m}_i$ | state vector describing the location of the $i$th ANs |
| $\mathbf{m}_{ap}$ | stacked vector of APs location |
| $\mathbf{m}_{fp}$ | stacked vector of FPs location |
| $\left\{ m_{i,x}, m_{i,y} \right\}$ | 2D location variables of an AN |
| $N_{AN}$ | number of ANs |
| $N_{AP}$ | number of APs |
| $N_{FP}$ | number of FPs |
| $N_d$ | dimension of dynamic variable in state vector |
| $N_s$ | dimension of stationary variable in state vector |
| $N_p$ | number of particles |
| $\mathbf{p}_t$ | MN location vector |
| $\mathbf{p}_{1:t}$ | history of MN locations |
| $\mathbf{q}_t$ | state vector at time step $t$ |

| $\mathbf{q}_{d,t}$ | dynamic portion of state vector at time step $t$ |
|---|---|
| $\mathbf{q}_s$ | stationary portion of state vector |
| $Q_d$ | covariance matrix of dynamic variables update process |
| $Q_P$ | motion process covariance matrix |
| $r(t)$ | geometric range between the AN and MN |
| $s(t)$ | bandpass signal |
| $\tilde{s}(t)$ | lowpass signal |
| $\mathbf{u}_t$ | control vector |
| $\mathbf{u}_{1:t}$ | history of update control inputs |
| $\mathbf{v}_t$ | motion update process noise |
| $w_{i,t}$ | measurement noise |
| $\mathbf{z}_t$ | measurement vector received at time step $t$ |
| $\mathbf{z}_{i,t}$ | observation vector from $i$-th AN at the time $t$ |
| $\mathbf{z}_{i,1:t}$ | history of observation from $i$-th AN |
| $\delta_{k+1}^{i,j}$ | $(k+1) \times (k+1)$ dimensional matrix whose elements are all zero except at the $i$-th row and the $j$-th column which is one |
| $\delta t_{MN}$ | MN clock bias |
| $\delta t_{AN}$ | AN clock bias |
| $\dot{\delta t}_{MN}$ | MN clock rate drift |
| $\dot{\delta t}_{AN}$ | AN clock rate drift |
| $\Delta \varphi(t)$ | carrier phase variation |
| $\Delta_\alpha^\beta$ | $\nabla_\alpha \nabla_\beta^T$, second order derivative operator |
| $\varepsilon_\varphi$ | carrier phase measurement noise |
| $\eta$ | normalizing constant |

| | |
|---|---|
| $\lambda$ | carrier wavelength |
| $N(b, B)$ | Gaussian process with the mean vector $b$ and covariance matrix $B$ |
| $\prod$ | overall transition matrix of sight states |
| $\prod_i$ | transition matrix of the $i$-th AN's sight state |
| $\sigma_b^2(Q_b)$ | range offset variance (covariance matrix) |
| $\varphi_0$ | carrier phase of AN transmitter at time of transmission |
| $\varphi(t)$ | partial carrier phase cycle measurement |
| $\chi^2$ | chi-square distribution |
| $\dim(.)$ | dimension function |
| $\text{Re}\{.\}$ | real part |
| $\nabla.$ | Jacobian function |

# Chapter 1   Introduction

In recent years, new developments in wireless systems have combined mobility features with personal communication devices, such as laptops and cell phones. However, advances in embedded sensing and high speed processing have enabled location-aware services built into handset devices. The most popular developed positioning systems used by handset devices are based on the Global Positioning System (GPS) and cellular networks which are widely accessible for navigation in outdoor environments.

Each GPS satellite transmits a narrowband signal modulated with a unique pseudo-random noise (PRN) sequence code that is known to the receiver. If the transmitter and receivers are synchronized, the corresponding receiver can correlate the received signal with a known PRN sequence to estimate the propagation delay between the transmitter and receiver antennas. The typical GPS navigation solution requires a minimum of 4 satellites that must be simultaneously visible to estimate the 3D location of the receiver and the time offset between receiver and transmitter clocks. However, in indoor and dense urban environments, satellite visibility is problematic.

On the other hand, the position accuracy obtained by existing cellular–based methods using cell-ID or enhanced observed time difference of arrival (E-OTDOA) is generally low and insufficient for indoor environments. To this end, indoor localization systems rely on other technologies such as UWB, RFID, Bluetooth (IEEE 802.15), ultrasonic badges, and computer vision technology. However, these approaches require developing a signaling system and/or installing the network infrastructure which make them time-consuming and costly approaches for indoor localization.

Particularly, the project of "Google Maps" extension inside buildings has sparked a technology race among all smartphone manufacturers such as Apple, Nokia , Samsung, and RIM; and ASIC manufactures such as Qualcomm and Broadcom. This is augmented by the

concept of using any opportunistic wireless signal that may be present. In this work, the opportunistic wireless localization system (OWLS) is developed where the wireless signals utilized for positioning are received from opportunistic and poorly defined sources that perhaps are uncooperative with the mobile handset device. This means that the mobile node (MN) is not registered with the network and merely exploits received signals as signals of opportunity.

This research has focused on the OWLS using existing wireless network infrastructure such as locally generated WiFi, WLAN and 4G LTE wireless signals as an inexpensive solution for indoor and dense urban environments. In addition to cost-effectiveness, opportunistic wireless localization offers scalability, not only in the cost of required network infrastructure, but also in the number of mobile devices/nodes (MNs) subscribing to positioning services, since each mobile device is responsible for its sensing and processing.

If the signal strength map is known, WiFi fingerprinting methods using signal of opportunity can achieve high localization accuracy in indoor environments [i], [ii]. [i] has obtained accuracy of 0.25 m using Monte Carlo localization based on a spatial discretized map of signal strength, combined with contact sensing. In [ii], the spatial discretized map of signal strength is fused with a low-cost image sensor to obtain a localization accuracy of 3 m. However, fingerprinting methods rely on expensive and time-consuming training phases to obtain the signal strength map. These methods require that the area must already have been surveyed and this makes them inefficient approaches for real time OWLS.

An ideal OWLS does not rely on prior knowledge of a signal map, but builds its own database during operation. Nevertheless, in absence of pre-existing information about the environment and the signal strength map, an OWLS must deal with reception of a multitude of signals with a large number of unknown channel and source parameters. Opportunistic wireless localization introduces the simultaneous localization and mapping problem (SLAM) as a systematic approach to not only localize the MN but also to estimate and track the unknown parameters due to signal reception from unregistered networks, including the AN locations [iii],

[iv]. SLAM, also known as Concurrent Mapping and localization (CML), is one of the most fundamental processing algorithms in robotics that has especially attracted immense attention in automation and control of the Mars Exploration Rover [v], [vi].

An OWLS must be solved for a large number of constraints applied while the MN moves in an unknown trajectory and receives signal from unknown sources. The most significant concept from SLAM that can be applied to OWLS is the introduction of a systematic way of incorporating all of the disparate nonlinear constraints of the MN dynamic motion and observables. The constraints define correlation between environment map parameters and MN locations estimates. Correlation always increases in time as more constraints are defined while the MN moves and/or receives new observations. The SLAM behavior in an OWLS is analogous to a network of springs where each constraint corresponds to a spring between unknowns [iii], as illustrated in Figure 0-1. An observation from an access node, at each time step, is analogous with a displacement in a spring network, and its correlation effect on its neighbors is proportional to their distances to other access nodes, i.e., the nearer they are, the greater is the effect. The minimum energy solution for this nonlinear network of springs self-organize the map parameters and the MN trajectory. As the MN moves through the environments and receives more observation, the spring becomes stiffer and fixes the map parameters.
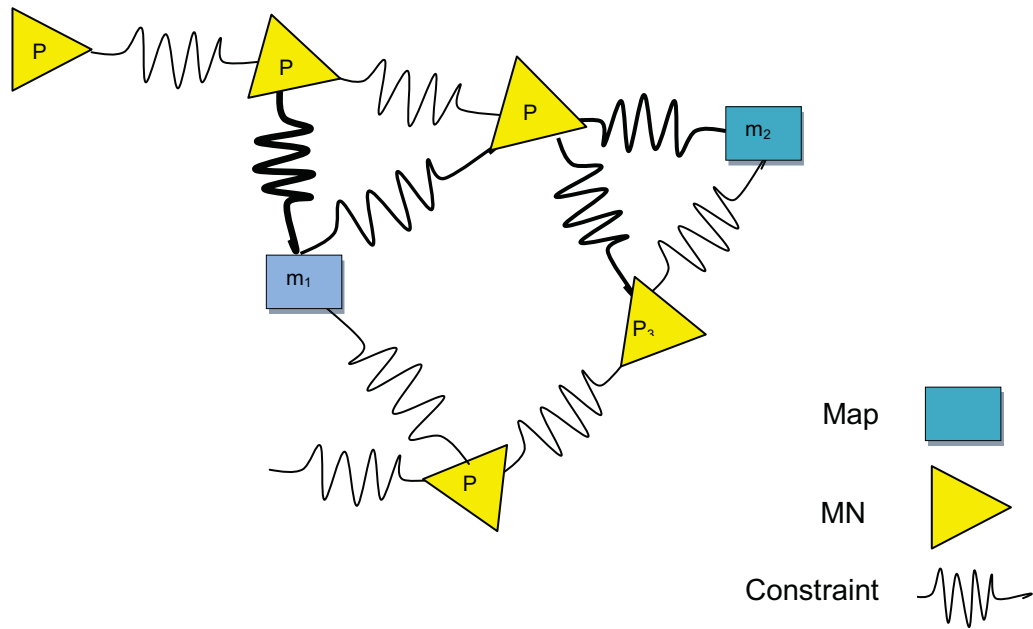
*Figure 0-1 SLAM as a network of springs problem*

Additionally, ANs' clocks may not necessarily be synchronized such as FDD LTE networks. The biased ranging issue is aggravated in a non-stationary multipath propagation environment where the signal is subject to spatial fading and signal attenuation due to shadowing and line-of sight (LOS) blockage [vii], [viii].

Furthermore, unlike traditional wireless localization systems, the wireless source locations are not necessarily unknown when the MN tends to estimate its location based on the signal receptions from an unregistered wireless network. Hence, the AN location parameters need to be estimated, along with the MN position states, which degrade the MN position estimates due to the increase in the number of unknown variables, while observables are unchanged. Tracking algorithms must be transformed to a solution for a SLAM problem which the MN localization is dependent on the quality of estimation of AN locations [iii], [iv].

The SLAM-based OWLS must deal with increase of unknown random variables such as the MN trajectory and the range error as the MN moves and receives new observations.

Consequently, the large set of unknown variables will be unobservable since the number of unknowns increases faster than the number of known equations. It will be shown the OWLS algorithm converges and is practically robust if two rather benign assumptions can be made:

1- The AN's are stationary in terms of physical position.

2- The MN undergoes a smooth albeit random trajectory.

The assumption of smooth trajectory is significant because there is high correlation between the positions that can be used to filter out noisy and false location estimates due to the multipath and clock instability [ix]. The Bayesian-based filter solution is proposed to improve the MN position estimation as it can take advantage of correlated information from previous observations. However, localization performance relies on the knowledge of the network map, the MN trajectory and quality of measurements.

Second stage involves obtaining an error metric to assess the system performance, as addressed in Chapter 3. In estimation theory, minimum mean square error (MMSE), calculated through the covariance matrix of posterior PDF, is generally considered as a measure of estimation accuracy. However, information theory can provide a deep analytical perspective to assess the information of observables regarding state space. One of the main components of this research is dedicated to determining the envelope of reasonably robust operability of the SLAM algorithms for opportunistic wireless localization. The Bayesian Fisher information matrix is a key to the SLAM problem, representing a quantitative summary of all available information in one matrix. For the SLAM-based OWLS, the Bayesian Fisher information matrix (BFIM) is derived as a quantitative measure of all available information from observables, the MN motion process and prior knowledge regarding the unknowns. BFIM and its variants are utilized to analyze the proposed SLAM-based solutions for OWLS performance in terms of efficiency, observability and consistency. Even though, the estimation relation to quantifiable Fisher information is only valid for a jointly linear Gaussian problem; as long as the nonlinearity is mild

and the measurement and state update noise are approximately Gaussian, it can still be regarded as a fundamental limit of accuracy [x].

To understand how much information each unknown variable contributes to the problem, SLAM-based OWLS is studied by four system models according to ranging measurements, varying from a simple synchronized scenario with stationary known propagation to the worse case with unsynchronized reception from unregistered and unsynchronized network in a non-stationary mixed LOS/NLOS propagation scenario.

Input-output mutual information (MI) is another interesting measure of information which quantifies the mutual dependence between input and output variables. Guo et al., 2005, revealed an insightful relationship between mutual information and MMSE in the Gaussian channel, regardless of the input statistics, given by [xi]:

$$\frac{\partial I\left(X;Y\right)}{\partial \rho} = \frac{1}{2}MMSE\left(\rho\right)$$

**0-1**

where $I\left(X;Y\right)$ is the mutual information between input $X$, and output $Y$, in units of nats; and $\rho$ is the signal-to-noise ratio. Guo's theorem illustrates that mutual information as well as Fisher information are powerful metrics which can lead to different insight into the localization performance. In this regard, the application of MI for localization problems with special focus on our SLAM-based problem is investigated in Chapter 3.

In a broad perspective, the SLAM-based OWLS can be viewed as a dynamic problem varying from mapping-only to tracking-only, or simultaneous localization and mapping, depending on the available knowledge from source locations and the MN trajectory, as depicted in Figure 0-2. However, as the number of unknown variables increases and they become more unpredictable, the SLAM accuracy, convergence, and hence robustness degrades.
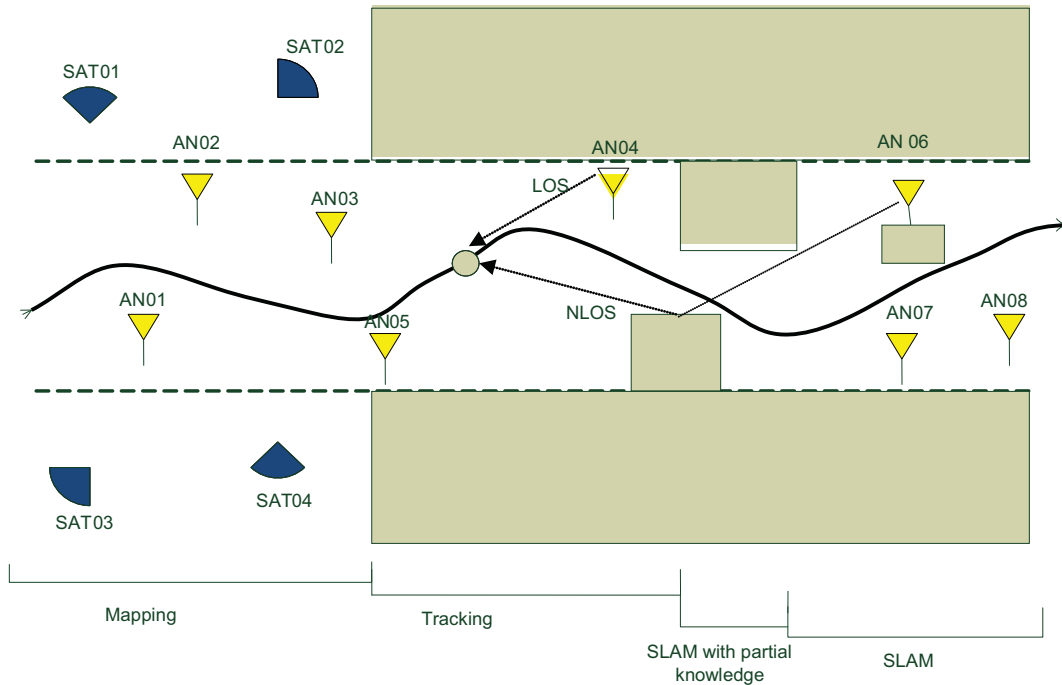
**Figure 0-2 Schematic scenarios of a SLAM problem in a broad prospective**

Consider a MN moving from left side of Figure 0-2 where the MN has access to LOS signals of at least 4 GPS satellites so that precise trajectory information is available. Opportunistic wireless localization can be solved for the estimation of the stationary ANs (for example, nearby LTE base stations) locations or the mapping problem. As the MN moves into a GPS-deprived environment such as an urban canyon area or an indoor building where the GPS signals are blocked, it has no access to the precise localization information but has prior knowledge about the ANs locations from the previous mapping step. The OWLS turns to the MN tracking problem using received signals of opportunity from wireless ANs with known locations.

As the MN moves, it may lose sight of some or all of the ANs where there will be partial/no knowledge about their source locations, as depicted in the right side of Figure 0-2. This is the worst case for the OWLS since it must not only map the source locations, but also track the MN trajectory. Four system models are suggested for this area, as addressed in Chapter 3 and Bayesian-based solutions are proposed as the final stage of designing the

tracking algorithm, as addresses in Chapter 4. In first system model, it is assumed that ANs are synchronized with MN and also all ANs are synchronized via a reference clock system (like GPS or a central hub). Moreover, multipath propagation is stationary or, if not, its condition is known to the MN. This means that for every AN-MN link, the propagation is either LOS or NLOS in the whole trajectory, or if the sight condition of ANs varies during trajectory as the MN moves, the ANs' LOS/NLOS conditions are known by the MN via prior detection processing, and NLOS measurements are discarded from the observation set.

Second system model considers the effect of MN clock drift where it is modeled by first-order Markov process based on the random smooth trajectory assumption; and further, in third system model, it is assumed that MN is no longer synchronized with ANs and ANs are also not synchronized with each other. This assumption introduces a range offset variable for every MN-AN link. For all four system models, both EKF-based and PF-based SLAM solutions, originally known as EKFSLAM and FastSLAM, are modified for newly-introduced nuisance parameters. Their performances are compared in terms of consistency and efficiency based on BFIM and other estimation and information metrics obtained in Chapter 3, and the strengths and weaknesses of each method are discussed.

In the forth system model, the ultimate objective of this thesis is addressed that is to develop a SLAM-based OWLS for the scenario where not only the MN trajectory and AN locations are unknown, but also where LOS/NLOS conditions in AN-MN links are non-stationary and unknown. To deal with different propagation conditions, two measurement models are introduced for LOS and NLOS conditions, where the transition between the LOS and NLOS modeled with a Markov chain. The binary state of LOS/NLOS conditions turns the OWLS to a jump Markov non-linear system (JMNLS) [xii]. Four novel SLAM-based solutions for this nonlinear JMNLS are suggested combining local maximum likelihood (LML) and interacting multiple model estimators with EKF-based and PF-based SLAM solutions: LML-EKFSLAM, IMM-EKFSLAM, LML-FastSLAM and MM-FastSLAM. IMM-EKFSLAM is derived by extension of

the EKF for joint estimation of the discrete sight states and continuous variable states including the MN location, AN locations and range error using interactive multiple model (IMM) estimator. In MM-FastSLAM, the Rao-Blackewellized (RB) PF–based SLAM [xxxiii] is modified based on the multiple model Particle filter (MMPF) [xii], where the posterior PDF samples represent both MN location dynamic state and AN sight condition states. LML-FastSLAM and LML-EKFSLAM are obtained by combining modified FastSLAM or EKFSLAM proposed for system model 3 with LML criteria for detecting ANs sight discrete state. Finally, the performance of each method is evaluated with the related BFIM and is compared with previously developed methods when the NLOS effect and/or range error are ignored.

## Chapter 2   OWLS Background Studies and Challenges

While the Global positioning system (GPS) is widely accessible, its position accuracy is compromised in dense urban areas and indoor environments due to low signal to noise ratio, LOS blockage and narrowband signaling [xiii]. Such factors are limiting when sub-meter accuracy is required. Taking advantage of opportunistic signals from the available local wireless networks, such as locally generated WiFi, WLAN or 4G LTE wireless signals of ample power and typically larger bandwidth can partially ameliorate these issues. The wireless signaling is assumed to be sourced from wireless network access nodes (ANs) which are primarily used for mobile data and voice communications [vii].

Similar to any wireless localization method, the opportunistic wireless localization exploits the received signal observables to extract the MN position information. In addition to unknown MN position variables in typical wireless localization methods, the tracking algorithm adopted for the opportunistic wireless localization must also deal with the estimation of unknown nuisance parameters of signals of opportunity from opportunistic sources [xiv], [iii]. Prior to design any tracking algorithm for an OWLS, it is required to present a fundamental study on

wireless localization methods, opportunistic wireless localization system parameters, and its challenges.

This chapter covers the required background studies for wireless localization based on signal of opportunity reception. Primarily, it explains the wireless positioning methods according to signal observables. However, the wireless signaling is assumed to be sourced from local wireless sources such as 4G LTE access nodes which are uncooperative with poorly defined source locations. In this thesis, the opportunistic sources are also referred as uncooperative or unregistered network; this means that the network location processing or assistance is not involved. The downlink signaling is specifically exploited, as the MN processing is desired to be capable of standalone localization. As mentioned earlier, since the MN receiver is not necessarily registered within wireless source networks; it must deal with the detection of a multitude of signals with unknown and random parameters including signal characteristics, such as bandwidth, the carrier frequency; or channel properties, such as shadowing, multipath and NLOS/LOS conditions; and network properties, such as the AN location and clock synchronization. In this regard, we also discuss the opportunistic wireless localization challenges due to signal, channel and network properties in more detail. Previous studies are also presented and recommended solutions are discussed. Finally, a systematic approach to formulate the opportunistic wireless localization problem is introduced including all nuisance parameters explained in former sections.

Signal characteristics used for positioning include the angle of arrival (AOA), the time of arrival (TOA) or the time difference of arrival (TDOA), the signal strength (SS), and the carrier phase or carrier phase difference (also known as the phase of arrival (POA/PDOA) ). Traditional positioning methods utilize triangulation algorithms that exploit the geometric properties of triangles to estimate the MN location through lateration or angulation.

Angulation estimates the location of a MN by computing the angle relative to multiple reference points via directive antennas or antenna arrays. The accuracy of the position

estimated by AOA methods is very sensitive on the distance, geometry, and multipath in the MN-AN link [xv]. In angulation or AOA-based approaches, the location of the desired target can be found at the intersection of several AOA direction measurements, which are in the form of ray emanating from the AN. As shown in Figure 0-3.a, this method may use at least two reference points for 2D position information. For AOA estimation, no synchronization is required between transmitters.  However, the application of directional antennas or antenna arrays in a handheld receiver is limited due to the complexity and size of antenna arrays. One of the disadvantages of AOA-based positioning methods is that their performance is very sensitive to accuracy of angle measurements. However, high accuracy angle measurements in indoor environments is limited by shadowing and multipath reflections arriving from misleading directions that may be as strong as LOS component or even stronger, or by the directivity of the measuring aperture.
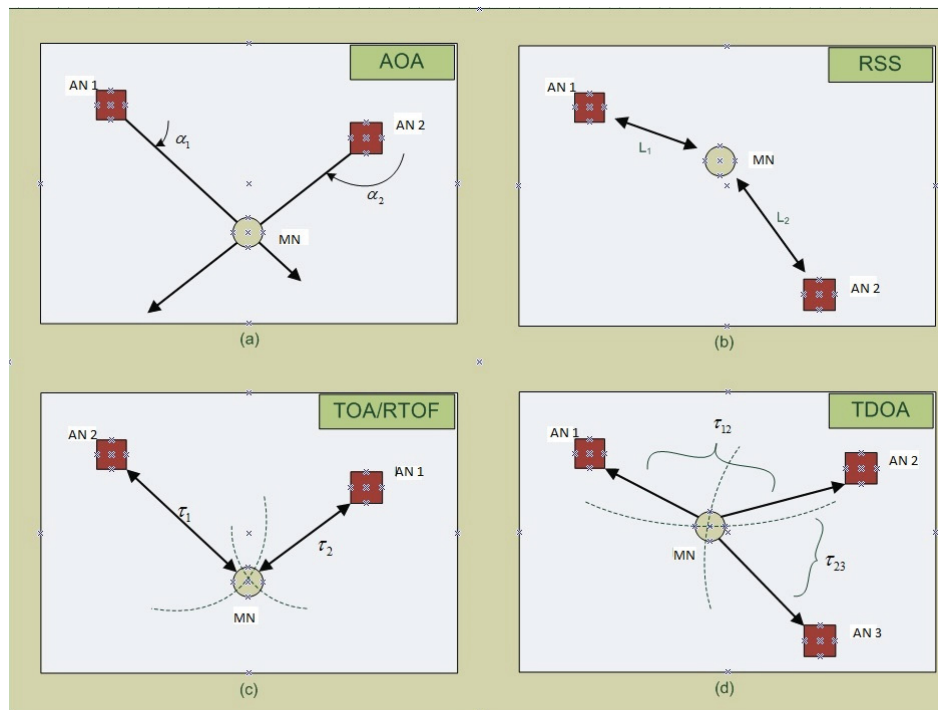


*Figure 0-3 Geometric locus of the MN location estimate in wireless positioning methods*

Lateration methods (also known as range-based methods) estimate the MN position by measuring the range from multiple ANs. Range-based methods utilize the SS, TOA/TDOA, round-trip time of flight (RTOF) or POA/PDOA measurements of the received signal. TOA-based algorithms are based on the fact that the distance from the AN to the MN is directly proportional to the propagation time. As shown in Figure 0-3.c, the position is computed by the intersection point of the circles of TOA measurements. One of the disadvantages of these methods is that all of the ANs and the MN must be time synchronized. In contrast, TDOA-based algorithms compute the relative position of the MN by examining the difference in TOAs from various ANs. Here, the MN location lies on a hyperboloid with a constant range difference between two ANs, as depicted in Figure 0-3.d. Unlike TOA-based methods, they only requires ANs to be synchronized.

RTOF-based methods, similar to radar, determine the time of flight of signal traveling from the AN to the MN and back, as illustrated in Figure 0-3.b. For these methods, a more moderate relative synchronization system is required in comparison with TOA methods. However, the exact delay/processing time caused by the reference/responder is unknown which cannot be ignored in short range indoor applications.

SS-based or signal attenuation-based methods try to compute the signal path loss due to propagation and then translate it into the range estimate. Due to the dynamic and unpredictable characteristics of indoor environment propagation, an explicit formulation between distance and path loss does not always hold. For this reason, SS-based positioning algorithms are mostly used in site-specific applications using fingerprinting and scene analysis methods.

Similar to time-based methods, carrier phase-based positioning methods are considered as range-based positioning methods. However, they provide better position accuracy compared to other time-based ranging methods, since the carrier phase can be measured with the precision of a 0.01-0.05 cycle. Assuming the transmitting signal is a pure sinusoid, the delay can be expressed as a fraction of wavelength. As long as the phase is in interval $[0, 2\pi)$, the range

estimate is unambiguous; otherwise, it is necessary to deal with ambiguity. GPS receivers acquire the phase lock with the transmitter signal, measure the initial partial phase difference between the received and transmitter signals (generated at the receiver), and then track changes in phase difference (i.e. counting full cycles and keeping track of the partial phase). In an ideal LOS condition, the integer full cycle numbers cannot be measured and have to be estimated; however, they remain constant as long as the carrier phase tracking loop is locked.

Generally, for absolute positioning based on the phase measurement, two receivers are required; one is the reference receiver at the stationary known location and the other is the MN receiver. This architecture is required for resolving ambiguity and initialization. After initialization, the MN receiver is expected to track the phase continuously. The integer ambiguity can be resolved using the least-squares ambiguity decorrelation adjustment (LAMBDA) method, carrier phase measurements, or multiple epochs from several transmitters. Since the integer ambiguity solution is not the main focus of this thesis, this information suffices for this research objective, and the interested reader is referred to [xvi].

The mathematical model for the carrier phase measurement in units of cycle in an opportunistic signal reception at the MN receiver is described as

$$\varphi(t) = \frac{1}{\lambda} r(t) + f(\delta t_{MN} - \delta t_{AN}) + N + \varphi_0 + \varepsilon_\varphi \qquad \textbf{\textit{0-2}}$$

where $\varphi(t)$ is the partial carrier phase cycle measured by the receiver, $\varepsilon_\varphi$ models the measurement noise, and $\varphi_0$ is the unknown carrier phase of the AN transmitter at the time of transmission. The $\lambda$ and $f$ are the carrier wavelength and the carrier frequency, respectively. $r(t)$ is the geometric range between the AN and MN at time $t$. The MN receiver and AN transmitter clock biases are represented as $\delta t_{MN}$ and $\delta t_{AN}$, both in units of second. $N$ is the integer ambiguity, which is the total number of full carrier cycles between the AN and the MN. It must be noted that since the range measurement from the carrier phase is ambiguous, it is

referred to as the pseudo range in many contexts. The pseudo-range measurement is defined as a function of the true range measurement which usually differs by an unknown offset.

The MN is not necessarily registered in the network, thus the ANs do not provide any synchronization information for the MN. Consequently, we are only interested in carrier phase changes in time that are independent of the initial carrier phase at the AN and the ambiguous integer number of cycles. Without the loss of generality, we assume that $\varphi(t=0)$ is zero that the MN tracking is initialized at the coordinate origin, so the Eq.(0-1) for carrier phase variation, $\Delta\varphi(t)$, as a function of time, is modified by

$$\Delta\varphi(t)=\varphi(t)-0=\frac{1}{\lambda}[r(t)-r(t=0)]+f.t(\dot{\delta t}_{MN}-\dot{\delta t}_{AN})+\dot{\varepsilon}_{\varphi} \qquad \textbf{0-3}$$

where $\dot{\delta t}_{MN}$ and $\dot{\delta t}_{AN}$ are the MN and the AN clock rate drifts , respectively. The unknown clock bias term, due to initial non-synchronization, is eliminated, since it is considered unchanged in time interval $[0,t]$. It is also assumed that, in the time interval $[0,t]$, the integer number of cycles is constant and there is no cycle slip in the tracking loop. Figure 0-4 shows general carrier phase relation with the AN-MN distance in LOS propagation, as defined in Eq. (0-2).
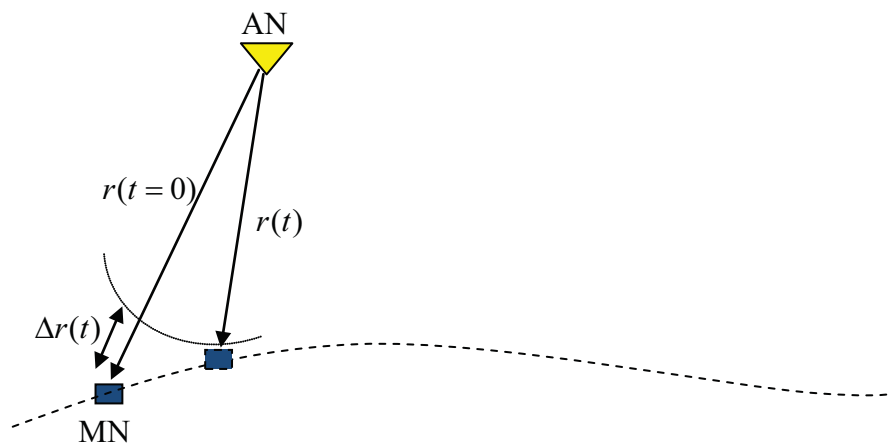


*Figure 0-4 Ranging based on the carrier phase measurement*

Consider a small portion of the MN trajectory where the signal is collected between M sampled positions, $\mathbf{p} = [\mathbf{p}_0, \mathbf{p}_1, ..., \mathbf{p}_M]^T$, within the trajectory. If the trajectory length is within the spatial coherence interval of the channel and also much shorter than the AN-MN distance $r(t)$, the plane wave propagation over the M sampled locations of the MN trajectory is justified. In this regard, the signal received at the *M* spatial sampling points, $\mathbf{p} = [\mathbf{p}_0, \mathbf{p}_1, ..., \mathbf{p}_{M-1}]^T$, is denoted as

**0-4**
$$\mathbf{s}(t, \mathbf{p}) = \begin{bmatrix} s(t, \mathbf{p}_0) \\ \vdots \\ s(t, \mathbf{p}_{M-1}) \end{bmatrix}$$

Consider the coordinate system origin at the initial location of the MN, Eq. (0-3) in terms of time delay, is written as

**0-5**
$$\mathbf{s}(t, \mathbf{p}) = \begin{bmatrix} s(t - \tau_0) \\ \vdots \\ s(t - \tau_{M-1}) \end{bmatrix}$$

where $\tau_m = \dfrac{\mathbf{K}_{AN}^{\mathbf{T}} \cdot \mathbf{p_m}}{c}$. $\mathbf{K}_{AN}$ is the unity vector of direction in a LOS propagation between the AN transmitter and the MN receiver, defined by

**0-6**
$$\mathbf{K}_{AN} = -\frac{1}{\sqrt{x_{AN}^2 + y_{AN}^2 + z_{AN}^2}} \begin{bmatrix} x_{AN} \\ y_{AN} \\ z_{AN} \end{bmatrix}$$

Assuming that $s(t)$ is a bandpass signal, we have

**0-7**
$$s(t) = \sqrt{2}\,\mathrm{Re}\{\tilde{s}(t)e^{j\omega_c t}\}, \quad m = 0, ..., M-1$$

where $\tilde{s}(t)$ is the lowpass band limited complex envelope of the received signal, and $\omega_c = 2\pi f_c$ is the carrier frequency in radians. Similarly, the signal at the $m^{\text{th}}$ spatial sampling point is modified in the complex envelop representation by

**0-8**
$$s(t, \mathbf{p}_m) = s(t - \tau_m) = \sqrt{2}\,\mathrm{Re}\{\tilde{s}(t - \tau_m)e^{j\omega_c(t - \tau_m)}\}, \quad m = 0, ..., M-1$$

If it can be assumed that incoming signals are narrowband, implying that the reciprocal of a maximum propagation delay across M MN locations is much greater than the signal bandwidth,

$$B_s \Box \ \frac{1}{\Delta T_{\max}}$$

where $B_s$ is the bandwidth of the complex envelope and $\Delta T_{\max}$ is the maximum propagation delay between each two MN locations [xvii], the narrowband assumption justifies as

$$\tilde{s}(t - \tau_m) \Box \ \tilde{s}(t), \quad m = 0,1,...,M-1$$

Hence, in the narrowband case, Eq.(0-7) reduces to

$$s(t, \mathbf{p}_m) = \sqrt{2} \, \mathrm{Re}\left\{ \tilde{s}(t) e^{j\omega_c t} e^{-j\omega_c \tau_m} \right\}, \quad m = 0,...,M-1$$

In a narrowband signal model, the sensor wise propagation delay is approximated by a phase shift as a function of the propagation direction, signal wavelength , MN position (here, the MN displacement)

$$\omega_c \tau_m = \frac{2\pi}{\lambda} \mathbf{k}_{AN}{}^T \mathbf{p_m}$$

On the other hand, the carrier phase measurement in units of cycle for positioning purpose is modified as

$$\varphi(t) = \frac{1}{\lambda} \mathbf{k}_{AN}{}^T \mathbf{p}(t) + \varphi_{clk} + \varepsilon_\varphi$$

where $\varphi_{clk}$ is clock instability due to free running clocks in receiver (here, the MN) and transmitter (here, the ANs), $\varepsilon_\varphi$ models the phase error due to both variation of antenna phase center along with the propagation direction and phase discriminator noise.
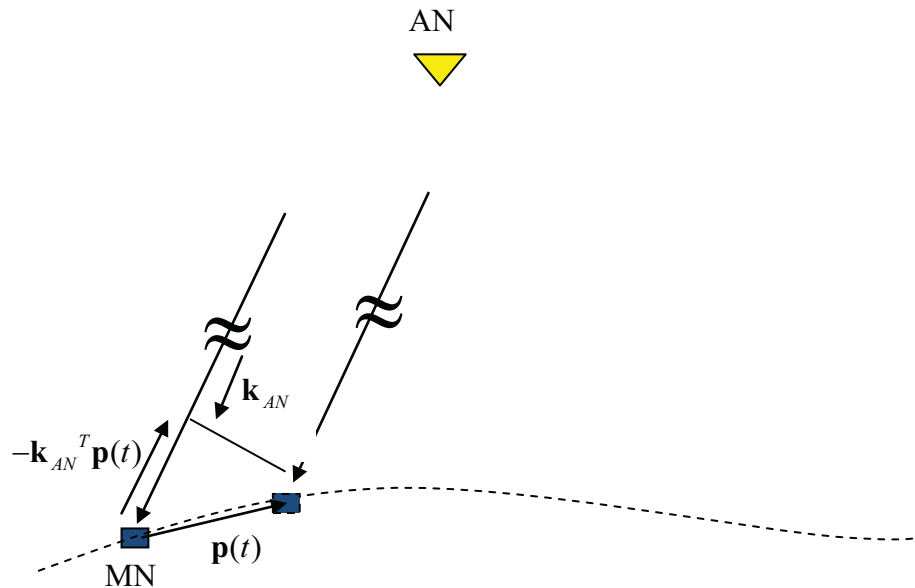
*Figure 0-5 Ranging based on carrier phase measurement in a plane wave propagation*

The performance of OWLS is highly dependent on both the quality of measurements and unknown characteristics of the signal which interfere as nuisance parameters in the position estimation problem. In this regard, it is important to explore the diverse set of factors that can affect localization accuracy. In summary, the main deficiency factors in the opportunistic wireless localization are classified as unsynchronized reception from an uncooperative network, non-stationary wireless propagation, lack of knowledge about source locations, and noise and interference from unwanted sources. The following sections discuss in more detail these four typical sources of error in opportunistic wireless localization.

Indoor localization requires precise timing measurement in at least nano-seconds since the accuracy level of several decimeter is desired. For this reason, clock synchronization is an important factor in the ranging and positioning performance. The carrier phase and time-based positioning methods require the receiver and transmitter nodes to be equipped with a stable oscillator from which an internal clock reference is derived to measure the true time with high

accuracy. However, various physical effects cause oscillators to experience frequency and phase drift, leading to large errors in phase and time measurements, and therefore in the position estimate. In a disciplined oscillator, the frequency is controlled by the internal microprocessor based on the measurement of its frequency relative to the received GPS or other wireless signals. Any interruption in signal reception may degrade the clock frequency.

In an opportunistic signal reception, while the MN receiver is not locked to the synchronization signal sent from the AN, an improved long-term and short-term stabilized oscillator is of great importance. The clock instability characteristics are defined by two terms, *holdover accuracy*, and *short-term stability*. Holdover accuracy refers to the time error accumulation during a free-running clock operation in a long term observation that is typically 1 day. For example, a medium-stability OCXO accumulates 100 microseconds of time error in 24 hours after the reference signal (like GPS or CDMA signal) is lost. Short-term stability refers to the frequency deviation relative to a reference frequency standard, measured over an observation time of one second or less. When measured in units of time, it is known as *jitter*, and when measured in units of phase, in a 1 Hz bandwidth at specific frequencies, is defined as *phase noise* [xviii]. It implies that short-term instability characteristics of the receiver/ transmitter clocks mainly affect positioning performance rather than holdover accuracy.

The local time of a clock can be expressed as $C(t)$ as a function of real time $t$. The oscillator frequency determines the rate at which the clock runs. In a perfect clock, the rate denoted as $dC(t)/dt$ would be equal to 1, or $C(t) = t$. However, all clocks are subject to clock drift due to various physical sources which result in uncertainty between the MN and the rest of the ANs network, as shown in Figure 0-6.
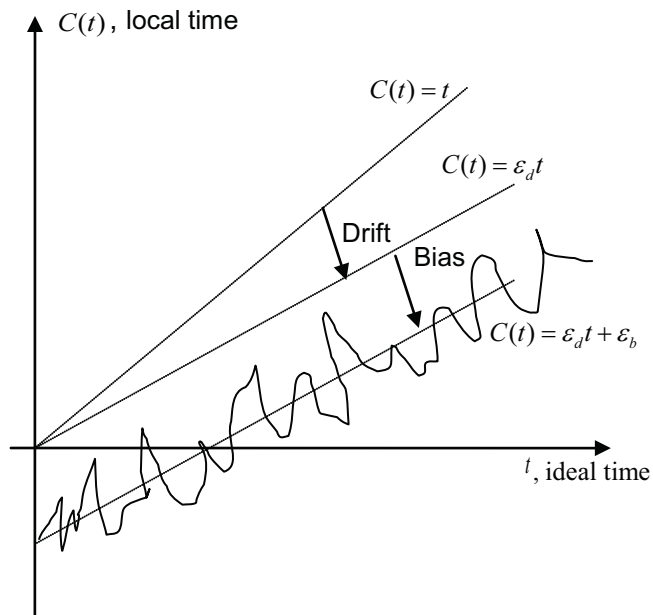
**Figure 0-6 Illustration of ideal time and local clock time (short term instability)**

A reasonable assumption that will be made here is that the ANs network is tightly synchronized perhaps locked to a central synchronizing clock or individually to a GPS source. This is a rather benign assumption to make as each AN will have a backhaul connection to a communication hub of sorts. However, the actual signal delay from this central hub to ANs is difficult to actually control and maintain. Regardless, it will be assumed that the AN clocks are perfectly stable and that the clock instability resides with the MN clock. As an example, the LTE hub is likely based on a higher quality clock than the consumer grade MN clock of a handset device.

For the MN free-running clock node without any synchronization scheme, one solution is that the MN receiver can adequately model the behavior of its own clock. The time reading error of a clock can be obtained as a function of oscillator quartz frequency given by

$$0\text{-}14$$

$$C(t_0) - t_0 = \frac{1}{f_0} \int_{t_0}^{t} f(t)dt$$

where $t_0$ and $C(t_0)$ are the reference time epoch and clock reading at the reference epoch;

and $f_i(t)$ and $f_0$ are the frequency of the oscillator and nominal oscillator frequency,

respectively. The oscillator frequency shows deterministic linear variations as well as random

errors [xix]. A standard model for the frequency of an oscillator is defined as

**0-15**

$$f(t) = f_b + \overline{f}(C(t_0) - t_0) + f_r(t)$$

where both $f_b$ and $\overline{f}$, as frequency bias and frequency drift, model the linear deterministic

portion, and $f_r(t)$ represents the unmodelled random frequency errors.

The standard approach to deal with clock frequency deviation is to model the

deterministic part by an explicit polynomial-like function and model the random part by its

sample variance known as Allen variance [vii], [xx], [xxi], [xxii]. Allen variance is defined as the

sample variance of $y(t) = \dfrac{f_r(t)}{f_0}$, given by

**0-16**

$$\sigma_y^2(M, \tau) = \frac{1}{2(M-1)} \sum_{m=1}^{M} \left( y_{m+1} - y_m \right)^2$$

where $y_m = \dfrac{1}{\tau} \int_{t_m}^{t_m + \tau} y(t) dt$

Allen deviation is the square root of Allen variance that is regarded as an indication of

the overall clock stability [xxiii], [xxiv], [xxv]. Figure 0-7 depicts the clock stability of several clock

sources in term of Allen deviation. The clock stability is defined as a function of observation time

of a particular clock. If it is assumed that, at the start of observation time, the clock is

synchronized with a true time scale, the RMS value by which the clock has deviated after a

certain time interval $\tau$ is stated by $\tau.\sigma_y(\tau)$.
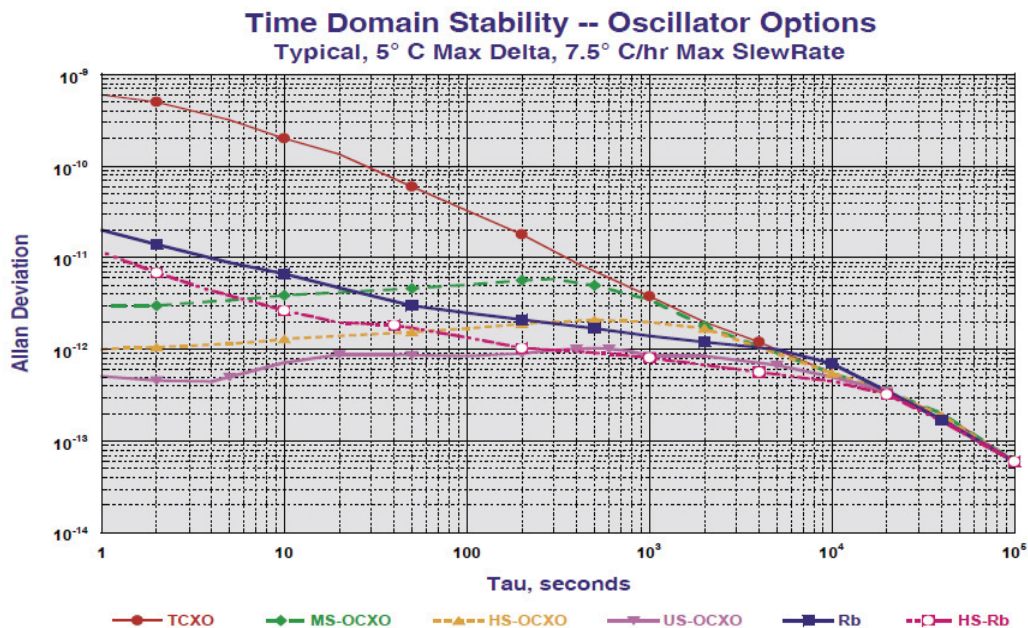
***Figure 0-7 Square-root of the Allan variance of typical oscillators (from
http://www.endruntechnologies.com/pdf/OscOptions.pdf, [xxvi])***

As an example, the Allen variance of $10^{-9}$ for a TCXO oscillator implies instability of about 0.6 nsec per second which roughly equates to 20 cm per second in range measurements. This means that if a localization scenario consists of a single MN and AN, and the location is perfectly known at t=0, then that location will randomly drift as a random walk at a deviation of about 20 cm per second. However, as it is a random walk, the deviation proportionally increases to the square root of the time lapse in seconds, and not linearly with time. From the Allen deviation, it is possible to estimate instability in terms of physical distance by a Markovian process.

However, mainstream published research on clock instability error has mostly focused on identifying models and their parameters from plots of Allen variance or of power spectral densities; whereas, the clock stability models based on the autocorrelation function of phase noise also show that the variation of clock deviation can be fitted as a Markov process. [xxvii] presents a clock deviation modeling based on a second order random process where the model parameters are obtained by its autocorrelation function. The Markovian process of clock drift

helps the clock deviation parameters to be modeled along with the dynamic MN trajectory state-space vector. Consequently, an optimum solution for the OWLS has to not only localize the MN position as it undergoes random motion, but also to track the clock deviation to mitigate the localization errors due to clock instability.

The main source of error in any wireless localization system is derived from multipath fading, shadowing and LOS blockage. In indoor environments, due to reflection, defraction, and scattering of radio waves by structures inside a building, several copies of transmitted signal reach the receiver; this phenomenon is called multipath. In narrowband signaling, different propagation paths are added constructively (in-phase) or deconstructively (out-of-phase) within signal propagation time, and cannot be resolved. The multipath delay spreading increases significantly the uncertainty of TOA measurements which leads to large bias error in the range estimate. The increased bandwidth partially ameliorates this situation because the channel acts more frequency selective, and the multipath components become resolvable. Therefore, the leading edge of received signal, corresponding to the LOS component is not biased with the resolvable multipath returns. As an example, the currently deployable LTE sources are limited to 20 MHz in terms of bandwidth. This is significantly better than the GPS or IS2000 signals which are typically limited to about 1 MHz; even though, this is not sufficient to provide accurate TOA measurements for indoor localization.

LOS propagation may also be obstructed completely or partially so that the transmitted signal, before receiving at the MN, is reflected by structures or travels through different obstacles like walls in a building. Both of these phenomena lead into a positive random excess delay in time measurements that render traditional methods of localization virtually ineffective. In other words, combating the effects of multipath is the most significant challenge in providing adequately accurate position estimates, and hence new methods are required.

In this regard, many research works have focused on LOS/NLOS identification as prior processing of any localization algorithm. The proposed methods to mitigate the NLOS effect are

categorized in two groups. In the first group, the NLOS/LOS conditions are detected in a prior processing to localization. Whenever the LOS/NLOS conditions are identified, NLOS measurements can simply be ignored or the measurement model is adopted based on the range error to improve accuracy. In a mixed scenario, the carrier phase of the AN transmission will be used when LOS conditions are evident; in NLOS situations, the code phase is used with multipath delay averaging.

In the second group, sight condition and/or its related parameters are jointly estimated and tracked along with location states. In a Jump-Markov system, the algorithm must solve for both discrete (here, binary state regarding NLOS/LOS conditions), and continuous (here, position variables) states at the same time. Jump Markov or switching Markov model is also extended for time-based systems where the range measurements in NLOS condition is modeled by jump in variance and mean of measurement noise [xlix-li], [lv]. In NLOS situations, the MN motion can be used to accumulate a number of TOA measurements from the AN, and hence averaging out the effects of multipath. This is essentially handled by the Bayesian processing which has enhanced indoor positioning performance in NLOS situations.

While the MN receiver must deal with detection and tracking of the signal of opportunity from a local wireless network, it has to combat the interference of unwanted signals from other coexisting devices using the same frequency band. The OWLS is expected to operate in the presence of both interferences from narrowband interferes such as Bluetooth devices and cordless phones and wideband interferers such as microwave ovens and WiFi devices. Beamforming methods [xxviii], [xxix] and nonlinear filtering are considered as effective approaches to mitigate the effect of interference on localization [xxx], [xxxi], [xxxii]. However, the effect of interference on OWLS and its mitigation techniques is out of the scope of this thesis and in the proposed OWLS modeling, the interference is simply treated as a part of system noise into a spread spectrum MN device.

The overall objective of a tracking problem is to generate the belief map of the MN location as the trajectory unfolds. The belief map will provide a posterior estimate of the MN location that is iterated at each time step based on all available data up to the current time. The Bayesian filtering methods such as PF and KF/EKF provide an incremental estimate of the posterior PDF based on the accumulation of the MN trajectory estimate and the measurements made up to current time with knowledge of AN locations.

However, in an opportunistic signal reception, it is not guaranteed that the location of ANs are known to the MN. This gives the impetus to employ the SLAM techniques for the OWLS as a systematic approach to take into account all available constraints regarding the large set of unknowns such as the MN trajectory and AN locations. The following sections provide a short history of the SLAM problem as well as its classifications and proposed solutions. Later, observability of the SLAM-based OWLS is discussed.

## Origin of SLAM

Simultaneous Localization and Mapping, which is also known as Concurrent Mapping and Localization (CML), addresses problems where the MN does not have access to the map of the environment, nor does it know its own location. SLAM will search for the possible tracking solution for a MN, if placed at an unknown location in an unknown environment, as it consistently builds the map of environment; while simultaneously, estimates its location within the map.

The roots of SLAM date back to 1986 IEEE Robotics and Automation Conference in San Francisco when probabilistic mapping as a fundamental robotic problem is addressed and discussed by Peter Cheeseman, Jim Crowley, and Hugh Durrant-Whyte, Raja Chatila, Oliver Faugeras, Randal Smith [xxxiii]. These discussions were mainly focused on application of

estimation-theoretic methods in Artificial Intelligence and Robotics. Subsequently, many research papers have come out on related problems such as Smith and Cheesman and Durrant-Whyte [xxxiv] Ayache and Faugeras [xxxv] , Crowley [xxxvi] and Chatila and Laumond [xxxvii]. The key result of these research studies proved that there is a high degree of correlation between the estimates of different landmarks locations in a map, which increase with future observations [xxxviii].

Later in 1990s, a key research on convergence issues was developed by Csorba [xxxix] and, then specifically, on Kaman-filter-based SLAM methods and the probabilistic localization and mapping methods by Thrun [xl]. The conceptual breakthrough in SLAM research was found that the combined mapping and localization problem, once formulated as a single estimation problem, is actually convergent. Most importantly, it was recognized that the correlations between landmarks were actually the critical part of the problem. In other words, the higher these correlations, the better the solution.

Today, the SLAM is introduced for many applications in a number of different domains from indoor robots to outdoor, underwater, and airborne systems. It has been formulated and solved as a theoretical problem in many different forms. The SLAM problem is a continuous and discrete estimation problem. Generally, the continuous estimation part pertains to both the location of the object in the map and the mobile node's own location, and the discrete nature is related with correspondences. When an object is detected, a SLAM algorithm must distinguish the relation of this object to the previously detected objects.

Consider a MN, such as a vehicle or a person carrying a handset device moving through an unknown environment and taking observations from opportunistic sources. Lets define the following variables in regards to the OWLS formulation:

$\mathbf{p}_t$ : the state vector describing the location of the MN at time $t$.

$\mathbf{u}_t$: the control vector, if available, applied at time $t-1$ to drive the MN location to $\mathbf{p}_t$ at time $t$; or observation vector that can model the MN motion state process such as computer vision outputs.

$\mathbf{m}_i$: the state vector describing the location of the $i$th ANs whose true location is assumed to be time invariant.

$\mathbf{m}$: the stacked vector of AN locations, $\mathbf{m} = \{\mathbf{m}_i, i = 1,.., N_{AN}\}$ where $N_{AN}$ is the number of ANs.

$\mathbf{m}_{ap}$: the stacked vector of ANs location whose locations are known to the MN, referred by anchor points (APs), $\mathbf{m}_{ap} = \{\mathbf{m}_i, i = 1,..., N_{AP}\}$, where $N_{AP}$ is the number of APs

$\mathbf{m}_{fp}$: the stacked vector of ANs location whose location are unknown to the MN, referred by feature points (FPs), $\mathbf{m}_{fp} = \{\mathbf{m}_i, i = N_{AP} + 1,..., N_{AP} + N_{FP}\}$, where $N_{FP}$ is the number of FPs.

$\mathbf{z}_{i,t}$: the observation vector received by the MN from $i$th AN at the time $t$.

$\mathbf{z}_t \, \square \, \{\mathbf{z}_{i,t}, i = 1,..., N_{AN}\}$; the stacked vector of observations received by the MN from all ANs at the time $t$.

In addition, the following sets are also defined:

$\mathbf{p}_{1:t} \, \square \, \{\mathbf{p}_1 \quad \mathbf{p}_2 \quad \cdots \quad \mathbf{p}_t\} = \{\mathbf{p}_{1:t-1} \quad \mathbf{p}_t\}$; the history of the MN locations.

$\mathbf{u}_{1:t} = \{\mathbf{u}_1 \quad \mathbf{u}_2 \quad \cdots \quad \mathbf{u}_t\} = \{\mathbf{u}_{1:t-1} \quad \mathbf{u}_t\}$; the history of update control inputs.

$\mathbf{z}_{i,1:t} \, \square \, \{\mathbf{z}_{i,1} \quad \mathbf{z}_{i,2} \quad \cdots \quad \mathbf{z}_{i,t}\} = \{\mathbf{z}_{i,1:t-1} \quad \mathbf{z}_{i,t}\}$; the history of observation received by the MN from $i$-th AN.

It must be noted that $N_{AN} = N_{AP} + N_{FP}$. The optimum solution for a SLAM-based OWLS must develop a systematic way of accounting for the all observations to compute the posterior belief map of state variables including the MN location, FP locations, and nuisance parameters

(if available). According to posterior PDF computation process, the SLAM techniques are classified into two categories: Online SLAM and full SLAM. The online SLAM problem includes estimating the posterior PDF over the current MN location, $\mathbf{p}_t$, along with the unknown source location $\mathbf{m}_{fp}$ (and other nuisance parameters, if available) represented as $p(\mathbf{p}_t, \mathbf{m}_{fp} \mid \mathbf{z}_{1:t}, \mathbf{u}_{1:t})$ [xxxiii]. Online SLAM algorithms are incremental, and they discard past measurements and update controls that have been processed. The second category is known as the full SLAM. The full SLAM involves calculating the posterior PDF over the entire path $\mathbf{p}_{1:t}$ along with the FP locations $\mathbf{m}_{fp}$, $p(\mathbf{p}_{1:t}, \mathbf{m}_{fp} \mid \mathbf{z}_{1:t}, \mathbf{u}_{1:t})$.

Figure 0-8 illustrates the graphical schemes for states dependency of a general SLAM problem and also the difference between the full SLAM and online SLAM. The arrows define the dependency between processes and dark grey boxes show the unknown states which must be estimated at time step $t$. The arrows connectivity between $\mathbf{p}_k$'s shows that given the control data at time $t$, $\mathbf{u}_t$ (if available), the MN location at time step $t$ is only dependent to MN location at previous time $t-1$. In other words, the MN location variables $\mathbf{p}_k$ are dependent is a specific way that the past and future are dependent only through the present. Moreover, it is seen that even though, state-dependent measurement process $\mathbf{z}_t$ evolves independently of each other and are only dependent on random process $\mathbf{p}_t$, since the FP map $\mathbf{m}_{fp}$ is unknown, estimate of $\mathbf{p}_t$ and $\mathbf{m}_{fp}$ are not independent. Consequently, the joint posterior PDF $\mathbf{p}_t$ and $\mathbf{m}_{fp}$ cannot be separated. The online SLAM and full SLAM are fundamentally different algorithms as the set of variables to be estimated is different in each algorithm as illustrated in Figure 0-8. However, online SLAM can be modified as the integration of the full SLAM over past locations.
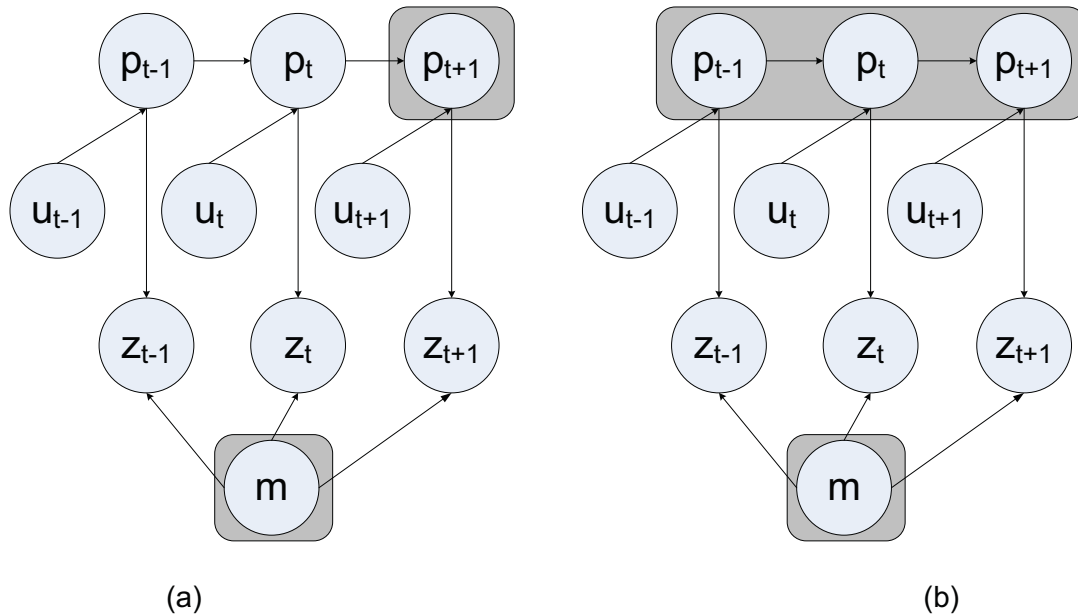
*Figure 0-8 Graphical schemes of the a) online SLAM in comparison with the b) full SLAM*

## Estimation error correlation effect on SLAM

One of the important aspects of SLAM is to understand the correlation between estimate of the MN trajectory and the estimate(s) of unknown parameters of environment map. For OWLS with no nuisance parameters except FP locations, Figure 0-9 shows the estimates of the MN trajectory and the FP locations compared to the actual MN trajectory and FP locations. It illustrates that the estimation error for the FP locations is highly correlated with the MN locations estimation error. This is because the main source of the estimation error originates from the uncertainty about the MN position where the observations are made [xl]. This common source of error makes estimation error of the feature points highly correlated as it shapes the joint probability density of feature points to be highly peaked, even if the marginal density of each individual FP's PDF has a skewed shape.
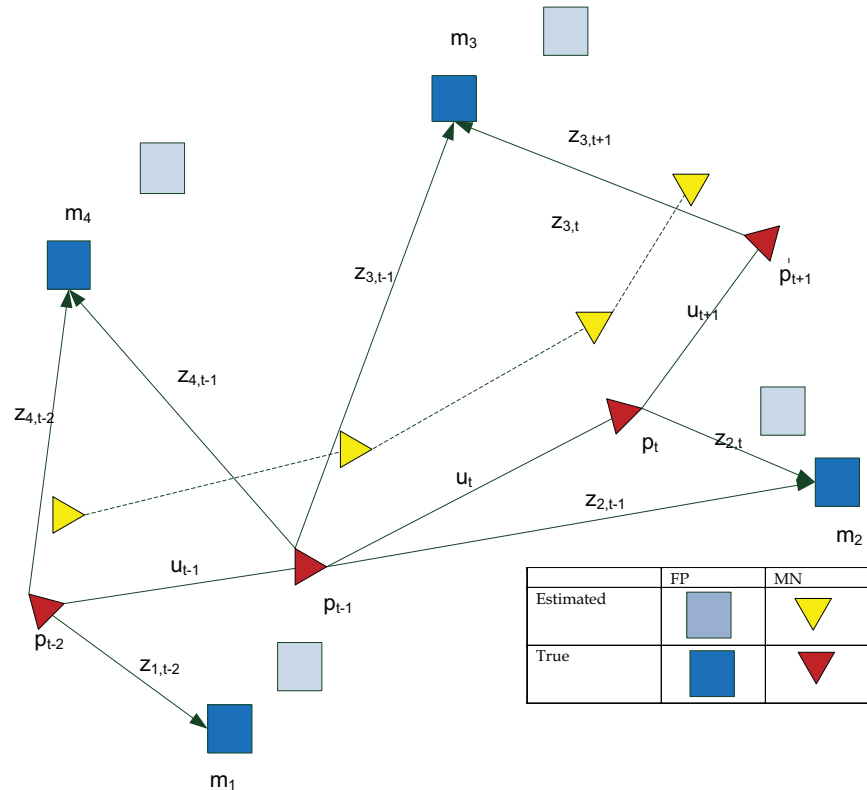
***Figure 0-9 Correlation between the estimation error of the MN trajectory and FP locations
compared with the true MN trajectory and the FP locations***

The interesting point is that the correlation between the estimates of FP locations

increases in time and makes the peak of the joint PDF sharper as more observations are

received. As discussed earlier, this correlation effect originates from the constraints defined by

disparate sources of information in OWLS such as MN motion process and observables from

unknown or known source locations. As already illustrated in Figure 0-1, the effect of correlation

between the MN trajectory estimates and FP locations cast the SLAM-based OWLS as a

network of springs where minimum energy solution of this spring system solves for the MN

trajectory and FP locations (and other nuisance parameters, if available). An observation at

each time step is analogous with a displacement in the spring network, and its correlation effect

on its neighbors is proportional to their distances to other feature points, i.e., the nearer they

are, the greater is the effect, as shown in Figure 0-10. As the MN moves, and receives more

observations from feature points, the correlation between the estimates of feature points increases and the spring becomes stiffer. The thicker link in Figure 0-10 denotes more stiffness and thus higher correlation.
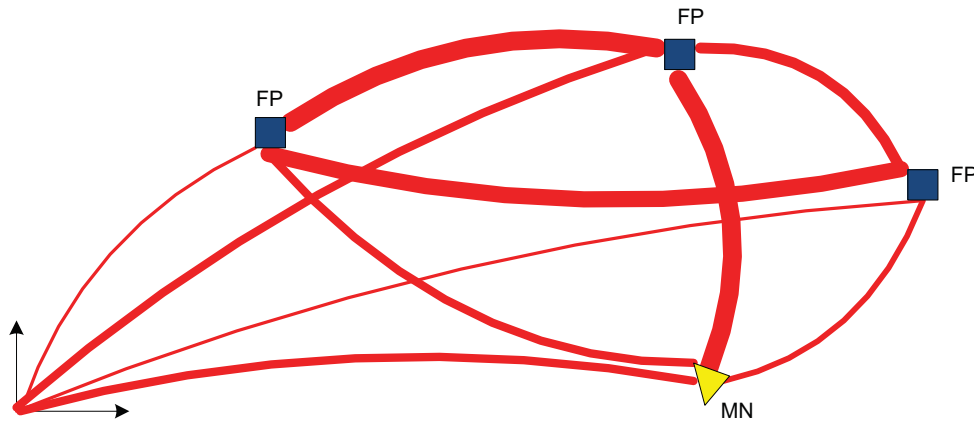


***Figure 0-10 Analogy of the estimation error correlation in a SLAM problem with a spring network***

In theoretical limit, the rigid or accurate relative map of ANs' location is obtained and the relative MN location accuracy becomes equal with the MN location accuracy achievable with a given map. The minimum energy solution for this spring network is the function of origin of coordinate systems and its unit vector. If there is no constraint to an absolute point or coordinate system, as illustrated in Figure 0-11.a, there is only constraints to the origin of the coordinate system but not the unit vectors, as illustrated in Figure 0-11.b, there are a family of lowest energy solutions which gives rise to the ambiguity relative to absolute space. The correlation is a result of the minimum energy solution mapping to such a family of solutions that are ambiguous as far as an affine transformation. That is the family of minimum energy solutions is a set of solutions, wherein an arbitrary affine transformation exists between its members.

In other words, the location accuracy of the MN, relative to the map, is bounded only by the quality of the map and the relating measurement sensors, whereas in the theoretical limit, it can be claimed that the MN relative location accuracy becomes equal to the localization accuracy achievable with a given map.
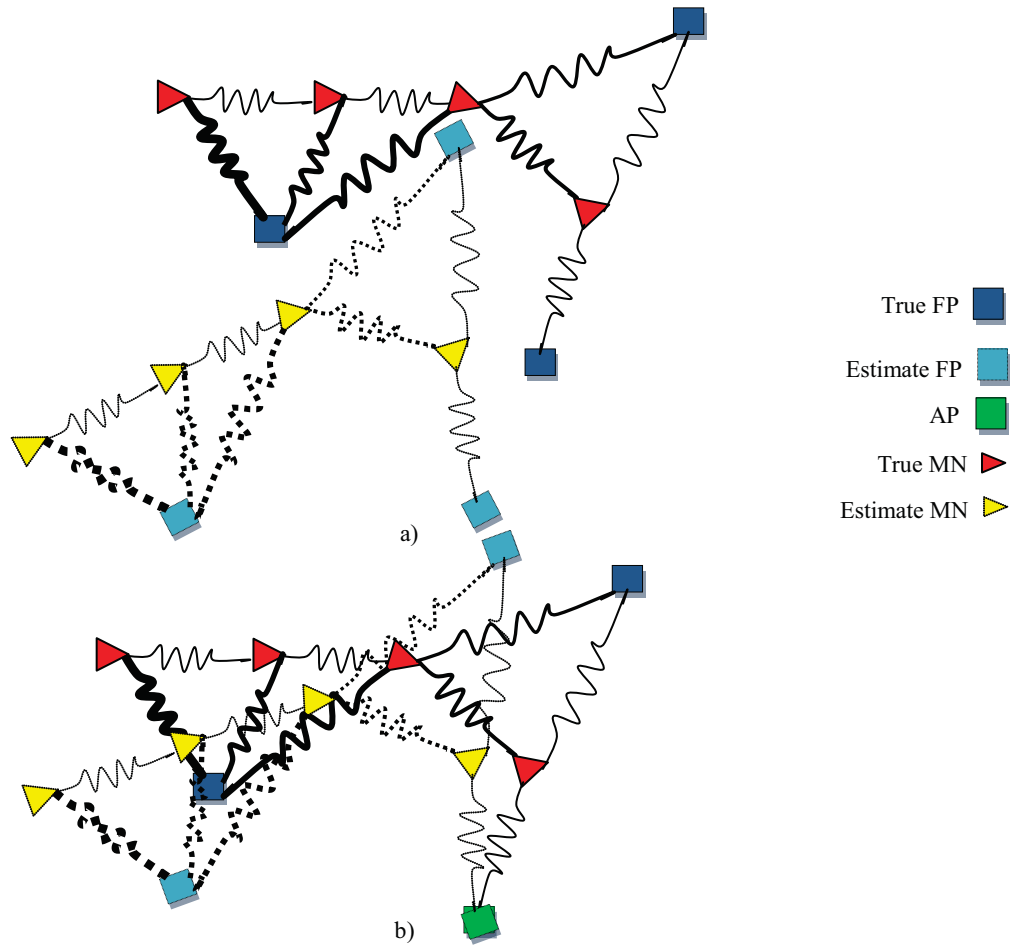
**Figure 0-11 Effect of coordinate system constraint on a SLAM problem**

Consider a MN that moves with an unknown trajectory and receives $N$ measurements at each time step from $N$ FPs, recalling that a FP is an AN with an unknown location to the MN. For a minimal 2D OWLS where there is no nuisance parameters except FP locations, there is at least $2 + 2N$ unknown variables, which is less than the number of the known constraints, $N$. Under no assumption on ANs or MN trajectory, after $K$ time steps, the number of unknown variables increases to $2K + 2K \times N$, while there are only $K \times N$ known equations, leading to an unobservable SLAM problem. The first assumption to make a SLAM problem observable is stationary ANs, meaning that there will be enough time steps like $K$, where $2K + 2N \leq NK$ or

$K \geq \dfrac{2N}{(N-2)}$. The effect of stationary ANs assumption for a two-time step SLAM problem with

two ANs is depicted in Figure 0-12. It can be seen that under stationary ANs assumption, four

unknown AN location states are merged to two, decreasing the number of unknowns to 8 for 2D

localization problem.
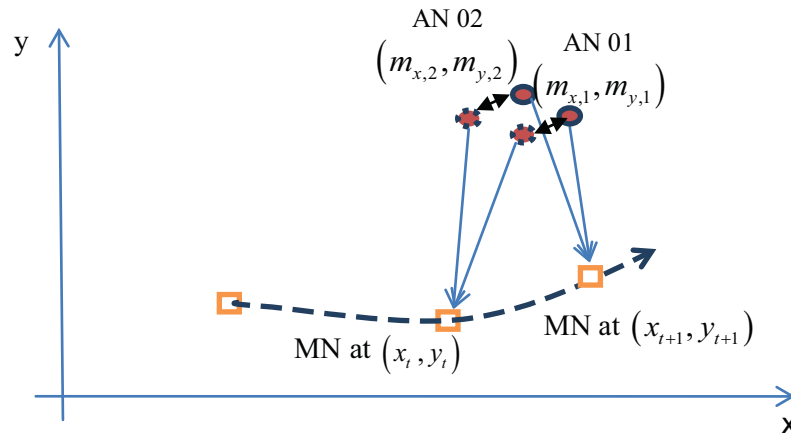


*Figure 0-12 Stationary ANs in a SLAM problem*

If the MN moves in an agile way or the distance between measurements is so far that

there is no correlation between the MN positions, no information related to the previous MN

location estimate is transformed for the next time step estimation. The problem becomes worse

when the SLAM problem also includes an estimation of random nuisance variables such as

range errors. After $K$ time steps, the number of unknowns is increased to $2K + KN + 2N$,

since, at each time step, a new bias variable is added for every AN-MN link, while there are only

$K \times N$ measurements available. In this case, the SLAM problem becomes unobservable unless

we can assume a smooth trajectory for the MN motion. The smooth trajectory assumption

proposes correlation between subsequent dynamic states such as the MN position and range

biases, i.e., the previous or future states estimate can add information for the current state

estimate, in addition to the current measurement. This information is conveyed by the update

information from previous states in the online SLAM, or from previous and future states in the full SLAM.

## Bayesian based SLAM

In probabilistic form, the optimum estimate for an online SLAM problem is obtained by evaluating the posterior PDF $p(\mathbf{q}_t \mid \mathbf{z}_{1:t}, \mathbf{u}_{1:t}, \mathbf{q}_0)$, where $\mathbf{q}_t = [\mathbf{q}_{d,t} \quad \mathbf{q}_s]^T$ is the vector of unknown variables including dynamic variables $\mathbf{q}_{d,t}$, such as the MN location at time $t$, $\mathbf{p}_t$, and random nuisance parameters, such as range error, and stationary variables $\mathbf{q}_s$, such as the FP location, $\mathbf{m}_{fp}$. Joint posterior densities of FP locations, MN location and other nuisance parameters embodies all the statistical information that can be extracted from observables $\mathbf{z}_{1:t}$, control data $\mathbf{u}_{1:t}$, and prior knowledge $\mathbf{q}_0$ about the state $\mathbf{q}_t$. A recursive solution for the SLAM problem is obtained using Bayes' rule, given by

$$p(\mathbf{q}_t \mid \mathbf{z}_{1:t}, \mathbf{u}_{1:t}, \mathbf{q}_0) = \frac{p(\mathbf{z}_t \mid \mathbf{q}_t, \mathbf{u}_{1:t}, \mathbf{z}_{1:t-1}) p(\mathbf{q}_t \mid \mathbf{z}_{1:t-1}, \mathbf{u}_{1:t}, \mathbf{q}_0)}{p(\mathbf{z}_t \mid \mathbf{z}_{1:t-1}, \mathbf{u}_{1:t})} \qquad \textbf{0-17}$$

Based on the first Markov assumption, as shown in Figure 0-6, given $\mathbf{q}_t$, $\mathbf{z}_t$ is dependent on previous measurements and control data; hence Eq. 0-16 can be re-written as

$$p(\mathbf{q}_t \mid \mathbf{z}_{1:t}, \mathbf{u}_{1:t}, , \mathbf{q}_0) = \frac{p(\mathbf{z}_t \mid \mathbf{q}_t) p(\mathbf{q}_t \mid \mathbf{z}_{1:t-1}, \mathbf{u}_{1:t}, \mathbf{q}_0)}{p(\mathbf{z}_t \mid \mathbf{z}_{1:t-1}, \mathbf{u}_{1:t})} \qquad \textbf{0-18}$$

$p(\mathbf{z}_t \mid \mathbf{q}_t)$ is the likelihood PDF that describes the probability of making an observation when FP locations, current MN location and nuisance parameters are known. Based on smooth random trajectory assumption, the dynamic state transition is considered as a first-order hidden Markov process, thus the prior PDF $p(\mathbf{q}_t \mid \mathbf{z}_{1:t-1}, \mathbf{u}_{1:t}, \mathbf{q}_0)$ can be calculated by

$$p(\mathbf{q}_t \mid \mathbf{z}_{1:t-1}, \mathbf{u}_{1:t}, \mathbf{q}_0) = \int p(\mathbf{q}_{d,t} \mid \mathbf{q}_{d,t-1}, \mathbf{u}_t) p(\mathbf{q}_{d,t-1}, \mathbf{q}_s \mid \mathbf{z}_{1:t-1}, \mathbf{u}_{1:t-1}, \mathbf{q}_0) d\mathbf{q}_{d,t-1} \qquad \textbf{0-19}$$

Eq. (0-17) and (0-18) provide a recursive procedure for calculating the joint posterior PDF based on history of observations and control data up to time step $t$. Since the denominator $p(\mathbf{z}_t \mid \mathbf{z}_{1:t-1}, \mathbf{u}_{1:t})$ in Eq. (0-17) is independent of $\mathbf{q}_t$, it can be replaced by a normalizing constant, $\eta$, and posterior PDF can be only modified in terms of prior and likelihood PDF:

$$p(\mathbf{q}_t \mid \mathbf{z}_{1:t}, \mathbf{u}_{1:t}, , \mathbf{q}_0) = \alpha\, p(\mathbf{z}_t \mid \mathbf{q}_t) p(\mathbf{q}_t \mid \mathbf{z}_{1:t-1}, \mathbf{u}_{1:t}, \mathbf{q}_0) \qquad \textbf{0-20}$$
$$\propto p(\mathbf{z}_t \mid \mathbf{q}_t) p(\mathbf{q}_t \mid \mathbf{z}_{1:t-1}, \mathbf{u}_{1:t}, \mathbf{q}_0)$$

The optimal Bayesian estimate of the state $\mathbf{q}_t$ can be obtained from $p(\mathbf{p}_t, \mathbf{m}_{fp} \mid \mathbf{z}_{1:t})$ by using the maximum *a posterior* (MAP) or the minimum mean-square error (MMSE) criterion. However, in the general case of nonlinear dynamic systems, as the SLAM-based OWLS problem, the posterior PDF cannot be determined analytically from Eq. (0-17) and (0-18). Particularly, it must be noted that the dynamic portion of the state vector (including the MN location) and the stationary portion of the state vector (including FP locations) are correlated through measurements, and it worth nothing to compute the conditional density of the stationary states $p(\mathbf{q}_s \mid \mathbf{z}_{1:t}, \mathbf{u}_{1:t}, \mathbf{q}_0)$, or the MN location $p(\mathbf{q}_{d,t} \mid \mathbf{z}_{1:t}, \mathbf{u}_{1:t}, \mathbf{q}_0)$, separately, since both are conditioned on the deterministic knowledge of other.

Suboptimal solution to the SLAM problem requires appropriate presentations of the measurement and transition processes based on reasonable assumptions that allow the evaluation of the posterior PDF with efficient computation. The EKF-SLAM and FastSLAM, as suboptimal Bayesian filters for SLAM problems, are proposed, whereby the former approximates the posterior PDF with a Gaussian PDF, and the latter describes the MN states as set of samples (known as particles) with a general non-Gaussian PDF.

## Extended Kalman Based SLAM

The most common solution to a SLAM problem in the form of a state-space model with additive noise is known as the extended Kalman SLAM (EKFSLAM). The first element and the

basis of EKFSLAM is to describe the evolution of the dynamic states as a first-order Markov process, in form of

$$\mathbf{q}_{d,t} = f(\mathbf{q}_{d,t-1}, \mathbf{u}_t) + \mathbf{v}_t \qquad \textbf{0-21}$$

where $f(*)$ is a known deterministic, possibly a nonlinear function of previous states $\mathbf{q}_{d,t-1}$, and $\mathbf{v}_t \sim p(\mathbf{q}_{d,t} \mid \mathbf{q}_{d,t-1}, \mathbf{u}_t)$ is additive, zero mean ,and uncorrelated Gaussian process with covariance $Q_t$.

The second element in the EKF-SLAM is the observation model, which defines the relation between observables and unknown state variables, given by

$$\mathbf{z}_t = h(\mathbf{q}_t) + \mathbf{w}_t \qquad \textbf{0-22}$$
$$= h(\mathbf{q}_{d,t}, \mathbf{q}_s) + \mathbf{w}_t$$

where $h(*)$ is a known deterministic, possibly nonlinear observation function, and

$w_t \sim p(\mathbf{z}_t \mid \mathbf{q}_{d,t}, \mathbf{q}_s)$ is an additive, zero mean, and uncorrelated Gaussian observation noise

with covariance matrix $R_t$.

The standard EKF-SLAM algorithm computes the estimation based on the mean of the conditional posterior PDF $p\left(\mathbf{q}_{d,t}, \mathbf{q}_s \mid \mathbf{z}_{1:t}, \mathbf{u}_{1:t}\right)$ as

$$\begin{bmatrix} \hat{\mathbf{q}}_{d,t|t} \\ \hat{\mathbf{q}}_s \end{bmatrix} = \begin{bmatrix} \mathbf{q}_{d,t} \\ \mathbf{q}_s \end{bmatrix} \mid \mathbf{z}_{1:t}, \mathbf{u}_{1:t} \qquad \textbf{0-23}$$

and covariance matrix of estimation is defined by the posterior PDF covariance matrix :

$$\Sigma_{t|t} \sim \begin{bmatrix} \Sigma_{q_d q_d,t|t} & \Sigma_{q_d q_s,t|t} \\ \Sigma_{q_d q_s,t|t}^T & \Sigma_{q_s q_s,t|t} \end{bmatrix} = E\left[ \begin{pmatrix} \mathbf{q}_{d,t} - \hat{\mathbf{q}}_{d,t} \\ \mathbf{q}_s - \hat{\mathbf{q}}_s \end{pmatrix} \begin{pmatrix} \mathbf{q}_{d,t} - \hat{\mathbf{q}}_{d,t} \\ \mathbf{q}_s - \hat{\mathbf{q}}_s \end{pmatrix}^T \mid \mathbf{z}_{1:t}, \mathbf{u}_{1:t} \right] \qquad \textbf{0-24}$$

The first stage of EKF-SLAM is the time-update of dynamic states or prediction stage.

$$\hat{\mathbf{q}}_{d,t} = f(\hat{\mathbf{q}}_{d,t-1}, \mathbf{u}_t) \qquad \textbf{0-25}$$
$$\Sigma_{q_d q_d,t|t-1} = \nabla f \Sigma_{q_d q_d,t-1|t-1} \nabla f^T + Q_t$$

where $\nabla f$ is the Jacobian of $f(*)$ evaluated at the previous estimate .

The second stage is the observation –update stage:

$$\begin{bmatrix} \hat{\mathbf{q}}_{d,t|t} \\ \hat{\mathbf{q}}_{s,t} \end{bmatrix} = \begin{bmatrix} \hat{\mathbf{q}}_{d,t|t} \\ \hat{\mathbf{q}}_{s,t} \end{bmatrix} + \mathbf{K}_t \left[ z_t - h(\hat{\mathbf{q}}_{d,t|t}, \hat{\mathbf{q}}_{s,t}) \right] \qquad \textbf{0-26}$$
$$\Sigma_{t|t} = \Sigma_{t|t-1} + \mathbf{K}_t \mathbf{D}_t \mathbf{K}_t^T$$

where

$$\mathbf{D}_t = H \sum_{t|t-1} H^T + R_t$$

$$\mathbf{K}_t = \sum_{t|t-1} H^T \mathbf{D}_t^{-1}$$

$H$ is the Jacobian of $h$, evaluated at the predicted state $\hat{\mathbf{q}}_{t|t-1} = [\hat{\mathbf{q}}_{d,t|t-1}, \hat{\mathbf{q}}_{s,t|t-1}]^T$. In a

EKF-SLAM, if the determinant of covariance matrix monotonically converges to zero, it is

defined that EKFSLAM is convergent in stationary states. However, the convergence is only

guaranteed in a jointly linear Gaussian system. It must be noted that standard deviation of an

individual FP estimate converges toward a lower bound imposed by initial uncertainties of the

MN location and observations.

Similar to EKF, EKFSLAM employs a linearized approximation of the nonlinear motion

and observation models; this inherits many caveats. Nonlinearity can be a significant problem in

EKFSLAM, which leads to inevitable and sometimes drastic inconsistency in solutions [xxxiii],

[xliv].


## FastSLAM

Online SLAM methods based on EKF can handle the large number of variables as the

update of the posterior PDF only involves the mean vector and the covariance matrix. However,

some of the state variables, notably the MN location variables are poorly approximated by a

joint Gaussian PDF where the measurement function represents a highly nonlinear relation with

the state vectors. Moreover, non-Gaussian prior belief maps cannot be accurately incorporated.

PFs or sequential Monte Carlo (SMC) methods is suggested as an alternative implementation of

Bayesian filters, where EKF fails, since it allows for a general PDF of the state variables

conditioned on non-Gaussian nonlinear observables. In a SLAM–based OWLS, the PF needs to

represent all state space variables such as the MN trajectory and the feature point locations, by

particles. The high dimensional state-space of the SLAM problem makes the complete

application of particles infeasible due to the high computational complexity.

An effective solution for this problem is the Rao-Blackwellized particle filters (RBPF). Rao-Blackwellization which is also known as variance reduction methods are based on partitioning the state vector so that one component of the partition is conditionally linear Gaussian state-space model [xli]. For this component, analytical solution can be found by exploiting the KF while the PF is only used for non-linear non-Gaussian portion of state-vector [xii].

A key feature to apply Rao-Blackwellization theorem in a SLAM problem is that the FP constraints become mutually independent when the MN trajectory variables are given. More precisely, when all of the mutually shared variables are given, then the remaining FP variables are independent. In this way, an EKF can be applied to each of the FP variable sets. For better understanding of FastSLAM implication, we limit dynamic states to MN location variables and stationary states to FPs location variables, where $\mathbf{q}_t = [\mathbf{p}_t \quad \mathbf{m}_{fp}]^T$, however the partitioning does not preclude the possible augmentation of additional variables.

In other words, the $i$-th FP location vector, $\mathbf{m}_i = [m_{i,x} \quad m_{i,y}]^T$, is independent of other FPs location variables, when the mutually shared variables including the MN position are given. Hence, the joint posterior PDF conditioned on the set of measurements and deterministic updates can be factorized as follows:

$$p\left(\mathbf{p}_{1:t}, \mathbf{m}_{fp} \mid \mathbf{z}_{1:t}, \mathbf{u}_{1:t}\right) = p\left(\mathbf{p}_{1:t} \mid \mathbf{z}_{1:t}, \mathbf{u}_{1:t}\right) \prod_{i=N_{AP}+1}^{N_{AN}} \left(\mathbf{m}_i \mid \mathbf{z}_{1:t}, \mathbf{u}_{1:t}\right)$$

<div align="right">*0-28*</div>

The product term indicates the independence of FP state variables, when conditioned on the MN position state variables, which are the part of the particles. There are a total of $N_p$ particles, with each particle consisting of the complete MN trajectory and a potential arrangement of the FPs. For $m$-th particle, we have the trajectory variables of $\mathbf{p}_{1:t}^{[m]} = \left\{x, y\right\}_{1:t}^{[m]}$, and the Gaussian FP parameters of $\left\{\mu_{1,t}^{[m]}\Sigma_{1,t}^{[m]},...,\mu_{N_{FP},t}^{[m]}\Sigma_{N_{FP},t}^{[m]}\right\}$. For each particle, a separate EKF is applied for each FP location state. Therefore, multiple possible MN trajectory solutions

are tracked instead of only the most probable one. The FastSLAM algorithm stages can be described as

**Retrieval** – obtain the MN location of the previous time step from $\mathbf{p}_{1:t-1}^{[m]}$

**Prediction** – draw new MN location variables based on the proposal distribution

$$\mathbf{p}_t^{[m]} \square\ p\left(\mathbf{p}_t \mid \mathbf{p}_{t-1}^{[m]}, \mathbf{m}_{fp,t-1}^{[m]}, \mathbf{u}_t\right)$$

**Measurement update** – update FP location estimate conditioned on the MN location. For each particle, an EKF update is performed over the observed ANs as a simple mapping operation under known MN location assumption. The outputs of this stage are $\left\{\mu_{i,t}^{[m]}, \Sigma_{i,t}^{[m]}\right\}$ for all particles and FPs locations.

**PF weight update** – calculate the importance weight $w_t^{[m]}$, which is based on the conditional probability of $p\left(\mathbf{z}_t \mid \mathbf{p}_t^{[m]}, \mathbf{m}_t^{[m]}\right)$ where $\mathbf{z}_t$ is the set of measurements from all ANs.

**Resampling** - sample with the replacement of $N_P$ particles, from the set $\left\{\mathbf{p}_{0:t}^{[m]}\right\}_{m=1}^{N_P}$, including their associated maps, considering each particle has probability proportional to $w_t^{[m]}$.

Given $N_P$ particles and $N_{FP}$ conditionally independent FPs, there will be $N_P N_{FP}$ EKFs, each with a small cluster of variables pertaining to the specific FP. Consider the details for the EKF of the $m$-th particle and the $i$-th FP. The output of this stage is $\left\{\mu_{i,t}^{[m]}, \Sigma_{i,t}^{[m]}\right\}$, defined by

$$\mu_{i,t}^{[m]} = \mu_{i,t|t-1}^{[m]} + K_t^{[m]}(z_t - h_i(\mu_{i,t-1}^{[m]}, \mathbf{p}_t^{[m]}))$$
$$\Sigma_{i,t}^{[m]} = \Sigma_{i,t|t-1}^{[m]} + K_t^{[m]} D_t^{[m]} K_t^{[m],T}$$
where, for $i$-th FP,

*0-29*

$$\mu_{i,t|t-1}^{[m]} = \mu_{i,t-1}^{[m]}$$
$$\Sigma_{i,t|t-1}^{[m]} = \Sigma_{i,t-1}^{[m]}$$
and

*0-30*

$$D_t^{[m]} = H_t^{[m]} \sum_{t|t-1}^{[m]} H_t^{[m],T} + R_{i,t}$$

$$K_t^{[m]} = \sum_{t|t-1}^{[m]} H_t^{[m],T} \left[ D_t^{[m]} \right]^{-1}$$

where $R_{i,t}$ is the covariance matrix of the measurement set $z_{i,t}$ from the ith FP.

Once the EKF is finished updating, the particle weights can be determined. The set of each FP measurement is assumed to be independent and the likelihood probability is determined. The likelihoods of the set of measurements can be multiplied, forming the overall weight of the particle. In the current version of FastSLAM, the particles are updated at each iteration such that the carryover of the previous weights is not done. The particle weight $w_{i,t}^{[m]}$ is calculated by

$$w_{i,t}^{[m]} = \eta \, p \left( \mathbf{z}_{i,t} \mid \mathbf{p}_t^{[m]}, \mathbf{m}_t^{[m]} \right)$$

where the constant $\eta$ which can be ignored since the set of weights is normalized such that the sum of weights is unity after each iteration.

## Comparison between EKFSLAM and FastSLAM performances

The two standard Bayesian approaches are explained for a SLAM-based OWLS. It is shown that the EKFSLAM linearizes the state transition and observation functions and represents the joint probability with a single high-dimensional Gaussian; however, FastSLAM, represents the MN trajectory using a set of particles and conditions the map on the MN trajectory. In particular, the EKF is subject to failure where significant MN uncertainty induces linearization errors. EKFSLAM represents the joint state posterior PDF by an approximate mean and variance. This can be problematic from two aspects. First, due to linearization error, these moments are approximate and may not accurately represent the true first and second moments. Secondly, where the true probability distribution is non-Gaussian, even the true mean and

variance may not be an adequate representation of the PDF. Particularly, the iterative nature of this algorithm leads the approximation errors to accumulate as time progresses [xlii], [xliii].

In contrast to the EKF, FastSLAM is much more robust against linearization error as the MN location can have an arbitrary PDF, and the update is constrained to be neither Gaussian nor linear. However, as more observations are received, particles which made poor association decisions in the past tend to be removed in the resampling process; hence, the majority of particles tend to converge onto the correct set of associations.

For the purposes of data association, FastSLAM automatically allows information to be integrated between online SLAM and full SLAM, as each particle is carrying a history of the MN path with an exponential forgetting memory. Furthermore, FastSLAM is simple to implement relative to complicated batch processing algorithms. The important feature of the FastSLAM algorithm is that each particle does not represent the current MN state, but the entire MN trajectory and associated ANs map. This can have important effects on consistency since it enables the filter to accurately estimate uncertainty.

However, the FastSLAM particle filter is really operating in a very high-dimensional space: the space of the MN trajectories (as opposed to the MN location at a specific time instance). Therefore, the required number of particles increases exponentially in the length of the trajectory. Using a smaller number of particles may result in underestimation of total uncertainty, and eventually an inconsistent solution, especially for the case whereby the full uncertainty is required such as when large loops need to be closed. Whenever resampling is performed, for each annihilated particle, the entire MN trajectory and map hypothesis is not represented in subsequent conditional PDF updates. This implies that the random ANs location estimates conditioned on these past locations (particles) are not sufficiently statistically sampled and the eventual state estimate based on the evolution of the conditional mean becomes inaccurate. For remembering long-term uncertainty, the EKF-SLAM performs in a far superior manner in comparison with FastSLAM since it uses a continuous Gaussian representation (the

mean vector and covariance matrix) for the posterior PDF, which does not degrade as a function of trajectory length [xliii], [xlii]. However, EKFSLAM is only applicable where all of the PDF's involved are near Gaussian.

This chapter presented an overview of wireless observables from local wireless sources which can be utilized for an OWLS. Taking advantage of the signals of opportunity was suggested as a solution for the indoor environment of dense urban areas, where the GPS cannot provide sufficient accuracy. To this reason, the deficiencies and problems of opportunistic wireless localization were discussed. In summary, the wireless localization algorithm, which exploits from an opportunistic signal from an unregistered local network, must combat the following challenges:

1- The downlink signals from the ANs may or may not be accurately time synchronized.

2- The MN clock is not synchronized with the ANs clock. Moreover, its clock may drift in time due to clock instability.

3- Time/range measurements from wireless sources are subject to excess delay/range error due to multipath fading. Moreover, the range error is not stationary due to the dynamic feature of sight conditions.

4- The AN locations are not completely known by the MN.

It was shown that the opportunistic wireless localization, in general, is an unobservable problem due to the inflation of unknown variables, unless certain conditions can be assumed: stationary ANs (or if mobile, they move in a deterministic way) and the MN smooth trajectory. The first assumption turns OWLS into an observable SLAM problem as the SLAM can take advantage of the correlation between subsequent measurements whenever the same AN is re-seen. The second assumption modeled the dynamic states including the MN position, range error, and sight conditions as a Markov process. The Markovian behavior of variables can be systematically captured by Bayesian-based methods. It was shown that the optimal joint

posterior belief map of system states cannot be calculated analytically in a closed form due to nonlinear dynamic nature of the OWLS. To this end, two suboptimal Bayesian solutions for the SLAM-based OWLS, EKFSLAM and FastSLAM, were introduced, and their benefits and deficiencies were discussed.

## Information and Estimation Bounds on OWLS

The main objective of this chapter is to derive the fundamental limits of OWLS performance in terms of both information and estimation metrics. This chapter illuminates connection between information theory and estimation theory with special focus on the SLAM-based OWLS. This gives an understanding of what a specific measurement is worth, based on the metric of quantifying its information content, which appears as an overly abstract quantity but is surprisingly practical. For instance, suppose the issue of whether a MEMS IMU can be added to the MN receiver. This will provide additional information regarding the update of the position of the MN in the SLAM algorithm. Is this worthwhile?  How much additional information does the IMU provide? A component of this thesis is the consideration of information in regards to the constraints of the SLAM formulation in the context of the OWLS.

In estimation theory, the MMSE and CRLB are considered as the most fundamental estimation measures to illustrate how accurately each individual parameter can be recovered from channel observables. Estimation theory is tightly coupled with the averaged squared error of estimation, regardless of whether the unknown state $\mathbf{q}$ is a deterministic parameter (as in classical approaches), or whether the unknown state $\mathbf{q}$ is a random variable (as in Bayesian approaches) [xliv], [xlv], given by

$$
\begin{aligned}
Unbiased\ Classical\ Estimator: &\quad \mathrm{var}(\hat{\mathbf{q}}(\mathbf{z})) = E_z[[\hat{\mathbf{q}}(\mathbf{z}) - \mathbf{q}]^2] \\
Bayesian\ Estimator: &\quad MSE(\hat{\mathbf{q}}(\mathbf{z})) = E_{z,q}[[\hat{\mathbf{q}}(\mathbf{z}) - \mathbf{q}]^2]
\end{aligned}
$$

*0-33*

However, to unify the concept of estimation error in classical and Bayesian philosophies, we use MSE as a general term for the averaged squared error of estimation for both classical and Bayesian methods, accepting the difference that the averaging is with respect to observation PDF (since there is no prior information available about non-random parameter) in classical philosophy, while the averaging is with respect to joint PDF of observations and random parameter in Bayesian philosophy.

Cramer Rao Lower Bound (CRLB) theorem says that the MSE corresponding to a unbiased estimator, $\hat{\mathbf{q}}(\mathbf{z})$, of a non-random parameter $\mathbf{q}$, given the observation vector $\mathbf{z}$, can be lower bounded [xlv], [xlvi], as follows:

$$E\left\{\left(\hat{\mathbf{q}}(\mathbf{z})-\mathbf{q}\right)\left(\hat{\mathbf{q}}(\mathbf{z})-\mathbf{q}\right)^{T}\right\} \geq J^{-1} \qquad \text{0-34}$$

where $J$ is the FIM of non-random parameter $\mathbf{q}$, obtained as

$$J \square E_{\mathbf{z}}\left\{\left[\nabla_{\mathbf{q}} \ln p_{\mathbf{z}|\mathbf{q}}(\mathbf{z}|\mathbf{q})\right]\left[\nabla_{\mathbf{q}} \ln p_{\mathbf{z}|\mathbf{q}}(\mathbf{z}|\mathbf{q})\right]^{T}\right\} \qquad \text{0-35}$$

However, the extended CRLB theorem for random parameters (also known as Bayesian CRLB, posterior CRLB, and Van Trees inequality) indicates that the MSE of an unbiased estimator $\hat{\mathbf{q}}(\mathbf{z})$ can also be lower-bounded [xlvi], [xlvii], as follows,

$$E\left\{\left(\hat{\mathbf{q}}-\mathbf{q}\right)\left(\hat{\mathbf{q}}-\mathbf{q}\right)^{T}\right\} \geq J_{tot}^{-1} \qquad \text{0-36}$$

where $J_{tot}$ is total Bayesian FIM (BFIM) of the random parameter $\mathbf{q}$, defined by

$$J_{tot} \square J_{Z} + J_{P} \qquad \text{0-37}$$

and $J_{Z}$ is the measurement information matrix, representing the information data obtained from the observables, $\mathbf{z}_{t}$, stated as

$$J_{Z} \square E_{\mathbf{z},q}\left\{\left[\nabla_{\mathbf{q}} \ln p_{\mathbf{z}|\mathbf{q}}(\mathbf{z}|\mathbf{q})\right]\left[\nabla_{\mathbf{q}} \ln p_{\mathbf{z}|q}(\mathbf{z}|\mathbf{q})\right]^{T}\right\} \qquad \text{0-38}$$

The expectation is taken under the joint PDF of measurements and states. The matrix $J_{P}$ denotes the apriori information about $\mathbf{q}_{t}$, whose elements are defined as

$$J_{P_{ij}} \; \Box \; E_{\mathbf{q}} \left[ \frac{\partial \ln p_q(\mathbf{q})}{\partial q_i} \frac{\partial \ln p_q(\mathbf{q})}{\partial q_j} \right] = -E \left[ \frac{\partial^2 \ln p_q(\mathbf{q})}{\partial q_i q_j} \right] \;, \quad i,j = 1,..K$$

where $K = \dim(\mathbf{q}_t)$ stands for the state space dimension. It must be noted that Bayesian CRLB theorem holds under some mild regularity conditions, implying that the joint PDF does not have infinite moments.

Information theory provides a deep analytical approach to assess tracking performance based on the available information. Information theory application in tracking problems is traditionally known by Fisher information (FI) regarding the CRLB calculation. Fisher information is recognized as a way to measure the amount of information that an observable carries about the parameters to be estimated upon either their joint (for random parameters) or likelihood (for non-random parameters) probability density functions.

Another important metric in information theory is the input–output mutual information (MI) that is used as an indicator of how much coded information can be pumped through a channel reliably given a certain input signaling. However, the main application of MI has been generally known in coding operations, Guo's theorem [xi] shows that MI can also represents a powerful measure to provide a deep insight into the performance of estimation problems such as the SLAM. Mutual information $I(X,Y)$ can be considered as a global measure of available information in channel observable Y, about state variable to be estimated $X$, since it does not make any assumptions regarding the receiver processing of $Y$. However, the minimum MSE (MMSE) criterion is obtained according to the quadratic cost function of error; this implies that posterior probability function needs to be of an exponential (Gaussian) type to reveal all related information about estimation error from the second order moment. As a consequence, CRLB or BCRLB may not fully characterize the accuracy of localization from a non-Gaussian posterior PDF which requires higher order moments, in addition to the mean and the covariance. Nevertheless, BCRLB/CRLB and BFIM/FIM is regarded as a useful metric not only to assess

the performance of implemented algorithms but also to predict the best achievable performance as a system design tool.

This chapter introduces both the information and the estimation metrics and their relations to evaluate OWLS performance in terms of efficiency, consistency and observability. Information matrix is introduced as a quantitative and visual benchmark for all the disparate sources of information utilized in OWLS. In this regard, the contribution of every source of information in a SLAM-based OWLS is explained by some basic cases. Based on the system parameters introduced for a range-based OWLS in Chapter 2, four system models are proposed to present a complete set of system state. BFIM is derived for each proposed system model as a fundamental limit of accuracy for a range-based OWLS. Later, the relation between FI and other estimation metrics is explained which can be exploited as useful tools to assess the SLAM algorithms in terms of consistency and localization accuracy. Finally, an applicable example of MI for a SLAM-based OWLS is provided through introduction of insightful connection between MI in information theory and MMSE in estimation theory from Guo's theorem.

## Fisher information and BCRLB application in a SLAM problem

The concept of the Bayesian information matrix, denoted by $J$, is key to SLAM algorithms. The SLAM filter efficiency can be investigated by comparing the extracted information with the existing information, quantified as $J$. It is loosely regarded as a quantitative summary of all information regarding the unknowns in one matrix. The relation to quantifiable information is only valid for the case where the problem is linear and jointly Gaussian (LJG); however, for problems where the nonlinearity is mild and the measurement and state update noise are approximately Gaussian, it is still applicable.

The MLE of the unknown variable vector $\mathbf{q}$ can be typically approximated as being jointly Gaussian represented by $N\left(\mathbf{q}, J^{-1}\right)$. Here, $\mathbf{q}$ represents the actual value of the state

variable vector. For typical problems that are not jointly Gaussian, the PDF approximation of the MLE as $N\left(\mathbf{q}, J^{-1}\right)$ is still generally valid. Regardless, $J$ is the information matrix and is the inverse of the covariance matrix of the MLE estimators for $\mathbf{q}$. In the OWLS, whenever the LJG assumption is justified, the Fisher information matrix can be derived as the fundamental limit of localization and mapping accuracy for the OWLS problem.

Information sources for a SLAM problem is generally derived from the MN motion process, measurements from ANs, and the prior knowledge about the MN initial state and AN locations. To understand the contribution of each information source on the SLAM problem, the FIM calculation process is explained by 6 simple linear Gaussian cases while the problem complexity is eventually increased for next case.

In the first case, consider the MN undergoes random motion in the $x$ direction according to the first-order Markov (random walk) model. Assuming that the initial state is distributed as $x_0 \sim N\left(0, \sigma_0^2\right)$, that represents the prior PDF. The update step from $x_0$ to $x_1$ is illustrated in Figure 0-13
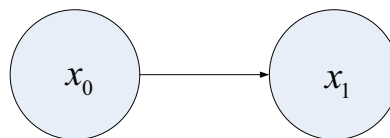


*Figure 0-13 One-step state update in a 1D linear problem*

The update model is defined by

$$0\text{-}40$$

$$x_1 = x_0 + u$$

where the process noise is distributed by $u \sim N\left(0, \sigma_u^2\right)$. The joint posterior PDF of $\left\{x_0, x_1\right\}$ is given by a normal PDF with the zero mean and the covariance matrix of

$$0\text{-}41$$

$$Q = \begin{bmatrix} \sigma_0^2 & \sigma_0^2 \\ \sigma_0^2 & \sigma_0^2 + \sigma_u^2 \end{bmatrix}$$

Note that the covariance of $x_1$ given $x_0$ is denoted as $\sigma_{1|0}^2$, determined by

$$\sigma_{1|0}^2 = \left(\sigma_0^2 + \sigma_u^2\right) - \frac{\sigma_0^4}{\sigma_0^2} = \sigma_u^2$$

Likewise, the covariance of $x_0 \mid x_1$ is given by

$$\sigma_{0|1}^2 = \sigma_0^2 - \frac{\sigma_0^4}{\sigma_0^2 + \sigma_u^2} = \frac{\sigma_0^2 \sigma_u^2}{\sigma_0^2 + \sigma_u^2}$$

which for the case where $\sigma_0^2 \gg \sigma_u^2$, is approximately $\sigma_u^2$. If there is no measurement then the variance of the estimate of $x_1$ is $\sigma_0^2 + \sigma_u^2$. The Fisher information matrix is obtained by

$$J = Q^{-1} = \begin{bmatrix} \dfrac{\sigma_0^2 + \sigma_u^2}{\sigma_0^2 \sigma_u^2} & -\sigma_u^{-2} \\ -\sigma_u^{-2} & \sigma_u^{-2} \end{bmatrix}$$

It is notable that diagonal elements of the information matrix are equal with the inverse of conditional covariances as follows,

$$[J]_{11} = \sigma_{0|1}^{-2}$$
$$[J]_{22} = \sigma_{1|0}^{-2}$$

Now, in the second case, consider another problem where only the measurement associated with the anchor point, $m_1$, is available, as illustrated in

Figure 0-14.
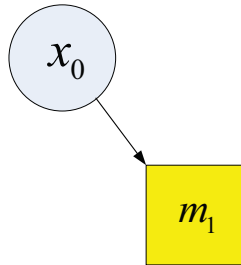


**Figure 0-14 Single measurement at a single point trajectory**

With the assumption of $z_1 \sim N(x_0, \sigma_z^2)$, the covariance of $x_0$ given the measurement is stated as

$$\sigma_{0|z}^2 = \sigma_0^2 - \frac{\sigma_0^4}{\sigma_z^2 + \sigma_0^2} = \frac{\sigma_z^2 \sigma_0^2}{\sigma_z^2 + \sigma_0^2}$$

In the third case, consider the measurement as an amendment to the prior one step update problem, as shown in Figure 0-15. Similarly, the covariance of $x_0$, given the previous state and measurement, is computed by

$$\sigma_{1|0,z}^2 = \sigma_{0|z}^2 + \sigma_u^2 = \frac{\sigma_z^2 \sigma_0^2}{\sigma_z^2 + \sigma_0^2} + \sigma_u^2$$
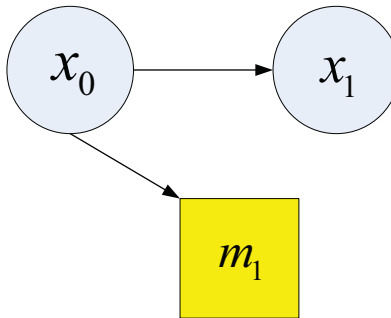


**Figure 0-15 Single update step with a single measurement**

The FI calculation procedure can be viewed differently with the procedure based on the state vector of $\mathbf{q} = \begin{bmatrix} x_0 & x_1 \end{bmatrix}^T$. Calculation of total information involved for the above cases can be determined by the following steps:

1. First, start with the covariance matrix of the state update:

$$Q = \begin{bmatrix} \sigma_0^2 & \sigma_0^2 \\ \sigma_0^2 & \sigma_0^2 + \sigma_u^2 \end{bmatrix}$$

2. The information matrix from the measurement is given by

$$J_z = \begin{bmatrix} \sigma_z^{-2} & 0 \\ 0 & 0 \end{bmatrix}$$

as it refers to the $x_0$ position state.

3. Compute the total information as the sum of prior information $J_P = Q^{-1}$ and

    measurement information $J_z$, expressed by

$$J_{tot} = J_P + \begin{bmatrix} \sigma_z^{-2} & 0 \\ 0 & 0 \end{bmatrix}$$

4. Determine the inverse

$$Q_{tot} = J_{tot}^{-1}$$

For the current case, the posterior PDF covariance matrix is determined as

$$Q_{tot} = \frac{\sigma_0^2 \sigma_z^2}{\sigma_0^2 + \sigma_z^2} \begin{bmatrix} 1 & 1 \\ 1 & \dfrac{\sigma_0^2 \sigma_z^2 + \sigma_z^2 \sigma_u^2 + \sigma_0^2 \sigma_u^2}{\sigma_0^2 \sigma_z^2} \end{bmatrix}$$

Note that the second diagonal term of $Q_{tot}$ defines the estimation variance of $x_1$ given $x_0$ and

$z$ as :

$$[Q_{tot}]_{22} = \frac{\sigma_0^2 \sigma_z^2 + \sigma_z^2 \sigma_u^2 + \sigma_0^2 \sigma_u^2}{\sigma_0^2 + \sigma_z^2} = \frac{\sigma_0^2 \sigma_z^2}{\sigma_0^2 + \sigma_z^2} + \sigma_u^2 = \sigma_{1|0,z}^2$$

Incrementing the information matrix, $J$, with a new incremental entity of information

such as a measurement, is shown in this example. The only processing problem is that $J$ has

to be eventually inverted to extract the actual variances of the state variables. Of course, the

other issue is that of the underlying assumption of the problem being jointly Gaussian. Note that

if the measurement provides no information, i.e. $\sigma_z^2 \to \infty$ , then $\sigma_{1|0,z}^2 \to \sigma_0^2 + \sigma_u^2$ as in the

previous example.

Now, in fourth case, it is assumed that the AP independent measurements are available

from both $x_0$ and $x_1$ , as illustrated in Figure 0-16.
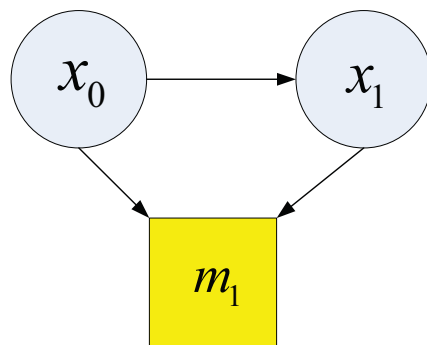


**Figure 0-16 Two independent measurements of two subsequent states**

The information matrix for the two independent measurements is given as

$$J_z = \begin{bmatrix} \sigma_z^{-2} & 0 \\ 0 & \sigma_z^{-2} \end{bmatrix}$$

0-54

The total covariance can be computed similarly as

0-55

$$Q_{tot} = J_{tot}^{-1} = \left( Q^{-1} + \begin{bmatrix} \sigma_z^{-2} & 0 \\ 0 & \sigma_z^{-2} \end{bmatrix} \right)^{-1} = \begin{bmatrix} \dfrac{\sigma_0^2 + \sigma_u^2}{\sigma_0^2 \sigma_u^2} + \sigma_z^{-2} & -\sigma_u^{-2} \\ -\sigma_u^{-2} & \sigma_u^{-2} + \sigma_z^{-2} \end{bmatrix}^{-1}$$

$$= \dfrac{1}{\dfrac{\sigma_0^2 + \sigma_u^2}{\sigma_0^2 \sigma_u^2} \sigma_u^{-2} + \dfrac{\sigma_0^2 + \sigma_u^2}{\sigma_0^2 \sigma_u^2} \sigma_z^{-2} + \sigma_z^{-2} \sigma_z^{-2}} \begin{bmatrix} \sigma_u^{-2} + \sigma_z^{-2} & \sigma_u^{-2} \\ \sigma_u^{-2} & \dfrac{\sigma_0^2 + \sigma_u^2}{\sigma_0^2 \sigma_u^2} + \sigma_z^{-2} \end{bmatrix}$$

In an estimation problem, a parameter is said to be observable if there is sufficient

information to estimate it without ambiguity.  FIM can also be used to investigate system

observability. In order to have an observable system, the FIM must be invertible. If the FIM (or

BFIM) is singular or  very ill-conditioned then CRLB (or BCRLB) does not meaningfully exist.

As shown in Eq.(0-48), the single observation of an AN results in a singular FI matrix; it means

that the amount of information is insufficient for the estimation problem. However,

unobservability can be resolved if the MN moves, as shown in Eq. 0-49, and/or the AN is

observed in more than a single MN state, as shown in Eq. (0-53).

In the fifth case, the previous localization problem is transformed to the SLAM problem

where the measurement is obtained from a feature point with initially unknown location, as

illustrated in Figure 0-16. The state vector is modified as $\mathbf{q} = \begin{bmatrix} x_0 & x_1 & m \end{bmatrix}^T$, where the

covariance matrix of the updates is given by

$$Q = \begin{bmatrix} \sigma_0^2 & \sigma_0^2 & 0 \\ \sigma_0^2 & \sigma_0^2 + \sigma_u^2 & 0 \\ 0 & 0 & \sigma_m^2 \end{bmatrix}$$

<div align="right">0-56</div>

The information added by the measurement between $m$ and $x_0$ is captured in the

information matrix as

$$J_{z,0} = \begin{bmatrix} \dfrac{1}{\sigma_z^2} & 0 & -\dfrac{1}{\sigma_z^2} \\ 0 & 0 & 0 \\ -\dfrac{1}{\sigma_z^2} & 0 & \dfrac{1}{\sigma_z^2} \end{bmatrix}$$

<div align="right">0-57</div>

where the component of the matrix is calculated by

<div align="right">0-58</div>

$$\left[ J_z \right]_{ij} = -E\left[ \frac{\partial^2}{\partial q_i \partial q_j} \ln\left( N\left(m - x_0, \sigma_z^2\right) \right) \right]$$

In a /similar way, the information added by the measurement between m and $x_1$ is given

by

<div align="right">0-59</div>

$$J_{z,1} = \begin{bmatrix} 0 & 0 & 0 \\ 0 & \dfrac{1}{\sigma_z^2} & -\dfrac{1}{\sigma_z^2} \\ 0 & -\dfrac{1}{\sigma_z^2} & \dfrac{1}{\sigma_z^2} \end{bmatrix}$$

Hence, the overall covariance matrix is obtained by

<div align="right">0-60</div>

$$Q_{tot} = \left( \begin{bmatrix} \sigma_0^2 & \sigma_0^2 & 0 \\ \sigma_0^2 & \sigma_0^2 + \sigma_u^2 & 0 \\ 0 & 0 & \sigma_m^2 \end{bmatrix}^{-1} + \begin{bmatrix} \dfrac{1}{\sigma_z^2} & 0 & -\dfrac{1}{\sigma_z^2} \\ 0 & \dfrac{1}{\sigma_z^2} & -\dfrac{1}{\sigma_z^2} \\ -\dfrac{1}{\sigma_z^2} & -\dfrac{1}{\sigma_z^2} & \dfrac{2}{\sigma_z^2} \end{bmatrix} \right)^{-1}$$

An interesting point in this example is that however, the observation information matrix of each state $J_{z,i}, i = 1, 2$, is a singular matrix, the multiple observation of a FP in a correlated trajectory makes the estimation problem observable. It must be noted that a single FP measurement that is only connected to one state variable does not convey information.

By now, a systematic approach to calculate information connectivity of FPs and the motion update from one time step to the next is established. It is shown that the information conveyed is therefore minimal if each FP is assumed to have only two associated observations; hence, the information matrix is sparse.

The final case complicates the SLAM problem to bring up the localization problem in cooperative networks where the mobile nodes can help each other by sharing their information. Although cooperative SLAM problems are out of scope of the current research, a simple illustrative example is given, as illustrated in Figure 0-17. The FIM calculation procedure, as systematic way of accounting for the diverse set of constraints, is extended for two MN cooperative tracking problem which two MNs meet a single FP.
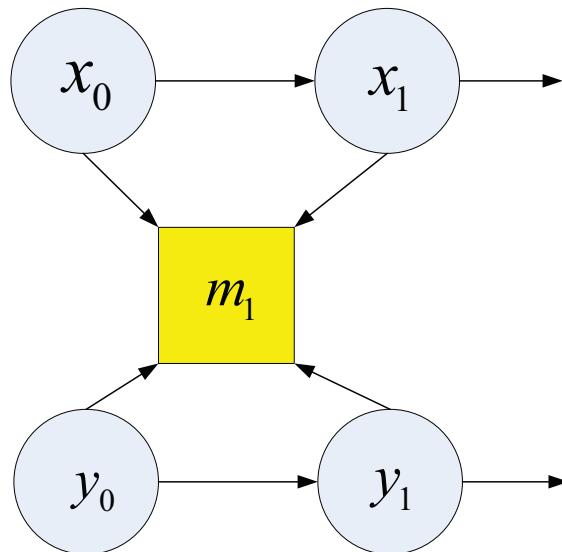


*Figure 0-17 Two cooperative MN localization problem*

The update covariance matrix is calculated by

$$
Q = \begin{bmatrix} \mathbf{Q_{ux}} & \mathbf{0} & \mathbf{0}_{(2\times 2)} \\ \mathbf{0} & \mathbf{Q_{ux}} & \mathbf{0} \\ \mathbf{0} & \mathbf{0} & \sigma_m^2 \end{bmatrix}
$$

$$
\mathbf{Q_{ux}} = \begin{bmatrix} \sigma_{0,x}^2 & \sigma_{0,x}^2 \\ \sigma_{0,x}^2 & \sigma_{0,x}^2 + \sigma_{u,x}^2 \end{bmatrix} ; \mathbf{Q_{uy}} = \begin{bmatrix} \sigma_{0,y}^2 & \sigma_{0,y}^2 \\ \sigma_{0,y}^2 & \sigma_{0,y}^2 + \sigma_{u,y}^2 \end{bmatrix}
$$

*0-61*

Similar to previous example, the measurement information matrix is given by

$$
J_{0,x} = \begin{bmatrix} \sigma_z^{-2} & 0 & 0 & 0 & \sigma_z^{-2} \\ 0 & 0 & 0 & 0 & 0 \\ 0 & 0 & 0 & 0 & 0 \\ 0 & 0 & 0 & 0 & 0 \\ \sigma_z^{-2} & 0 & 0 & 0 & \sigma_z^{-2} \end{bmatrix} ; J_{1,x} = \begin{bmatrix} 0 & 0 & 0 & 0 & 0 \\ 0 & \sigma_z^{-2} & 0 & 0 & \sigma_z^{-2} \\ 0 & 0 & 0 & 0 & 0 \\ 0 & 0 & 0 & 0 & 0 \\ 0 & \sigma_z^{-2} & 0 & 0 & \sigma_z^{-2} \end{bmatrix} ;
$$

*0-62*

$$
J_{0,y} = \begin{bmatrix} 0 & 0 & 0 & 0 & 0 \\ 0 & 0 & 0 & 0 & 0 \\ 0 & 0 & \sigma_z^{-2} & 0 & \sigma_z^{-2} \\ 0 & 0 & 0 & 0 & 0 \\ 0 & 0 & \sigma_z^{-2} & 0 & \sigma_z^{-2} \end{bmatrix} ; J_{1,y} = \begin{bmatrix} 0 & 0 & 0 & 0 & 0 \\ 0 & 0 & 0 & 0 & 0 \\ 0 & 0 & 0 & 0 & 0 \\ 0 & 0 & 0 & \sigma_z^{-2} & \sigma_z^{-2} \\ 0 & 0 & 0 & \sigma_z^{-2} & \sigma_z^{-2} \end{bmatrix} ;
$$

The total covariance matrix and so the information is computed as follows

$$
Q_{tot} = \left[ Q^{-1} + \begin{bmatrix} \sigma_z^{-2} & 0 & 0 & 0 & \sigma_z^{-2} \\ 0 & \sigma_z^{-2} & 0 & 0 & \sigma_z^{-2} \\ 0 & 0 & \sigma_z^{-2} & 0 & \sigma_z^{-2} \\ 0 & 0 & 0 & \sigma_z^{-2} & \sigma_z^{-2} \\ \sigma_z^{-2} & \sigma_z^{-2} & \sigma_z^{-2} & \sigma_z^{-2} & 4\sigma_z^{-2} \end{bmatrix} \right]^{-1}
$$

*0-63*

$$
Q_{tot} = \begin{bmatrix} \sigma_z^{-2} + \dfrac{\sigma_{0,x}^2 + \sigma_{u,x}^2}{\sigma_{0,x}^2 \sigma_{u,x}^2} & \sigma_{u,x}^{-2} & 0 & 0 & \sigma_z^{-2} \\ \sigma_{u,x}^{-2} & \sigma_z^{-2} + \sigma_{u,x}^{-2} & 0 & 0 & \sigma_z^{-2} \\ 0 & 0 & \sigma_z^{-2} + \dfrac{\sigma_{0,y}^2 + \sigma_{u,y}^2}{\sigma_{0,y}^2 \sigma_{u,y}^2} & \sigma_{u,y}^{-2} & \sigma_z^{-2} \\ 0 & 0 & \sigma_{u,y}^{-2} & \sigma_z^{-2} + \sigma_{u,y}^{-2} & \sigma_z^{-2} \\ \sigma_z^{-2} & \sigma_z^{-2} & \sigma_z^{-2} & \sigma_z^{-2} & 4\sigma_z^{-2} + \sigma_m^{-2} \end{bmatrix}^{-1}
$$

$$
J_{tot} = Q_{tot}^{-1}
$$

The diagonal elements of $Q_{tot}$ are defined by

$$\sigma^2_{x_0|x_1,y_0,y_1,m} = [Q_{tot}]_{11}$$

$$\sigma^2_{x_1|x_0,y_0,y_1,m} = [Q_{tot}]_{22}$$

$$\sigma^2_{y_0|x_0,x_1,y_1,m} = [Q_{tot}]_{33}$$

$$\sigma^2_{y_1|x_0,x_1,y_0,m} = [Q_{tot}]_{44}$$

$$\sigma^2_{m|x_0,x_1,y_1,y_0} = [Q_{tot}]_{55}$$

0-64

In a dense obstacle environment, the opportunistic sources may not be able to provide sufficient localization information to the MN because of radio blockage and limited range. In such situations, cooperation between MNs can significantly improve opportunistic localization performance. Cooperative OWLS can be investigated by the case where the FPs are also moving and have their own update motion models, as shown in Figure 0-18. In this case, the new states associated with FPs will be augmented to the state space as

$y = \begin{bmatrix} x_0 & x_1 & m_0 & m_1 \end{bmatrix}^T$. For each time step, the covariance matrix for the update state will be defined as

$$Q = \begin{bmatrix} \mathbf{Q_{ux}} & \mathbf{0} \\ \mathbf{0} & \mathbf{Q_{um}} \end{bmatrix};$$

$$Q_{ux} = \begin{bmatrix} \sigma^2_{0,x} & \sigma^2_{0,x} \\ \sigma^2_{0,x} & \sigma^2_{0,x} + \sigma^2_{u,x} \end{bmatrix} ; Q_{um} = \begin{bmatrix} \sigma^2_{0,m} & \sigma^2_{0,m} \\ \sigma^2_{0,m} & \sigma^2_{0,m} + \sigma^2_{u,m} \end{bmatrix}$$

0-65
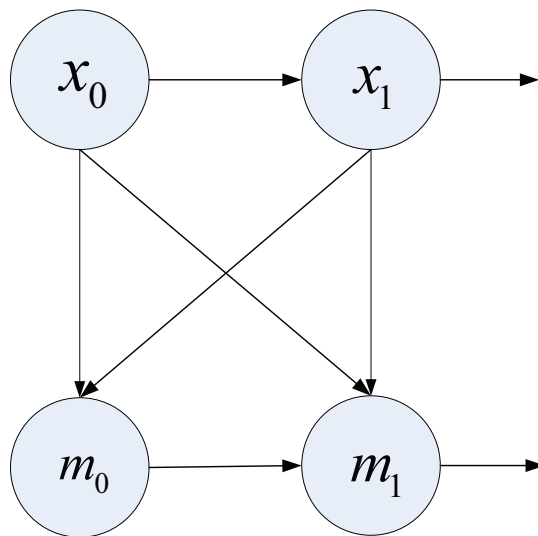


**Figure 0-18 Cooperative SLAM with moving FPs**

In similar way, the measurement information matrix is shown as

$$
J_{0,z} = \begin{bmatrix} \sigma_z^{-2} & 0 & \sigma_z^{-2} & 0 \\ 0 & 0 & 0 & 0 \\ \sigma_z^{-2} & 0 & \sigma_z^{-2} & 0 \\ 0 & 0 & 0 & 0 \end{bmatrix}; J_{1,z} = \begin{bmatrix} 0 & 0 & 0 & 0 \\ 0 & \sigma_z^{-2} & 0 & \sigma_z^{-2} \\ 0 & 0 & 0 & 0 \\ 0 & \sigma_z^{-2} & 0 & \sigma_z^{-2} \end{bmatrix};
$$

*0-66*

$$
J_z = J_{0,z} + J_{1,z}
$$

A systematic approach to calculate FI elements and unify all information from different sources of information into one single matrix is explained with some simple linear Gaussian cases. In the next subsection, the FI concept is generalized for the nonlinear OWLS problem in a SLAM framework.

## Opportunistic wireless localization system models

Consider a single MN moving smoothly through a 2D space in a random trajectory and receiving signals from an opportunistic wireless network that consists of an arbitrary number, $N_{AN}$, of stationary ANs. The location of ANs may not be known to the MN; however, their correspondence is not an issue; therefore, the additional mapping variables associated with mapping do not have to be carried in the state vector. Figure 0-19 shows a 2D illustration of an OWLS scenario, where blue lines represent the continuous MN trajectory, and red circles on the MN trajectory represent the MN locations where the measurements are taken and state estimates are updated. FPs and APs are shown by red and green squares, respectively, and LOS blockage is created by a wall shown by a light green rectangular.

The MN location $\mathbf{p}_t$ is modeled as a random walk process ruled by the system equation $\mathbf{p}_t = \mathbf{p}_{t-1} + \mathbf{v}_t$, where the $\mathbf{v}_t \in \square^2$ is the motion driving process with the known zero mean Gaussian distribution, $f_v(\mathbf{v}_t)$, or $\mathbf{v}_t \square N(\mathbf{0}, Q_p)$. The first-order Markov model for motion is the most non-informative model for the smooth MN trajectory assumption, which considers the

velocity to be zero and $f_v(\mathbf{v}_t)$ to describe the velocity variation. Higher-order motion

parameters such as velocity and acceleration can also be modeled for the MN motion process

for a smoother and more informative trajectory assumption. Moreover, the motion control data

or trajectory estimation from CV or IMU sources can be replaced by the random walk model to

insert more information in tracking algorithms, whenever available.
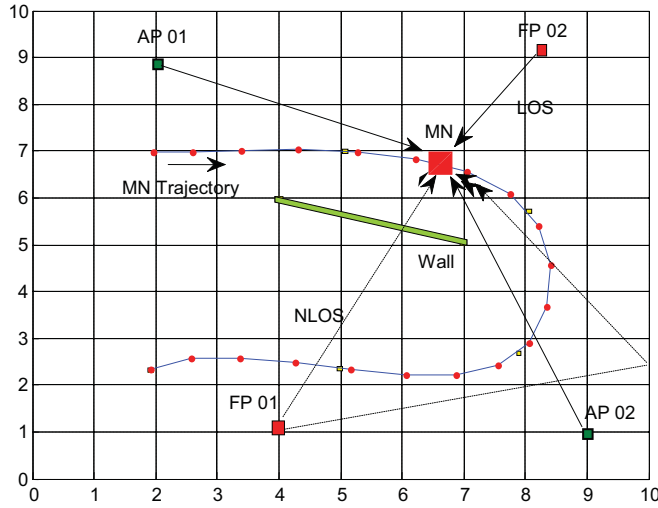


*Figure 0-19 MN tracking in mixed LOS/NLOS conditions*

Let $N_{AP}$ denote the number of all APs whose locations, represented by

$\left\{ m_{i,x}, m_{i,y} \right\}, i = 1 : N_{AP}$, are precisely known to the MN, and $N_{FP}$ denote the number of FPs

whose locations $\left\{ m_{i,x}, m_{i,y} \right\}, i = N_{AP} + 1 : N_{FP} + N_{AP}$ are unknown to the MN. The range

measurements obtained from opportunistic signal reception from ANs can be subject to range

offset error due to non-synchronization, multipath, and NLOS/LOS effects.

In this research, the SLAM-based opportunistic localization problem is investigated in

four system models. In the first case, it is assumed that the MN receives a synchronized signal

from a synchronized network of ANs. In addition, ANs provide LOS measurements, or if not,

ANs sight conditions are known to the MN, and NLOS measurements are discarded from the measurement data set.

The pseudo range measurement, obtained at the $t$ th time instant from the $i$ th AN, is explicitly presented by

$$z_{i,t} = |\mathbf{p}_t - \mathbf{m}_i| + w_{i,t}$$

**0-67**

$$= \sqrt{\left(m_{i,x} - x_t\right)^2 + \left(m_{i,y} - y_t\right)^2} + w_{i,t}, \ i = 1, 2, ..., N_{AN}$$

where $\mathbf{p}_t = [x_t, y_t]^T$ is the MN location vector at time step $t$, and $\mathbf{m}_i = \left[m_{i,x}, m_{i,y}\right]^T$ is the $i$-th AN location vector. $w_{i,t}$ is an additive white Gaussian noise with a mean power $E\left\{w_{i,t}^2\right\} = \sigma_{z,i}^2$.

In this case, the state vector is denoted by $\mathbf{q}_t = \begin{bmatrix} \mathbf{p}_t & \mathbf{m}_{fp} \end{bmatrix}^T$, where

$$\mathbf{m}_{fp} = \begin{bmatrix} m_{N_{AP+1},x} & m_{N_{AP+1},y} & \cdots & m_{N_{AN},x} & m_{N_{AN},y} \end{bmatrix}^T$$ is the stacked vector of the FP locations. Since the ANs are stationary, the transition PDF from the MN position- ANs position state

$\mathbf{q}_{t-1} = \begin{bmatrix} \mathbf{p}_{t-1} & \mathbf{m}_{fp} \end{bmatrix}^T$ to the next one $\mathbf{q}_t = \begin{bmatrix} \mathbf{p}_t & \mathbf{m}_{fp} \end{bmatrix}^T$ is defined only by the MN motion update,

$$p(\mathbf{q}_t \mid \mathbf{q}_{t-1}) = p(\mathbf{p}_t \mid \mathbf{p}_{t-1}).$$

The second system model assumes that synchronized ANs are in the MN's line of sight but are not synchronized with the MN. The range measurement obtained at the $t$-th time step, from the $i$-th AN, is explicitly presented by the pseudo-range biased due to the random MN-AN clock offset as

$$\mathbf{z}_{i,t} = \sqrt{\left(m_{i,x} - x_t\right)^2 + \left(m_{i,y} - y_t\right)^2} + b_t + w_{i,t}$$

**0-68**

$$i = 1, 2, ..., N_{AN}$$

where $b_t$ is the random range offset which takes into account both the deterministic clock time offset between the ANs and MN and random MN receiver clock instability properties. The random range offset is modeled by an independent random walk from the MN motion process as $p(b_t \mid b_{t-1}) \ \square \ N(0, \sigma_b^2)$ where $\sigma_b^2$ is commensurate with Allen variance of the MN clock. In this

case, the state vector is defined by $\mathbf{q}_t = \begin{bmatrix} \mathbf{p}_t & b_t & \mathbf{m}_{fp} \end{bmatrix}^T$. If the ANs are not synchronized, the

bias variable for each AN will be different and the state vector is modified by

$\mathbf{q}_t = \begin{bmatrix} \mathbf{p}_t & \mathbf{b}_t & \mathbf{m}_{fp} \end{bmatrix}^T$, where $\mathbf{b}_t = \begin{bmatrix} b_{1,t} & \cdots & b_{N_{AN},t} \end{bmatrix}^T$ is the vector of ANs range offsets; this will

be studied as the third system model, given by

$$\mathbf{z}_{i,t} = \sqrt{\left(m_{i,x} - x_t\right)^2 + \left(m_{i,y} - y_t\right)^2} + b_{i,t} + w_{i,t} \qquad \textbf{0-69}$$
$$i = 1, 2, ..., N_{AN}$$

The clock drift process of each AN evolves independently from the clock drift processes

of other ANs, so the transition PDF of range offset variables is given by $p(\mathbf{b}_t \mid \mathbf{b}_{t-1}) \square \, N(0, Q_b)$,

where $Q_b = diag \left\{ \sigma_{b_1}^2 \quad \sigma_{b_2}^2 \quad \cdots \quad \sigma_{b_{N_{AN}}}^2 \right\}$

The fourth system model considers a general multipath scenario where the

measurement is also affected by non-stationary channel behavior. Multipath and LOS blockage

are the most penalizing error sources in wireless localization. It can be classically modeled by a

white noise in the signal bandwidth. NLOS measurements are detected as an abrupt change in

mean and/or variance of a Gaussian noise [xlviii]. However, if the NLOS condition is left

undetected, it substantially degrades localization accuracy. One approach to deal with the

NLOS conditions is to introduce a noise model for LOS propagation and a noise model for

NLOS propagation, where the transition between the LOS and NLOS mode is modeled with a

Markov chain. In this case, the state vector is characterized by the MN position, FP locations,

range offset vector, and ANs' sight conditions $\mathbf{s}_t = \begin{bmatrix} s_{1,t} & \cdots & s_{N_{AN},t} \end{bmatrix}^T$, given by

$$\mathbf{q}_t = \begin{bmatrix} \mathbf{p}_t & \mathbf{b}_t & \mathbf{s}_t & \mathbf{m} \end{bmatrix}^T \qquad \textbf{0-70}$$

where each AN sight condition, $s_{i,t}$, is modeled by a binary Markov Chain, with the value $s_{i,t} = 0$

is assigned to the LOS event, and $s_{i,t} = 1$ is assigned to the NLOS event. As earlier discussed,

in mixed NLOS/LOS conditions, the suggested range measurement model is characterized by

introducing sight state-dependent measurement noise distributions for fourth system model, given by

$$\mathbf{z}_{i,t} = \sqrt{\left(m_{i,x} - x_t\right)^2 + \left(m_{i,y} - y_t\right)^2} + b_{i,t} + w_{i,t}$$
$$i = 1, 2, ..., N_{AN}$$

**0-71**

where

$$w_{i,t} \sim \begin{cases} N(0, \sigma_{i,lo\,s}^2) & if \ s_{i,t} = 0 \\ N(\mu_{i,nlos}, \sigma_{i,nlos}^2) & if \ s_{i,t} = 1 \end{cases}$$

**0-72**

Under LOS condition, the measurement is only corrupted by additive receiver noise, which is described by a zero-mean Gaussian distribution with a variance of $\sigma_{i,los}^2$. The NLOS excess delay is modeled by the abrupt jump in the mean and variance of measurement noise, where $\sigma_{i,nlos}^2 > \sigma_{i,los}^2$ and $\mu_{i,nlos} > 0$ [xlix], [l], [li]. We assume that the $\mu_{i,nlos}$, $\sigma_{i,nlos}^2$, and $\sigma_{i,los}^2$ are known from prior information about the room size and the calibration stage.

The $N_{AN}$ Markov chains are combined into a single, augmented Markov chain, denoted by $\mathbf{s}_t$ which have $2^{N_{AN}}$ possible states. As long as the range measurements are collected from ANs at different locations, the LOS/NLOS transition can be assumed to be independent. Therefore, the transition probability matrix $\prod$ of the augmented Markov chain can be expressed in terms of the transition probability matrices of $\prod_i, i = 1, ..., N_{AN}$ of each AN, according to $\prod = \prod_1 \otimes \prod_2 \otimes ... \otimes \prod_{N_{AN}}$, where $\otimes$ denotes the Kronecker product. The description of four proposed system models is summarized in Table 0-1.

*Table 0-1 System models' description*

| System Model scenario | ANs location | MN clock instability | ANs synchronization | NLOS conditions |
|---|---|---|---|---|
| 1 | Unknown<br><br>Solution: ANs unknown locations are treated as FP's of unknown location. | The MN are synchronized with ANs | ANs are synchronized | Sight conditions are known and NLOS measurements are discarded |
| 2 | Unknown | The MN are not synchronized with ANs | ANs are synchronized | Sight conditions are known and NLOS measurements |

| | | | |
|---|---|---|---|---|
| | Solution: similar to the system model 1 | Solution: MN clock instability is treated as random first-order Markov process. | | are discarded |
| **3** | Unknown | The MN are not synchronized with ANs | ANs are not synchronized | Sight conditions are known and NLOS measurements are discarded |
| | Solution: similar to the system model 1 | Solution For every MN-AN link, the clock drift is treated as a random first-order Markov process | | |
| **4** | Unknown | The MN are not synchronized with ANs | ANs are not synchronized | Sight conditions are unknown |
| | Solution: similar to the system model 1 | Solution: similar to the system model 3 | | Solution: Sight conditions are modeled by Boolean switch. |

## Fisher information for a SLAM-based OWLS

A direct approach to quantify the potential accuracy of a trajectory estimation based on the observed data samples is formulated by the Fisher information matrix. However, as stated earlier, the quantifiable information is only valid where the problem is linear and jointly Gaussian or at least nonlinearity is mild and the measurement and state update noise are approximately Gaussian. FI determines a fundamental limit for localization accuracy by using information inequality through the CRLB theorem. This information bound predicts the best achievable performance even before the OWLS is built, so that it can be utilized as a system design tool.

For the SLAM-based OWLS, where $\mathbf{q}_{0:t}$ represents the history of unknown system state vector, the BCRLB as a lower bound on the MSE matrix of any unbiased estimator $\hat{\mathbf{q}}_{0:t}(\mathbf{z}_{1:t})$ is obtained by substituting $\mathbf{q}_{0:t}$ by $\mathbf{q}$ and $\mathbf{z}_{1:t}$ by $\mathbf{z}$ in Eq. (0-35)-(0-38), yielding

$$E\left\{\left(\hat{\mathbf{q}}_{0:t} - \mathbf{q}_{0:t}\right)\left(\hat{\mathbf{q}}_{0:t} - \mathbf{q}_{0:t}\right)^{T}\right\} \geq J_{to}^{-1}(\mathbf{q}_{0:t})$$

*0-73*

where $J_{tot}(\mathbf{q}_{0:t})$ denotes the BFIM in regards with history of state vector. $J_{tot}(\mathbf{q}_{0:t})$ is quantifiable information associated with full SLAM processing; however, in OWLS, the current system state $\mathbf{q}_{t}$ is of particular interest. It can be easily proved [lii] that BCRLB for $\mathbf{q}_{t}$ is given by the $K \times K$

lower right submatrix of $J_{tot}^{-1}(\mathbf{q}_{0:t})$, where $K = \dim(\mathbf{q}_t)$. Let decompose $\mathbf{q}_t$ as $[\mathbf{q}_{0:t-1}{}^T, \mathbf{q}_t{}^T]^T$,

$J_{tot}(\mathbf{q}_{0:t})$ can be written by

$$J_{tot}(\mathbf{q}_{0:t}) = \begin{bmatrix} A_t & B_t \\ B_t^T & C_t \end{bmatrix} \qquad \textbf{0-74}$$

$$\square \begin{bmatrix} E\{-\Delta_{\mathbf{q}_{0:t-1}}^{\mathbf{q}_{0:t-1}} \ln p_{\mathbf{z},\mathbf{q}}(\mathbf{z}_{1:t},\mathbf{q}_{0:t})\} & E\{-\Delta_{\mathbf{q}_{0:t-1}}^{\mathbf{q}_t} \ln p_{\mathbf{z},\mathbf{q}}(\mathbf{z}_{1:t},\mathbf{q}_{0:t})\} \\ E\{-\Delta_{\mathbf{q}_t}^{\mathbf{q}_{0:t-1}} \ln p_{\mathbf{z},\mathbf{q}}(\mathbf{z}_{1:t},\mathbf{q}_{0:t})\} & E\{-\Delta_{\mathbf{q}_t}^{\mathbf{q}_t} \ln p_{\mathbf{z},\mathbf{q}}(\mathbf{z}_{1:t},\mathbf{q}_{0:t})\} \end{bmatrix}$$

where $\Delta_\alpha^\beta$ is the operator of the second order derivative and is also defined versus the first-order gradient as $\Delta_\alpha^\beta = \nabla_\alpha \nabla_\beta{}^T$. Given Eq. (0-73) decomposition, the Fisher information matrix regarding the current state $\mathbf{q}_t$, $J_{tot}(\mathbf{q}_t)$, is obtained by

$$J_{tot}(\mathbf{q}_t) = C_t - B_t^T A_t^{-1} B_t \qquad \textbf{0-75}$$

Generally, there are two types of algorithms that calculate the Fisher information for online processing. The first type avoids inversion of the large matrix of $J_{tot}(\mathbf{q}_{0:t})$ and calculates the $J_{tot}(\mathbf{q}_t)$ recursively based on Eq. (0-93) [xii], [lii] as

$$J_{tot}(\mathbf{q}_k) \square D_k^{22} - D_k^{21}(D_k^{11} + J_{tot}(\mathbf{q}_{k-1}))^{-1} D_k^{12} \qquad \textbf{0-76}$$

where

$$
\begin{aligned}
& J_{tot}(\mathbf{q}_k) \square D_k^{22} - D_k^{21}(D_k^{11} + J_{tot}(\mathbf{q}_{k-1}))^{-1} D_k^{12} && \textbf{0-77} \\
& D_k^{22} = E\{-\Delta_{\mathbf{q}_k}^{\mathbf{q}_k} \ln p(\mathbf{q}_{k+1} | \mathbf{q}_k)\} \\
& D_k^{12} = E\{-\Delta_{\mathbf{q}_k}^{\mathbf{q}_{k+1}} \ln p(\mathbf{q}_{k+1} | \mathbf{q}_k)\} \\
& D_k^{21} = E\{-\Delta_{\mathbf{q}_{k+1}}^{\mathbf{q}_k} \ln p(\mathbf{q}_{k+1} | \mathbf{q}_k)\} = [D_k^{12}]^T \\
& D_k^{22} = E\{-\Delta_{\mathbf{q}_{k+1}}^{\mathbf{q}_{k+1}} \ln p(\mathbf{q}_{k+1} | \mathbf{q}_k)\} + E\{-\Delta_{\mathbf{q}_{k+1}}^{\mathbf{q}_{k+1}} \ln p(\mathbf{z}_{k+1} | \mathbf{q}_{k+1})\}
\end{aligned}
$$

For a LJG case, the recursion for $J_{tot}(\mathbf{q}_t)$ is identical to inverse of the posterior PDF covariance matrix calculated from the Kalman filter. However, in a nonlinear SLAM problem, due to correlation between state vector estimates, as earlier discussed, the recursive methods partially discard the correlated information between the current state and older states.

The second types of methods focus on calculating full SLAM BFIM $J_{tot}(\mathbf{q}_{0:t})$ numerically [lv] or based on reasonable approximations [liv]. For the problem at hand, we utilized the second approach since the inversion of $J_{tot}(\mathbf{q}_{0:t})$ is not an issue for the dimension of the simulated problem; otherwise the recursive methods need to be used. Except the forth system model which is described by a hybrid discrete and continuous state space and must be treated differently, the proposed system models for the SLAM-based OWLS can be described by a linear model for state update and a nonlinear model for the measurement function, yielding

$$\mathbf{q}_t = \mathbf{q}_{t-1} + F^T \mathbf{v}_{d,t} \qquad \qquad \text{0-78}$$
$$z_{i,t} = h_i(\mathbf{q}_t) + w_{i,t} \ , \ \ i = 1, 2, ..., N_{AN}$$

where

$$\text{0-79}$$

$$F = \begin{bmatrix} 1 & 0 & \cdots & 0 & 0 & \cdots & 0 \\ 0 & 1 & \ddots & \vdots & 0 & \dots & 0 \\ \vdots & \ddots & \ddots & 0 & \vdots & \cdots & \vdots \\ 0 & \dots & 0 & 1 & 0 & \dots & 0 \end{bmatrix}$$
$$\underbrace{\phantom{1 \ 0 \ \cdots \ 0}}_{L_d} \underbrace{\phantom{0 \ \cdots \ 0}}_{L_s}$$

$L_d$ and $L_s$ denote the dimension of dynamic variables and stationary variables of state vector, respectively. The noise vectors are mutually independent white process distributed as $\mathbf{v}_{d,t} \sim N(0, Q_d)$ and $w_{i,t} \sim N(0, \sigma_{i,z}^2)$. $Q_d$ is a nonsingular covariance matrix of joint dynamic variables process where for the system model 1, $Q_d = Q_p$; for the system model 2, $Q_d = diag\{Q_p, \sigma_b^2\}$ and for the system model 3 and 4, $Q_d = diag\{Q_p, Q_b\}$. It is assumed that the MN clock instability process evolves independently from the MN motion process. From Eq. (0-91), the BFIM $J_{tot}(\mathbf{q}_{0:t})$ for a SLAM-based OWLS is given by

$$\text{0-80}$$

$$J_{to}(\mathbf{q}_{0tt}) = E\left\{-\Delta_{\mathbf{q}_{0:t}}^{\mathbf{q}_{0:t}} \ln p_{\mathbf{z},\mathbf{q}}(\mathbf{z}_{1:t}, \mathbf{q}_{0:t})\right\}$$

According to Eq. (0-35)-(0-38), the total BFIM is decomposed using Bayes' rule, stated as

$$J_{tot}(\mathbf{q}_{0:t}) = J_Z(\mathbf{q}_{0:t}) + J_P(\mathbf{q}_{0:t})$$

where $J_Z(\mathbf{q}_{0:t})$ denotes the BFIM of measurement data, defined as

$$J_Z(\mathbf{q}_{0:t}) = E_{\mathbf{z}_{1:t},\mathbf{q}_{0:t}} \left\{ -\Delta_{\mathbf{q}_{0:t}}^{\mathbf{q}_{0:t}} \ln p_{\mathbf{z}|\mathbf{q}}(\mathbf{z}_{1:t} \mid \mathbf{q}_{0:t}) \right\}$$

and where $J_P(\mathbf{q}_{0:t})$ denotes the BFIM of prior data, defined as

$$J_P(\mathbf{q}_{0:t}) = E_{\mathbf{q}_{0:t}} \left\{ -\Delta_{\mathbf{q}_{0:t}}^{\mathbf{q}_{0:t}} \ln p_{\mathbf{q}}(\mathbf{q}_{0:t}) \right\}$$

The evaluation of BFIM of the measurement data involved the computation of expectation, which is difficult to express analytically for the nonlinear model given in Eq. (0-77) unless some reasonable approximations can be assumed. We utilize first-order Taylor expansion to construct a linear approximation of $h_i(.)$ around $\hat{\mathbf{q}}_t$ which is the most likely system state deemed at the time of linearization:

$$h_i(\mathbf{q}_t) \approx h_i(\hat{\mathbf{q}}_t) + H_{i,t}(\mathbf{q}_t - \hat{\mathbf{q}}_t)$$

with $H_{i,t} = \dfrac{\partial h_i(\mathbf{q}_t)}{\partial \mathbf{q}_t}$, the gradient of $h_i(.)$. Therefore, the Gaussian approximation of the liberalized measurement process is given by

$$p_{\mathbf{z}|\mathbf{q}}(\mathbf{z}_t \mid \mathbf{q}_t) = \frac{1}{\sqrt{2\pi\sigma_{i,z}^2}} \exp\left\{ -\frac{1}{2} \frac{\left( z_{i,t} - h_i(\hat{\mathbf{q}}_t) - H_{i,t}(\mathbf{q}_t - \hat{\mathbf{q}}_t) \right)^2}{\sigma_{i,z}^2} \right\}$$

Using the linearized measurement model approximation, the BFIM from measurement data can be expressed by

$$J_Z(\mathbf{q}_{0:t}) = \sum_{k=1}^{t} E\left\{-\Delta_{\mathbf{q}_{0:k}}^{\mathbf{q}_{0:k}} \ln p(\mathbf{z}_k | \mathbf{q}_k)\right\}$$

$$= \sum_{k=1}^{t} E\left\{-\delta_{k+1}^{k+1,k+1} \otimes \Delta_{\mathbf{q}_{d,k}}^{\mathbf{q}_{d,k}} \ln p(\mathbf{z}_k | \mathbf{q}_k)\right\}$$

$$= \sum_{k=1}^{t} E\left\{-\delta_{k+1}^{k+1,k+1} \otimes J_Z(\mathbf{q}_k)\right\}$$

where $\delta_{k+1}^{i,j}$ denotes a $(k+1) \times (k+1)$ dimensional matrix whose elements are all zero except at the $i$-th row and the $j$-th column which is one, and $J_Z(\mathbf{q}_k)$ denotes the BFIM portion from the measurement data at the $k$-th time step. It must be noted that the FPs are stationary, so unlike dynamic state variables such as MN location variables, there is no need to define a new state vector portion regarding to FP location variables at each time step. To unify the information regarding FP location variables from all time steps, the state vector variables are divided in two dynamic and stationary portions as $\mathbf{q}_k = \begin{bmatrix} \mathbf{q}_{d,k}, \mathbf{q}_s \end{bmatrix}^T$ and the history of state vectors is re-sorted as $\mathbf{q}_{0:k} = \begin{bmatrix} \mathbf{q}_{d,0:k}, \mathbf{q}_s \end{bmatrix}^T$. In this regard, the BFIM for mixed stationary and dynamic states from measurement data is modified by

$$J_Z(\mathbf{q}_{0:t}) = \sum_{k=1}^{t} E\left\{-\Delta_{\mathbf{q}_{0:k}}^{\mathbf{q}_{0:k}} \ln p(\mathbf{z}_k | \mathbf{q}_k)\right\}$$

$$= \sum_{k=1}^{t} E\left\{-\delta_{t+2}^{k+1,k+1} \otimes \Delta_{\mathbf{q}_{d,k}}^{\mathbf{q}_{d,k}} \ln p(\mathbf{z}_k | \mathbf{q}_k)\right\}$$

$$+ E\left\{-\delta_{t+2}^{k+1,t+2} \otimes \Delta_{\mathbf{q}_{d,k}}^{\mathbf{q}_s} \ln p(\mathbf{z}_k | \mathbf{q}_k)\right\}$$

$$+ E\left\{-\delta_{t+2}^{t+2,k+1} \otimes \Delta_{\mathbf{q}_s}^{\mathbf{q}_{d,k}} \ln p(\mathbf{z}_k | \mathbf{q}_k)\right\}$$

$$+ E\left\{-\delta_{t+2}^{t+2,t+2} \otimes \Delta_{\mathbf{q}_s}^{\mathbf{q}_s} \ln p(\mathbf{z}_k | \mathbf{q}_k)\right\}$$

To calculate the prior information, we need to consider the update model of dynamic state variables as well as initial conditions. Since the FPs are assumed to be stationary, the update information is only applied for dynamic variables. The initial conditions are divided into two portions: the stationary portion which is later added to the measurement information to calculate the total information, and the dynamic portion which is combined with the update

information. According to the LJG model of the state update process, and assuming that initial state $\mathbf{q}_0$ is Gaussian distributed as $\mathbf{q}_0 \sim N(0, Q_0)$ which is composed of initial condition for dynamic variables, $\mathbf{q}_{0,d} \sim N(0, Q_{d,0})$, and stationary variables, $\mathbf{q}_{0,s} \sim N(0, Q_{s,0})$, the prior information about dynamic states $\mathbf{q}_{d,0}$ and $\mathbf{q}_{d,1}$ with the update state model

$\mathbf{q}_{d,1} - \mathbf{q}_{d,0} \sim N(\mathbf{0}, Q_d)$ is given by

$$J_P(\mathbf{q}_{d,0:1}) = Q_u(\mathbf{q}_{d,0:1})^{-1} \qquad\qquad \textbf{0-88}$$

$$Q_u(\mathbf{q}_{d,0:1}) = \left[ \begin{bmatrix} Q_{d,0}^{-1} & \mathbf{0} \\ \mathbf{0} & \mathbf{0} \end{bmatrix} + J_d \right]^{-1}$$

where

$$J_d = \begin{bmatrix} Q_d^{-1} & -Q_d^{-1} \\ -Q_d^{-1} & Q_d^{-1} \end{bmatrix} \qquad\qquad \textbf{0-89}$$

The prior information of the state vector after two time steps, $\mathbf{q}_{0:1} = \left[ \mathbf{q}_{d,0:1}, \mathbf{q}_s \right]^T$, is calculated by inserting initial information from stationary states as follows

$$J_P(\mathbf{q}_{0:1}) = Q^{-1} \qquad\qquad \textbf{0-90}$$

$$Q = \begin{bmatrix} Q_u(\mathbf{q}_{d,0:1}) & \mathbf{0} \\ \mathbf{0} & Q_{s,0} \end{bmatrix}$$

Generalizing Eq. (0-104)- Eq. (0-106), for $t$ time steps, the BFIM from prior data, $J_P(\mathbf{q}_{0:t})$ can analytically be computed by

$$J_P(\mathbf{q}_{0:t}) = E_{\mathbf{q}_{d,0:k}} \left\{ -\Delta_{\mathbf{q}_{0:k}}^{\mathbf{q}_{0:k}} \ln p(\mathbf{q}_0) \right\} \qquad\qquad \textbf{0-91}$$

$$+ \sum_{k=1}^{t} E_{\mathbf{q}_{0:k}} \left\{ -\Delta_{\mathbf{q}_{0:k}}^{\mathbf{q}_{0:k}} \ln p(\mathbf{q}_k \mid \mathbf{q}_{k-1}) \right\}$$

$$= \delta_{t+2}^{1,1} \otimes Q_{d,0}^{-1} + \delta_{t+2}^{t+2,t+2} \otimes Q_{s,0}^{-1} + \sum_{k=1}^{t} \delta_{t+2}^{k,k} \otimes Q_d^{-1}$$

$$- \delta_{t+2}^{k,k+1} \otimes Q_d^{-1} - \delta_{t+2}^{k+1,k} \otimes Q_d^{-1} + \delta_{t+2}^{k+1,k+1} \otimes Q_d^{-1}$$

The BFIM elements for each proposed model are different as the proposed system models vary in terms of state variables and measurement and state update models. In this

regard, the following subsections explain the calculation of BFIM elements for all four proposed models in more detail. The BFIM calculation is described in particular for the fourth system model as its state space includes both discrete and continuous variables.

## MODEL 1: SYNCHRONIZED ANS, MN SYNCHRONIZED WITH ANS, KNOWN SIGHT CONDITIONS

Given $z_{i,k} \square N\left(h_i\left(\mathbf{q}_k\right), \sigma_{i,z}^2\right)$, the Fisher information obtained from a single measurement from the $i$-th AN is obtained by

$$J_{Z,i}\left(\mathbf{q}_k\right) = \sigma_{z,i}^{-2} \frac{\partial h_i\left(\mathbf{q}_k\right)^T}{\partial \mathbf{q}_k} \frac{\partial h_i\left(\mathbf{q}_k\right)}{\partial \mathbf{q}_k} \tag{0-92}$$

where $h_i\left(\mathbf{q}_k\right) = \sqrt{\left(m_{i,x} - x_k\right)^2 + \left(m_{i,y} - y_k\right)^2}$, as described in Eq. (0-66). The gradient of measurement/likelihood PDF is calculated by

$$\frac{\partial h_i\left(\mathbf{q}_k\right)}{\partial \mathbf{q}_k} = \left[ -\frac{\left(m_{i,x} - x_k\right)}{r_{i,k}} \quad -\frac{\left(m_{i,y} - y_k\right)}{r_{i,k}} \quad \mathbf{0}_{1 \times 2N_{FP}} \right] \tag{0-93}$$

$$for \ i = 1, 2, ... N_{AP}$$

and

$$\frac{\partial h_i\left(\mathbf{q}_k\right)}{\partial \mathbf{q}_k} = \tag{0-94}$$

$$\left[ -\frac{\left(m_{i,x} - x_k\right)}{r_{i,k}} \quad -\frac{\left(m_{i,y} - y_k\right)}{r_{i,k}} \quad \left[ \frac{\left(m_{i,x} - x_k\right)}{r_{i,k}} e_{1 \times 2N_{FP}}^{2(i-N_{AP})-1} + \frac{\left(m_{i,y} - y_k\right)}{r_{i,k}} e_{1 \times 2N_{FP}}^{2(i-N_{AP})} \right] \right]$$

$$for \ i = N_{AP}+1, N_{AP}+2, ..., N_{AP}+N_{FP}$$

where $r_{i,k} = \sqrt{\left(m_{i,x} - x_k\right)^2 + \left(m_{i,y} - y_k\right)^2}$ and $e_{1 \times m}^i$ is the $1 \times m$ row vector whose elements are zero, except the $i$-th element which is equal to one. Then, the measurement Fisher information matrix from a single measurement available at time step $t$ from the $i$-th AN is calculated by

$$J_{Z,i}(\mathbf{q}_k) = \sigma_{z,i}^{-2}
\begin{bmatrix}
\dfrac{(m_{i,x}-x_k)^2}{r_{i,k}^2} & \dfrac{(m_{i,x}-x_k)(m_{i,y}-y_k)}{r_{i,k}^2} & \mathbf{0}_{1\times 2N_{FP}} \\[3mm]
\dfrac{(m_{i,x}-x_k)(m_{i,y}-y_k)}{r_{i,k}^2} & \dfrac{(m_{i,y}-y_k)^2}{r_{i,k}^2} & \mathbf{0}_{1\times 2N_{FP}} \\[3mm]
\mathbf{0}_{2N_{FP}\times 1} & \mathbf{0}_{2N_{FP}\times 1} & \mathbf{0}_{2N_{FP}\times 2N_{FP}}
\end{bmatrix}$$

$$\text{0-95}$$

$$\text{for } i = 1,2,...N_{AP}$$

and

$$J_{Z,i}(\mathbf{q}_k) = \sigma_{z,i}^{-2}
\begin{bmatrix}
\dfrac{(m_{i,x}-x_k)^2}{r_{i,k}^2} & \dfrac{(m_{i,x}-x_k)(m_{i,y}-y_k)}{r_{i,k}^2} & A \\[3mm]
\dfrac{(m_{i,x}-x_k)(m_{i,y}-y_k)}{r_{i,k}^2} & \dfrac{(m_{i,y}-y_k)^2}{r_{i,k}^2} & B \\[3mm]
A^T & B^T & D
\end{bmatrix}$$

$$\text{0-96}$$

$$\text{for } i = N_{AP}+1, N_{AP}+2,..., N_{AP}+N_{FP}$$

where

$$\text{0-97}$$

$$A = [-\dfrac{(m_{i,x}-x_k)^2}{r_{i,k}^2} e_{1\times 2N_{FP}}^{2(i-N_{AP})-1} - \dfrac{(m_{i,y}-y_k)(m_{i,x}-x_k)}{r_{i,k}^2} e_{1\times 2N_{FP}}^{2(i-N_{AP})}]$$

$$B = [-\dfrac{(m_{i,x}-x_k)(m_{i,y}-y_k)}{r_{i,k}^2} e_{1\times 2N_{FP}}^{2(i-N_{AP})-1} - \dfrac{(m_{i,y}-y_k)^2}{r_{i,k}^2} e_{1\times 2N_{FP}}^{2(i-N_{AP})}]$$

$$C = [\dfrac{(m_{i,x}-x_k)}{r_{i,k}} e_{N_{AN}\times 2N_{FP}}^{i,2(i-N_{AP})-1} + \dfrac{(m_{i,y}-y_k)}{r_{i,k}} e_{N_{AN}\times 2N_{FP}}^{i,2(i-N_{AP})}]$$

$$D = [\dfrac{(m_{i,x}-x_k)^2}{r_{i,k}^2} e_{2N_{FP}\times 2N_{FP}}^{2(i-N_{AP})-1,2(i-N_{AP})-1} + \dfrac{(m_{i,x}-x_k)(m_{i,y}-y_k)}{r_{i,k}^2} e_{2N_{FP}\times 2N_{FP}}^{2(i-N_{AP})-1,2(i-N_{AP})}$$

$$+ \dfrac{(m_{i,x}-x_k)(m_{i,y}-y_k)}{r_{i,k}^2} e_{2N_{FP}\times 2N_{FP}}^{2(i-N_{AP}),2(i-N_{AP})-1} + \dfrac{(m_{i,y}-y_k)^2}{r_{i,k}^2} e_{2N_{FP}\times 2N_{FP}}^{2(i-N_{AP}),2(i-N_{AP})}]$$

The measurements from different ANs are assumed to be independent. This is

reasonable as the measurement noise comes from two sources which are the receiver noise

and the multipath. The propagation paths from the ANs to the MN are statistically independent

provided that the ANs are sufficiently separated spatially (which may be violated in the MIMO

cases), and there is no tunneling propagation or keyhole effect at the receiver. However, in

some cases, the multipath occurs close to the MN receiver; hence, if two ANs are at similar bearings relative to the MN, then the multipath will be correlated. However, this correlation is not considered in the current analysis. Based on the assumption that the noise in the receiver is uncorrelated as the synchronization signals from the ANs have different spreading codes; hence, the noise subspaces are orthogonal. Consequently, the BFIMs from additional statistically-independent AN signals can simply be added as

$$J_Z(\mathbf{q}_k) = \sum_{i=1}^{N_{AN}} J_{Z,i}(\mathbf{q}_k) = \sum_{i=1}^{N_{AN}} \sigma_{z,i}^2 \frac{\partial h_i(\mathbf{q}_k)^T}{\partial \mathbf{q}_k} \frac{\partial h_i(\mathbf{q}_k)}{\partial \mathbf{q}_k}$$

<div align="right">0-98</div>

To comply with the re-sorted state history vector, $\mathbf{q}_{0:t} = \begin{bmatrix} \mathbf{q}_{d,0:t} & \mathbf{q}_s \end{bmatrix}^T$, the elements of

Eq. (0-102) is described as $\Delta_{\mathbf{q}_{d,k}}^{\mathbf{q}_{d,k}} \ln p(\mathbf{z}_k \mid \mathbf{q}_k)$ is the upper left $L_d \times L_d$ submatrix of $J_Z(\mathbf{q}_k)$,

$\Delta_{\mathbf{q}_{d,k}}^{\mathbf{q}_s} \ln p(\mathbf{z}_k \mid \mathbf{q}_k)$ is the the upper right $L_d \times L_s$ submatrix of $J_Z(\mathbf{q}_k)$, $\Delta_{\mathbf{q}_s}^{\mathbf{q}_{d,k}} \ln p(\mathbf{z}_k \mid \mathbf{q}_k)$ is the

lower left $L_s \times L_d$ submatrix of $J_Z(\mathbf{q}_k)$, and $\Delta_{\mathbf{q}_s}^{\mathbf{q}_s} \ln p(\mathbf{z}_k \mid \mathbf{q}_k)$ is the lower left $L_s \times L_s$ submatrix

of $J_Z(\mathbf{q}_k)$.

To calculate the BFIM from prior information, as shown in Eq. (0-107), $Q_0$ and $Q_d$ must be defined based on the state space and the state update process for each system model. In the system model 1, the vector of dynamic states $\mathbf{q}_{d,k}$ is only described by MN location variables as $\mathbf{q}_{d,k} = \begin{bmatrix} x_k & y_k \end{bmatrix}^T$ with the dimension $L_d = \dim(\mathbf{q}_{d,t}) = 2$. Subsequently, the update process for dynamic states $\mathbf{q}_{d,0}$ and $\mathbf{q}_{d,1}$ is described by $\mathbf{q}_{d,1} - \mathbf{q}_{d,0} \square N(\mathbf{0}_{2\times1}, Q_P)$, and the prior PDF at the initial point is defined by

<div align="right">0-99</div>

$$\mathbf{q}_0 \square N(0, Q_0)$$

where $Q_0 = diag\left\{ \sigma_{x,0}^2 \quad \sigma_{y,0}^2 \quad \sigma_{mx_1,0}^2 \quad \sigma_{my_1,0}^2 \quad \cdots \quad \sigma_{mx_{N_{FP}},0}^2 \quad \sigma_{my_{N_{FP}},0}^2 \right\}$. $Q_0$ is decomposed into the stationary and dynamic portions as

$$Q_{d,0} = diag\left\{\sigma_{x,0}^2 \quad \sigma_{y,0}^2\right\}$$

<div align="right">**0-100**</div>

$$Q_{s,0} = diag\left\{\sigma_{mx_1,0}^2 \quad \sigma_{my_1,0}^2 \quad \cdots \quad \sigma_{mx_{N_{FP}},0}^2 \quad \sigma_{my_{N_{FP}},0}^2\right\}$$

## MODEL 2: SYNCHRONIZED ANS, MN NOT SYNCHRONIZED WITH ANS, KNOWN SIGHT CONDITIONS

For this system model, the Fisher information from the measurement of $i$-th AN is calculated as

<div align="right">**0-101**</div>

$$\frac{\partial h_i(\mathbf{q}_k)}{\partial \mathbf{q}_k} = \left[ -\frac{(m_{i,x} - x_k)}{r_{i,k}} \quad -\frac{(m_{i,y} - y_k)}{r_{i,k}} \quad 1 \quad \mathbf{0}_{1\times 2N_{FP}} \right]$$

$$for \ i = 1, 2, ... N_{AP}$$

and

<div align="right">**0-102**</div>

$$\frac{\partial h_i(\mathbf{q}_k)}{\partial \mathbf{q}_k} =$$

$$\left[ -\frac{(m_{i,x} - x_k)}{r_{i,k}} \quad -\frac{(m_{i,y} - y_k)}{r_{i,k}} \quad 1 \quad \left[\frac{(m_{i,x} - x_k)}{r_{i,k}} e_{1\times 2N_{FP}}^{2(i-N_{AP})-1} + \frac{(m_{i,y} - y_k)}{r_{i,k}} e_{1\times 2N_{FP}}^{2(i-N_{AP})}\right] \right]$$

$$for \ i = N_{AP}+1, N_{AP}+2, ..., N_{AP}+N_{FP}$$

where $h_i(\mathbf{q}_k) = \sqrt{(m_{i,x} - x_k)^2 + (m_{i,y} - y_k)^2} + b_k$ .

Similarly, the measurement BFIM from all MN-AN links is calculated by the sum of the FIM from each MN-AN link as stated in Eq. (0-97). It must be noted the elements of FIM from measurement data for re-sorted state history in Eq. (0-85) are obtained in a similar way to the procedure explained for the system model 1.

To calculate prior information, the initial information must be modified by adding the initial condition of the range offset, given by

<div align="right">**0-103**</div>

$$\mathbf{q}_0 \square \ N(0, Q_0)$$

where $Q_0 = diag\left\{\sigma_{x,0}^2 \quad \sigma_{y,0}^2 \quad \sigma_{b,0}^2 \quad \sigma_{mx_1,0}^2 \quad \sigma_{my_1,0}^2 \quad \cdots \quad \sigma_{mx_{N_{FP}},0}^2 \quad \sigma_{my_{N_{FP}},0}^2\right\}$

The initial condition for the stationary portion remains the same; however, dynamic portion is modified as $Q_{d,0} = diag\left\{\sigma_{x,0}^2 \quad \sigma_{y,0}^2 \quad \sigma_{b,0}^2\right\}$. The dynamic portion of state vector is defined by $\mathbf{q}_{d,k} = \begin{bmatrix} x_k & y_k & b_k \end{bmatrix}^T$ with a dimension of $L_d = 3$. The update information is calculated similar to Eq. (0-97)-(0-107) where $Q_d$ is modified for newly added range offset variables as $Q_d = diag\left\{Q_P \quad \sigma_b^2\right\}$.

## MODEL 3: UNSYNCHRONIZED ANS, MN NOT SYNCHRONIZED WITH ANS, KNOWN SIGHT CONDITIONS

The measurement Fisher information is calculated similar to system model 1, as stated in Eq. (0-91), except for each AN-MN link, a single range offset variable is added to the state space, and $h_i(\mathbf{q}_k)$ is modified by, $h_i(\mathbf{q}_k) = \sqrt{(m_{i,x} - x_k)^2 + (m_{i,y} - y_k)^2} + b_{i,k}$. Therefore,

$$\frac{\partial h_i(\mathbf{q}_k)}{\partial \mathbf{q}_k} = \left[ -\frac{(m_{i,x} - x_k)}{r_{i,k}} \quad -\frac{(m_{i,y} - y_k)}{r_{i,k}} \quad e^i_{1 \times N_{AN}} \quad \mathbf{0}_{1 \times 2N_{FP}} \right]$$

$$for \ i = 1, 2, ... N_{AP}$$

0-104

and

$$\frac{\partial h_i(\mathbf{q}_k)}{\partial \mathbf{q}_k} =$$

$$\left[ -\frac{(m_{i,x} - x_k)}{r_{i,k}} \quad -\frac{(m_{i,y} - y_k)}{r_{i,k}} \quad e^i_{1 \times N_{AN}} \quad [\frac{(m_{i,x} - x_k)}{r_{i,k}} e^{2(i-N_{AP})-1}_{1 \times 2N_{FP}} + \frac{(m_{i,y} - y_k)}{r_{i,k}} e^{2(i-N_{AP})}_{1 \times 2N_{FP}}] \right]$$

$$for \ i = N_{AP} + 1, N_{AP} + 2, ..., N_{AP} + N_{FP}$$

0-105

Consequently, the measurement FIM is obtained by

$$J_{Z,i}\left(\mathbf{q}_k\right) =$$

$$= \sigma_{z,i}^{-2} \begin{bmatrix} \dfrac{\left(m_{i,x}-x_k\right)^2}{r_{i,k}^{\;2}} & \dfrac{\left(m_{i,x}-x_k\right)\left(m_{i,y}-y_k\right)}{r_{i,k}^{\;2}} & -\dfrac{\left(m_{i,x}-x_k\right)}{r_{i,k}}.e^i_{1\times N_{AN}} & \mathbf{0}_{1\times N_{FP}} \\[2ex] \dfrac{\left(m_{i,x}-x_k\right)\left(m_{i,y}-y_k\right)}{r_{i,k}^{\;2}} & \dfrac{\left(m_{i,y}-y_k\right)^2}{r_{i,k}^{\;2}} & -\dfrac{\left(m_{i,y}-y_k\right)}{r_{i,k}}.e^i_{1\times N_{AN}} & \mathbf{0}_{1\times N_{FP}} \\[2ex] -\dfrac{\left(m_{i,x}-x_k\right)}{r_{i,k}}.e^i_{1\times N_{AN}}{}^T & -\dfrac{\left(m_{i,y}-y_k\right)}{r_{i,k}}.e^i_{1\times N_{AN}}{}^T & e^{i,i}_{N_{AN}\times N_{AN}}{}^T & \mathbf{0}_{1\times N_{FP}} \\[2ex] \mathbf{0}_{N_{FP}\times 1} & \mathbf{0}_{N_{FP}\times 1} & \mathbf{0}_{N_{AN}\times 1} & \mathbf{0}_{N_{FP}\times N_{FP}} \end{bmatrix}$$

$$for\ \ i = 1,2,...,N_{AP}$$

and

$$J_{Z,i}\left(\mathbf{q}_k\right) =$$

$$= \sigma_{z,i}^{-2} \begin{bmatrix} \dfrac{\left(m_{i,x}-x_k\right)^2}{r_{i,k}^{\;2}} & \dfrac{\left(m_{i,x}-x_k\right)\left(m_{i,y}-y_k\right)}{r_{i,k}^{\;2}} & -\dfrac{\left(m_{i,x}-x_k\right)}{r_{i,k}}.e^i_{1\times N_{AN}} & A \\[2ex] \dfrac{\left(m_{i,x}-x_k\right)\left(m_{i,y}-y_k\right)}{r_{i,k}^{\;2}} & \dfrac{\left(m_{i,y}-y_k\right)^2}{r_{i,k}^{\;2}} & -\dfrac{\left(m_{i,y}-y_k\right)}{r_{i,k}}.e^i_{1\times N_{AN}} & B \\[2ex] -\dfrac{\left(m_{i,x}-x_k\right)}{r_{i,k}}.e^i_{1\times N_{AN}}{}^T & -\dfrac{\left(m_{i,y}-y_k\right)}{r_{i,k}}.e^i_{1\times N_{AN}}{}^T & e^{i,i}_{N_{AN}\times N_{AN}}{}^T & C \\[2ex] A^T & B^T & C^T & D \end{bmatrix}$$

$$for\ \ i = N_{AP}+1, N_{AP}+2,...,N_{AP}+N_{FP}$$

where

$$A = [-\frac{(m_{i,x} - x_k)^2}{r_{i,k}^2} e_{1 \times 2N_{FP}}^{2(i-N_{AP})-1} - \frac{(m_{i,y} - y_t)(m_{i,x} - x_k)}{r_{i,k}} e_{1 \times 2N_{FP}}^{2(i-N_{AP})}]$$

$$B = [-\frac{(m_{i,x} - x_k)(m_{i,y} - y_k)}{r_{i,k}^2} e_{1 \times 2N_{FP}}^{2(i-N_{AP})-1} - \frac{(m_{i,y} - y_k)^2}{r_{i,k}^2} e_{1 \times 2N_{FP}}^{2(i-N_{AP})}]$$

$$C = [\frac{(m_{i,x} - x_k)}{r_{i,k}} e_{N_{AN} \times 2N_{FP}}^{i,2(i-N_{AP})-1} + \frac{(m_{i,y} - y_k)}{r_{i,k}} e_{N_{AN} \times 2N_{FP}}^{i,2(i-N_{AP})}]$$

$$D = [\frac{(m_{i,x} - x_k)^2}{r_{i,k}^2} e_{2N_{FP} \times 2N_{FP}}^{2(i-N_{AP})-1,2(i-N_{AP})-1} + \frac{(m_{i,x} - x_k)(m_{i,y} - y_k)}{r_{i,k}^2} e_{2N_{FP} \times 2N_{FP}}^{2(i-N_{AP})-1,2(i-N_{AP})}$$

$$+ \frac{(m_{i,x} - x_k)(m_{i,y} - y_k)}{r_{i,k}^2} e_{2N_{FP} \times 2N_{FP}}^{2(i-N_{AP}),2(i-N_{AP})-1} + \frac{(m_{i,y} - y_k)^2}{r_{i,k}^2} e_{2N_{FP} \times 2N_{FP}}^{2(i-N_{AP}),2(i-N_{AP})}]$$

Similarly, the measurement BFIM from all MN-AN links is calculated by the sum of the FIM from each MN-AN link as stated in Eq. (0-97). It must be noted the elements of FIM from measurement data for re-sorted state history in Eq. (0-85) are obtained in a similar way to the procedure explained for the system model 1.

The range offset terms make the rank of $J_z$ equal to one, so the portion of Fisher information that relates to observation is not invertible. The smooth spatial assumption of the MN movement is necessary to make the FIM invertible and the SLAM problem observable. To describe the prior information transformed by the update model, the initial information needs to be modified by

$$\mathbf{q}_0 \square N(0, Q_0)$$

where $Q_0 = diag\{\sigma_{x,0}^2 \quad \sigma_{y,0}^2 \quad \sigma_{b_1,0}^2 \quad \cdots \quad \sigma_{b_i,0}^2 \quad \sigma_{mx_1,0}^2 \quad \sigma_{my_1,0}^2 \quad \cdots \quad \sigma_{mx_{N_{FP}},0}^2 \quad \sigma_{my_{N_{FP}},0}^2\}$. The initial condition for the stationary portion remains the same as the system model; whereas the dynamic portion is modified by $Q_{d,0} = diag\{\sigma_{x,0}^2 \quad \sigma_{y,0}^2 \quad \sigma_{b_1,0}^2 \quad \cdots \quad \sigma_{b_i,0}^2\}$. In this case, the dynamic state vector $\mathbf{q}_{d,k} = [x_k \quad y_k \quad \mathbf{b}_k]^T$ has a dimension of $L_d = 2 + N_{AN}$. The update

information is calculated similar to Eq. (0-97)-(0-90) where $Q_d$ is modified for newly added

range offset variables as $Q_d = diag\{Q_P \quad Q_b\}$.

## MODEL 4: UNSYNCHRONIZED ANS, MN NOT SYNCHRONIZED WITH ANS, UNKNOWN SIGHT CONDITIONS

As mentioned earlier, one approach to deal with mixed NLOS/LOS propagation is to introduce two different noise models for LOS and NLOS propagation conditions, whereby the transition between the LOS and NLOS states is modeled with a binary Markov chain. This modeling turns the OWLS to a jump Markov nonlinear Gaussian system (JMNLGS). Since the FI calculation involves taking derivative with respect to all state variables, it cannot handle discrete values parameters such as binary sight conditions. Therefore, the discrete parameters need to be marginalized from all probability densities.

In [liii], [xii], an enumeration method is proposed to approximate the desired BCRLB as the expected value over all the discrete state sequences, referred as the Enumer-BCRLB. The method initially obtains a lower bound on the MSE matrix for any conditional estimator for the continuous-valued portion of $\mathbf{q}_t$, denoted by $\mathbf{q}_t^c$, based on the calculation of the conditional MSE matrix, given by

$$MSE(\hat{\mathbf{q}}_t \mid s_{1:t}^i) \square \mathrm{E}_{p(\mathbf{q}_t, \mathbf{z}_{1:t} \mid s_{1:t}^i)} \left\{ \left[ \hat{\mathbf{q}}_t^c(\mathbf{z}_{1:t} \mid s_{1:t}^i) - \mathbf{q}_t^c \right] \left[ \hat{\mathbf{q}}_t^c(\mathbf{z}_{1:t} \mid s_{1:t}^i) - \mathbf{q}_t^c \right]^T \right\} \qquad \textbf{\textit{0-110}}$$

$$\geq J\left( \mathbf{q}_t^c \mid s_{1:t}^i \right)^{-1}$$

where $\hat{\mathbf{q}}_t^c(\mathbf{z}_{1:t} \mid s_{1:t}^i)$ denotes the conditional estimator for a particular sight state sequence $s_{1:t}^i$ and $J\left( \mathbf{q}_t^c \mid s_{1:t}^i \right)$ denotes the conditional BFIM for $\mathbf{q}_t^c$ which is the $K \times K$ lower right submatrix of

$J_{tot}^{-1}\left( \mathbf{q}_{0:t}^c \mid s_{1:t}^i \right)$. Similar to the procedure explained previously, $J\left( \mathbf{q}_t^c \mid s_{1:t}^i \right)$ can be calculated recursively as shown in Eq. (0-75) as or based on linearization approximations as shown in Eq. (0-83). Then, to evaluate the unconditional MSE lower bound, the conditional CRLB is averaged over all possible discrete state sequences.

$$MSE(\hat{\mathbf{q}}_t^c) \,\square\, \mathrm{E}_{\mathrm{Pr}\{s_{1:t}\}} \left\{ \mathrm{E}_{p(\mathbf{q}_t^c, \mathbf{z}_{1:t}|s_{1:t}^i)} \left\{ \left[ \hat{\mathbf{q}}_t^c(\mathbf{z}_{1:t}) - \mathbf{q}_t^c \right] \left[ \hat{\mathbf{q}}_t^c(\mathbf{z}_{1:t} \mid \mathbf{s}_{1:t}^i) - \mathbf{q}_t^c \right]^T \right\} \right\} \qquad \textbf{\textit{0-111}}$$

$$\geq \sum_{i=1}^{s^k} \mathrm{Pr}\left\{ \mathbf{s}_{1:t}^i \right\} J\left( \mathbf{q}_t^c \mid \mathbf{s}_{1:t}^i \right)^{-1}$$

Therefore, the total BFIM is obtained by the inverse of the Enumer-CRLB. It can be seen that calculation complexity of Enumer-CRLB algorithm increases tremendously with time, yielding a complexity order of $o(t.2^t)$ for a binary sight state model since this requires the calculation of conditional FIMs for all possible discrete state sequences. In addition to computational complexity, it is stated in [xii], [liv], [lv], [[lvi] that the Enumer-BCRLB can be an overly optimistic bound.

To obtain a tighter bound, [liv]-[lvi] proposed a new method for jump Markov linear Gaussian systems where the Enumer-BCRLB is modified based on Monte Carlo (MC) methods. Since the state update process is described by a LJG model and is not a function of discrete states, the prior information for continuous-valued state vector can be calculated analytically as described in Eq. (0-90). However, the BFIM from measurement data, $J_Z(\mathbf{q}_{0:t}^c)$ is numerically approximated by [lv-lvi],

$$J_Z(\mathbf{q}_{0:t}^c) \approx \frac{1}{N} \sum_{n=1}^{N} \left\{ \left[ \nabla_{\mathbf{q}_{0:t}^c} \ln p_{\mathbf{z}_{1:t}|\mathbf{q}_{1:t}^c}\left( \{\mathbf{z}_{1:t}\}^n \mid \{\mathbf{q}_{1:t}^c\}^n \right) \right] \left[ \nabla_{\mathbf{q}_{0:t}^c} \ln p_{\mathbf{z}_{1:t}|\mathbf{q}_{1:t}^c}\left( \{\mathbf{z}_{1:t}\}^n \mid \{\mathbf{q}_{1:t}^c\}^n \right) \right]^T \right\} \qquad \textbf{\textit{0-112}}$$

where $\left\{ \mathbf{q}_{1:t}^c \right\}^n$ and $\left\{ \mathbf{z}_{1:t} \right\}^n$ are the independent and identically distributed vectors generated from $p(\mathbf{q}_{1:t}^c, \mathbf{z}_{1:t})$ for $N$ Monte Carlo simulation runs. The algorithm to compute $J_z(\mathbf{q}_{1:t}^c)$ approximately is adopted from [lvi]. It is reminded that for the problem at hand, $\mathbf{q}_t^c$ is defined by joint vector of location of MN, AN locations and range offsets as $\mathbf{q}_t^c = [\mathbf{p}_t \quad \mathbf{b}_t \quad \mathbf{m}]^T$.

Unlike the Enumer-CRLB , this later bound does not require explicit calculation of all possible discrete state sequences which reduce the complexity to the order of $o(2.N.t)$. However, [lvi] shows that for $N = 20000$, the method has obtained a tighter bound than Enumer-

CRLB for an tracking example; for an nonlinear SLAM-based OWLS with the high dimensional state space, the required number of MC runs is unknown and much higher.

Another approach for calculating BCRLB for jump Markov systems is suggested in [xii] that is based on deterministic trajectory of discrete states $\mathbf{s}_{1:t}^{*}$. However, it can be overly optimistic as it assumes the knowledge of discrete state; practically, it has suffced requirements for error assessment in most tracking problems [xii], [xlv]. In chapter 4, it will be shown that the BCRLB obtained based on the knowledge discrete state sequence still provides a reasonable bound to evaluate the result of the proposed algorithms for the OWLS.

## Other estimation metrics in terms of the BFIM

An accuracy metric is important in that it gives an indication of confidence in OWLS solution and if the tracking algorithm works successfully. In previous section, the BFIM is obtained as a quantitative metric of all available information in a SLAM-based OWLS. The BFIM comprises all information regarding the parameters of interest including the MN trajectory and nuisance parameters including AN locations, range offsets, and/or sight conditions. Since the main purpose of OWLS is MN localization, a concise accuracy metric which only focuses on positioning accuracy can be more useful than a high dimensional BFIM. In this regard, Position Error Bound (PEB) is introduced which interprets the BFIM in terms of localization accuracy. Moreover, a quantitative confidence metric can be extracted from BFIM known as confidence region of state vector. Not only in terms of accuracy and confidence, the BFIM introduces an useful tool, known as Normalized Estimation Error Squared (NEES), to evaluate OWLS solutions in terms of consistency. In following subsection, the relation of these three important metrics with the BFIM is explained in more detail.

In terms of localization accuracy, the error variance of the MN position $\{\hat{x}_t, \hat{y}_t\}$ is of interest, which is the upper left 2by2 submatrix of $J_{tot}\left(\mathbf{q}_t\right)^{-1}$,

$$E\left\{(\hat{\mathbf{p}}_t - \mathbf{p}_t)(\hat{\mathbf{p}}_t - \mathbf{p}_t)^T\right\} \geq \left[J_{to}\left(\mathbf{q}_{tt}\right)^{-1}\right]_{2\times 2}$$

**0-113**

or

$$E\left\{(x_t - \hat{x}_t)^2 + (y_t - \hat{y}_t)^2\right\} \geq tr\left\{\left[J_{tot}\left(\mathbf{q}_t\right)^{-1}\right]_{2\times 2}\right\}$$

**0-114**

where $tr\left\{\left[J\left(\mathbf{q}_t\right)^{-1}\right]_{2\times 2}\right\}$ is known as Position Error Bound (PEB).

The Normalized Estimation Error Squared (NEES) for the state $\mathbf{q}_t$ is defined as [xlv]

$$\varepsilon_q = \left(\mathbf{q}_t - \hat{\mathbf{q}}_t\right)^T J\left(\mathbf{q}_t\right)(\mathbf{q}_t - \hat{\mathbf{q}}_t)$$

**0-115**

and is chi-square distributed , $\chi^2$, with $\dim(\mathbf{q}_t)$ degrees of freedom under the hypothesis that the filter is consistent and approximately linear-Gaussian. In an estimation problem, particularly SLAM, NEES is used as a measure of filter consistency by the examination of average NEES over N Monte Carlo runs of filters [xliii], [xlv]; [lvii]. Given N simulation runs, the average NEES is obtained by

$$\bar{\varepsilon}_q = \frac{1}{N}\sum_{i=1}^{N}\varepsilon_q$$

**0-116**

The quantity of $N\bar{\varepsilon}_q$ is chi-squared distributed with $N\dim(\mathbf{q}_t)$ degrees of freedom under consistent filter hypothesis. The 95% probability concentration region for $\bar{\varepsilon}_q$ can be used to test whether the SLAM filter is optimistic if the error rises significantly higher than bound, or is pessimistic, if it tends below the lower bound. Moreover, $\bar{\varepsilon}_q$ can be asymptotically estimated by $N\dim(\mathbf{q}_t)$.

## Confidence Region for the state vector

When $\mathbf{q}_t$ is the unknown parameter to be estimated, one can say that $\hat{\mathbf{q}}_t$ must be within some neighborhood of $\mathbf{q}_t$. This neighborhood is determined by the confidence region of the state vector $\mathbf{q}_t$, as defined by the inside of "g-sigma" ellipsoid,

$$\varepsilon_q = \left(\mathbf{q}_t - \hat{\mathbf{q}}_t\right)^T J\left(\mathbf{q}_t\right)\left(\mathbf{q}_t - \hat{\mathbf{q}}_t\right) = g^2$$

0-117

This is actually a hyper-ellipsoid of dimension $\dim(\mathbf{q}_t)$ where the semi-axes are $g$ times of the square roots of the Eigen values of $\left[J\left(\mathbf{q}_t\right)\right]^{-1}$. For an efficient estimator, the normalized error $\varepsilon_q$ must follow

$$\Pr\left\{\varepsilon_q \leq g^2\right\} = 1 - Q$$

0-118

where $Q$ represents the small tail probabilities. For a one-sided probability region of 95%, the ellipsoid boundary will be used to assess the SLAM algorithm error performance in comparison with the efficient estimator.

Mutual information (MI), $I(X,Y)$, measures the mutual dependence of two random variables, $X$ and $Y$. If $X$ and $Y$ are the input and output of a channel, respectively, $I(X,Y)$ does not make any assumptions regarding the receiver processing of $Y$, but requires the source entropy. It can be shown that if the signal to noise of each degree of freedom (DOF) is small, then $I(X,Y)$ is independent of the source distribution [lviii], [lix], [lx]. Hence, an asymptotic assessment of the tracking performance based on the mutual information is possible for any source distribution. We can select a source distribution of $X$ that facilitates the mathematics and results in the most convenient expressions. Assuming a low SNR per signal DOF, such that the source distribution becomes asymptotically irrelevant, then it is possible to consider the symmetry of the problem such that the mutual information can be assessed for a specific value of $X$. However, instead of determining the overall $I(X,Y)$, where the probability

structure of $X$ needs to be specified, we can consider the simpler problem of determining

$I(X,Y \mid X = A)$ or just $I(Y,A)$. Mutual information quantifies how much information of a specific

value of $A$ is contained in $Y$. In other words, determine the statistics of the optimum estimator

of $A$ based on the data in $Y$ which is expressed as $\hat{A}(Y)$. The quantity of information

regarding the parameter $A$ that is contained in Y is also given by the Fisher information

denoted in this case as $J(A;Y)$. Hence, the quantity that is used to assess the estimation and

tracking performance is the effective signal to noise given as $A^2 J(A;Y)$.

Guo et al [xi] revealed an interesting relation between the mutual information and the

MMSE. Guo theorem says that regardless of the input statistics the relation between mutual

information and MMSE in an additive Gaussian channel can be described by

$$\frac{\partial I\left(X,Y;SNR\right)}{\partial SNR} = \frac{1}{2} MMSE\left(SNR\right) \qquad \textbf{\textit{0-119}}$$

where $SNR$ is the signal-to-noise ratio of the channel; $I\left(X;Y\right)$ is the input-output mutual

information in nats, and the $MMSE$ is the minimum mean square error of input estimation given

output as a function of SNR. Eq. 0-118) reflects a strong relevance of mutual information to

estimation and filtering which can provide a non-coding operational application. The input-output

mutual information demonstrates how much information can be transferred through a channel

reliably given a certain input signaling, while the MMSE quantifies how efficiently each input

sample can be recovered using the channel output. The significance of this relation is that this is

not only simple and intriguing but is also independent of input distribution which holds under

arbitrary signaling conditions and the broadest setting of the Gaussian channel, including both

discrete-time and continuous-time channels in both scalar and vector versions. Two explanatory

proofs for Guo's theorem are presented in Appendix A where the first proof is inspired by

independence of MI from input distribution in low SNRs and incremental channel concept and

the second proof uses the relation between FI and differential entropy in de Bruijn's identity [xi], [lxii].

The intuitive Guo's theorem introduces a novel application of another information metric, that is mutual information, in tracking and estimation problems [lxi]. However, the Guo theorem only proposed a MI application in a linear Gaussian problem for random stationary parameter. In this section, it is explained how the mutual information concept can be applied for a SLAM-based OWLS which includes not only random stationary parameters such as FP locations but also random dynamic variables such as the MN location. The elements of MI, their contribution to stationary and dynamic parameter estimation are depicted via a Venn diagram based on a Markovian structure of OWLS.

We define a SLAM-based wireless localization problem where the MN moves within an unregistered network and receives wireless observables from a mixture of stationary ANs with unknown or known positions. The MN trajectory is assumed to be random but smooth in the way that the motion dynamical process is modeled by a Markovian process. At any discrete time instant $t \in \square$, the state variable $\mathbf{q}_t$ includes stationary parameters such as FP locations $\mathbf{m}_{fp}$, and dynamic variables, such as the MN location, and other nuisance parameters such as range offset $\mathbf{q}_{d,t} = \begin{bmatrix} \mathbf{p}_t & \mathbf{b}_t \end{bmatrix}^T$, is denoted as

$$\mathbf{q}_t = \begin{bmatrix} \mathbf{q}_{d,t} & \mathbf{m}_{fp} \end{bmatrix}^T$$
<div align="right">*0-120*</div>

Mutual information, $I(\mathbf{q}_t, \hat{\mathbf{q}}_t)$ is a measure of information which the sufficient statistic or estimator, $\hat{\mathbf{q}}_t$, can provide for estimating $\mathbf{q}_t$ in terms of shared entropy [lxii]. The first element of MI is defined by Markovian process between subsequent dynamic states. Note that the stationary portion of state vector $\mathbf{m}_{fp}$ can be also considered as a dynamic variable with a zero mean and variance Markov process. Figure 0-20 shows a Venn diagram of entropy change in two and three-step Markov process. The entropy of states are shown by color-filled ellipse areas

and their common information or MI shown by overlapped areas between entropies. For example, the green left area in left-side depicts the maximum-decreased entropy of $\mathbf{q}_{d,t}$ if the previous state is known as a result of filtering in a online processing, while green area in right side diagram shown the maximum-decreased entropy of $\mathbf{q}_{d,t}$ if previous and next states are known as a result of smoothing in a batch processing.
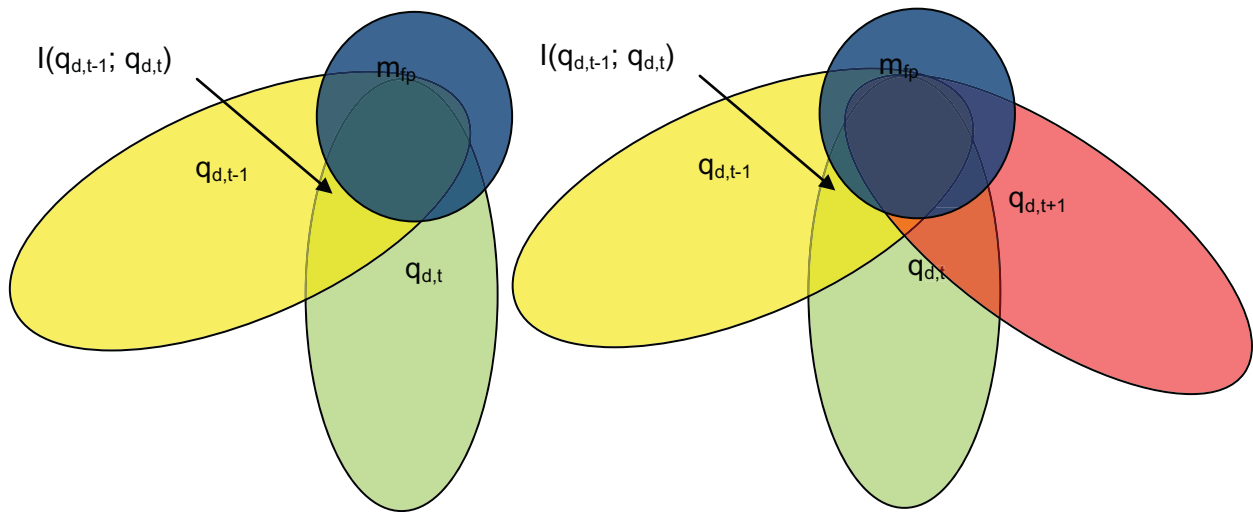


***Figure 0-20 Venn diagram of entropy change in a Markov process***

Since the underlying Markov process ($\mathbf{q}_{d,t-1} \rightarrow \mathbf{q}_{d,t} \rightarrow \mathbf{q}_{d,t+1}$) evolves unaware of the observations, when at the time instant $t$, the observation $\mathbf{z}_t$ depends only on the state at time instant $t$. This means, given $\mathbf{q}_{d,t}$, the observation at the time instant $t$, $\mathbf{z}_t$ and $\mathbf{q}_{d,t-1}$ are independent so that $\mathbf{q}_{d,t}$, $\mathbf{z}_t$ and $\mathbf{q}_{d,t-1}$ form a Markov Chain as $\mathbf{q}_{d,t-1} \rightarrow \mathbf{q}_{d,t} \rightarrow \mathbf{z}_t$ or $\mathbf{z}_t \rightarrow \mathbf{q}_{d,t} \rightarrow \mathbf{q}_{d,t-1}$ that is equivalent with $I(\mathbf{q}_{d,t-1};\mathbf{z}_t \mid \mathbf{q}_{d,t}) = 0$. Note that this independency is also applied to the whole state vector $\mathbf{q}_t$, since the stationary portion of state vector can also be treated as dynamic variable as earlier discussed. Therefore, the second element of MI is defined by measurement data; however, this independency property must be considered when

combining the MI elements. Figure 0-21 shows entropy change in presence of measurement data and MI dependency in this Markov process.
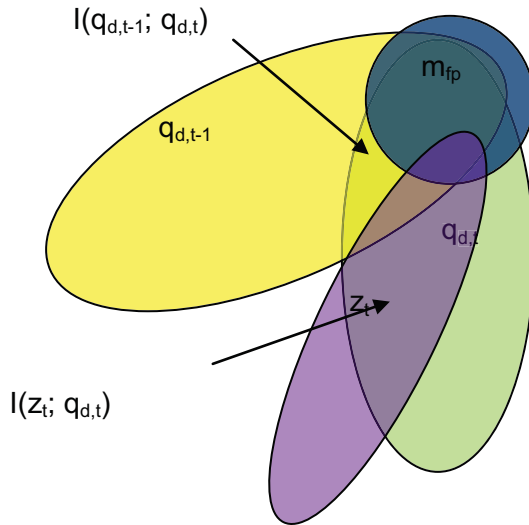


***Figure 0-21 Venn diagram of the entropy change in presence of measurement data***

With Markovian chain assumption between states and also state-measurement, two important points is taken into account in plotting Venn diagrams. First $I(\mathbf{q}_{t-1};\mathbf{z}_t \,|\, \mathbf{q}_t)=0$, then

$$h(\mathbf{q}_{t-1};\mathbf{z}_t)=h(\mathbf{q}_{t-1};\mathbf{z}_t \,|\, \mathbf{q}_t)$$

<div align="right">

*0-121*

</div>

where $h(.)$ denotes the entropy. It means that not only $I(\mathbf{q}_{t-1};\mathbf{z}_t)<I(\mathbf{q}_{t-1};\mathbf{q}_t)$ but also

$(\mathbf{q}_{t-1}\cap\mathbf{z}_t)\subset(\mathbf{q}_{t-1}\cap\mathbf{q}_t)$.

Second, since $p(\mathbf{q}_t \,|\, \mathbf{q}_{t-1},\mathbf{z}_{t-1})=p(\mathbf{q}_t \,|\, \mathbf{q}_{t-1})$, it is inferred that given the previous states, previous measurement doesn't add new information for the current and future states, which complies with Markovian assumption.

Therefore, the maximum mutual information for state estimate at time step $t$ in terms of nats or bits is obtained by combining the MI elements with considering the Markov properties , given by

$$I(\mathbf{q}_t, \hat{\mathbf{q}}_{t-1}) \leq I(\mathbf{q}_t; \mathbf{q}_{t-1}, \mathbf{z}_t) = I(\mathbf{q}_t; \mathbf{z}_t) + I(\mathbf{q}_t; \mathbf{q}_{t-1}) - I(\mathbf{q}_{t-1}; \mathbf{z}_t) \qquad \textbf{\textit{0-122}}$$
$$= I(\mathbf{q}_t; \mathbf{z}_t) + I(\mathbf{q}_t; \mathbf{q}_{t-1} \mid \mathbf{z}_t)$$
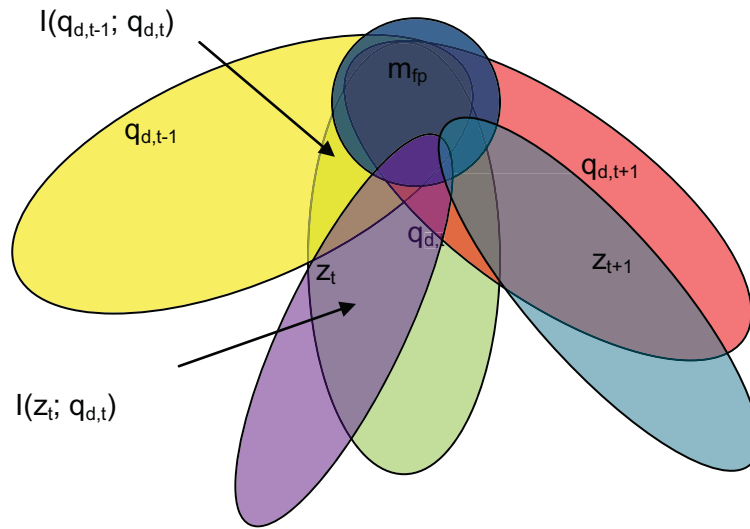


***Figure 0-22 Venn diagram of the MI and entropy change in a Bayesian problem***

Finally, the entropy reduction and total MI increase procedure of three subsequent states in a SLAM problem is illustrated in Figure 0-22 which fulfills these two criteria. In an online SLAM problem, Eq. (0-121) determines the upper bound of information for $\mathbf{q}_t$ ; while in the full SLAM problem, the added information from future states must be considered, as shown Figure 0-20, where the decreased entropy of $\mathbf{q}_t$ after taking into account the information from is $\mathbf{q}_{t+1}$ and $\mathbf{z}_{t+1}$ illustrated by the pure green area. However, the MI calculation for state variables given in Eq. 0-121) can be difficult in comparison to MMSE calculation; it gives a global criterion for any state statistics and channel noise distributions in units of bits or nats. The more detailed

pros and cons of MI application in estimation problems will be discussed in next subsection by some examples.

## Guo's theorem applications and its limitation for the SLAM-based OWLS

The main advantages of MI application to estimation problems in comparison with FI or Bayesian CRLB is that it provides a global measure of shared information between the state vector and observables and prior information regardless of linearity or Gaussianity of the problem. The Guo's theorem has built the bridge between estimation theory in terms of MMSE and information theory in terms of MI under certain conditions. However, Guo's theorem and MI calculation have their own disadvantages which lead us to mainly focus on the FIM for our SLAM-based wireless localization problem. Following example are designed to illustrate the MI and Guo's theorem limitations for OWLS application in more detail.

*Example 01: Linear Gaussian random input in additive Gaussian channel*

Consider a simple channel model with continuous-valued input and noise process

$$y = \sqrt{\delta}x + n \tag{0-123}$$

where $n, x \sim N(0,1)$. Therefore, the output distribution is given by

$$y \sim N(0, \delta + 1) \tag{0-124}$$

For a Gaussian channel with linear Gaussian input, the input-output mutual information in terms of nats is derived as

$$I(x; y) = H(y) - H(y \mid x) = \frac{1}{2}\ln(2\pi e(\delta + 1)) - \frac{1}{2}\ln(2\pi e) = \frac{1}{2}\ln(\delta + 1) \tag{0-125}$$

Figure 0-23 shows the mutual information calculated numerically from entropy and analytical result in Eq. (0-124). Although the MI calculation from entropy is trivial when the closed form is obtainable, both plots are presented in order to observe possible errors of numerical integration. From Guo's theorem, it is inferred that the mutual information of a

Gaussian channel is concave function of SNR as shown in Figure 0-21. Moreover, the mutual

information can be bounded as

$$mmse(SNR) \le \frac{2}{SNR} I(SNR) \le mmse(0) = \text{var}(X)$$
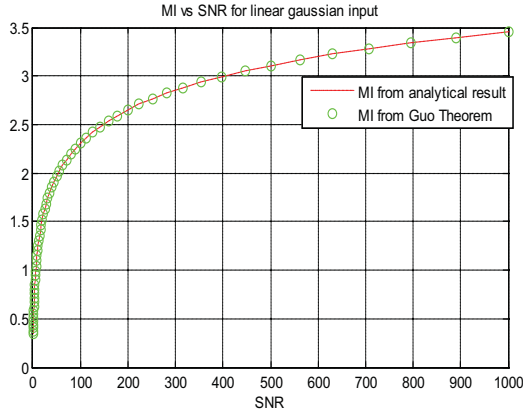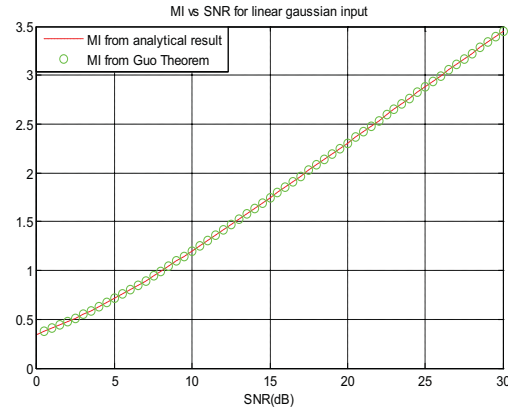


a. linear scale SNR          b. SNR in dB

**Figure 0-23 Mutual information versus SNR in a linear Gaussian channel with a Gaussian input**

The MMSE of the input estimate given the output is computed as the averaged mean of

the posterior PDF :

$$f_{X|y}(x \mid y) = \frac{f_{Y|X}(y \mid x) f_X(x)}{f_Y(y)}$$

$$= \frac{\frac{1}{\sqrt{2\pi}} \exp\left(-\frac{1}{2}\left(y - \sqrt{\delta}x\right)^2\right) \frac{1}{\sqrt{2\pi}} \exp\left(-\frac{1}{2}x^2\right)}{\frac{1}{\sqrt{2\pi(1+\delta)}} \exp\left(-\frac{\left(y - \sqrt{\delta}x\right)^2}{2(1+\delta)}\right)}$$

$$\square\ N\left(\frac{\sqrt{\delta}}{1+\delta}y, \frac{1}{1+\delta}\right)$$

Since the variance of posterior PDF is constant for all value of $y$, the MMSE is given by

$$mmse(\hat{x} \mid \delta, y) = \frac{1}{1+\delta}$$

GUO's theorem is confirmed not only by analytical results in Eq. 0-128) for both continuous Gaussian signal and noise in a linear system but also by numerical calculation as shown in Figure 0-22:

$$\frac{\partial I(x; y)}{\partial \delta} = \frac{1}{2} mmse(\hat{x} \mid \delta, y) = \frac{1}{1+\delta}$$

0-129

Small difference between analytical and numerical results for SNR<10dB in Figure 0-24 is mainly due to numerical error in MI first derivative calculation. However, it is not mentioned in [xi], Eq. (0-128) is only valid when the variance of $x$ is normalized to 1.
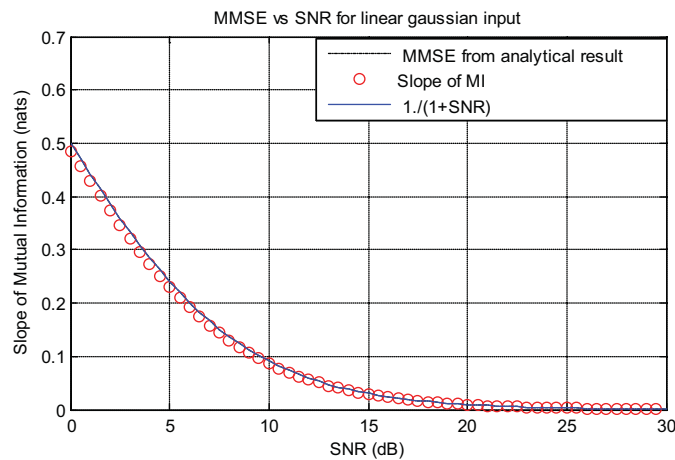


**Figure 0-24 MMSE and MI versus SNR in linear Gaussian channel with Gaussian input**

*Example 02 : Nonlinear discrete random input in an additive Gaussian channel*

Range and TOA measurements provide observables for tracking algorithms that have nonlinear relation with state space. In this case, the verification of Guo's theorem for nonlinear system is investigated. Even if the input $x$ is Gaussian , the output PDF through nonlinear function is not Gaussian. One of main disadvantages of MI application in tracking problems will be the difficulty in generating the PDF for a general nonlinear process with some correlation. In this regard, numerical calculation is generally solution such as approximation of the continuous PDF of input by a discrete PDF. Consider a input-output nonlinear system with additive Gaussian noise channel:

$$y = \sqrt{\delta} f(x) + n$$

where $n \square N(0,1)$ and $x \square \sum_{i=1}^{M} p_i \delta(x - x_i)$ as $\sum_{i=1}^{M} p_i = 1$.

In this example, a Gaussian PDF of input $x$ is approximated by a discretized version of

Gaussian PDF with cell width $\Delta$. To apply Guo's theorem, it is also required to normalized the

variance of $f(x)$, $\sigma_{fx}$; therefore the total SNR is stated by $\sqrt{\delta} \sigma_{fx}$ where

$$y = \sqrt{\delta} \sigma_{fx} \frac{f(x)}{\sigma_{fx}} + n$$

Lets define $\sqrt{snr} = \sqrt{\delta} \sigma_{fx}$ and. $g(x) = \frac{f(x)}{\sigma_{fx}}$; the output distribution is given by

$$f(y) = \frac{1}{\sqrt{2\pi}} \sum_{i=1}^{M} p_i \exp\left(-\frac{\left(y - \sqrt{snr}\, g(x)\right)^2}{2}\right)$$

The posterior PDF is calculated as

$$f_{g(x)|y}(g(x)|y) = \frac{f_{Y|X}(y|x) f_{g(x)}(g(x))}{f_Y(y)}$$

$$= \frac{\frac{1}{\sqrt{2\pi}} \sum_{i=1}^{M} p_i \exp\left(-\frac{\left(y - \sqrt{\delta}\, g(x)\right)^2}{2}\right) \delta\big(g(x) - g(x_i)\big)}{\frac{1}{\sqrt{2\pi}} \sum_{i=1}^{M} p_i \exp\left(-\frac{\left(y - \sqrt{\delta}\, g(x)\right)^2}{2}\right)}$$

and the conditional mean estimate is given by

$$\hat{g}(x) = \int_{R \subset g(x)} g(x)\, f_{g(x)|y}(g(x)|y)\, d\, g(x)$$

$$= \frac{\frac{1}{\sqrt{2\pi}} \sum_{i=1}^{M} g(x_i) p_i' \exp\left(-\frac{\left(y - \sqrt{\delta}\, g(x)\right)^2}{2}\right)}{\frac{1}{\sqrt{2\pi}} \sum_{i=1}^{M} p_i' \exp\left(-\frac{\left(y - \sqrt{\delta}\, g(x)\right)^2}{2}\right)}$$

The averaged variance of posterior PDF which is equal to MMSE is given by

$$MMSE(\hat{g}(x)\,|\,y) = \int_y f_Y(y)\,\mathrm{var}(f_{g(x)|y}(g(x)\,|\,y)dy$$

$$= \int \left( \frac{1}{\sqrt{2\pi}} \sum_{i=1}^M g(x_i)^2 p_i' \exp\left( -\frac{\left(y-\sqrt{\delta}g(x_i)\right)^2}{2} \right) \right) dy$$

$$- \int \frac{\left( \frac{1}{\sqrt{2\pi}} \sum_{i=1}^M g(x_i) p_i' \exp\left( -\frac{\left(y-\sqrt{\delta}g(x_i)\right)^2}{2} \right) \right)^2}{\frac{1}{\sqrt{2\pi}} \sum_{i=1}^M p_i' \exp\left( -\frac{\left(y-\sqrt{\delta}g(x_i)\right)^2}{2} \right)} dy$$

$$= \sum_{i=1}^M g(x_i)^2 p_i' - \int \frac{\left( \frac{1}{\sqrt{2\pi}} \sum_{i=1}^M g(x_i) p_i' \exp\left( -\frac{\left(y-\sqrt{\delta}g(x_i)\right)^2}{2} \right) \right)^2}{\frac{1}{\sqrt{2\pi}} \sum_{i=1}^M p_i' \exp\left( -\frac{\left(y-\sqrt{\delta}g(x_i)\right)^2}{2} \right)} dy$$

**SLAM-Based Opportunistic Wireless Localization**

OWLS is proposed as a solution for localization in environments where GPS fails or the local wireless network signaling is not intended for positioning purposes. It is shown that the SLAM can introduce a systematic approach of accounting for the various disparate sources of information to track MN trajectory in an unknown environments. The significance of SLAM application in an OWLS problem is that it can incorporate all available information from the motion process, observables and prior knowledge to track the MN trajectory while jointly estimates the unknown environment map parameters including FP locations and other nuisance parameters such as range offset due to unsynchronized reception and multipath effects. Chapter 2 introduced the OWLS system parameters which based on, Chapter 3 presented four system models for an OWLS according to range measurements data. It is shown in Chapter 2 that optimal recursive Bayesian solution for an OWLS requires the complete posterior PDF of the system state to be determined as a function of time. However, a closed form solution for an OWLS cannot be formulated due to system nonlinearity. Despite the absence of closed form analytical solution, Bayesian FIM was formulated for all four proposed system models as the best achievable performance of the OWLS in Chapter 3.

This chapter presents two suboptimal Bayesian solutions for an OWLS based on EKF and PF, known as EKF-SLAM and FastSLAM. The proposed suboptimal EKF-based and PF-based solutions are implemented for four proposed OWLS models ranging from a synchronized scenario with known sight conditions, as in system model 1, to where there is no knowledge about the MN trajectory, AN locations in a non-stationary multipath situation. Figure 0-25 illustrates a flow chart of how proposed algorithms interacts with system models. This step-by-step modeling provides a deep understanding of how much information each additional variable contributes to solution. BFIM and its derivatives' bounds (BCRLB, NEES, PEB and confidence region), formulated in Chapter 3, are used as benchmarks for comparison of implemented suboptimal algorithms and assessment of the effect of introduced system parameters.

Performance bounds are also used to investigate the effect of introduced approximation in suboptimal solutions in terms of consistency and efficiency.
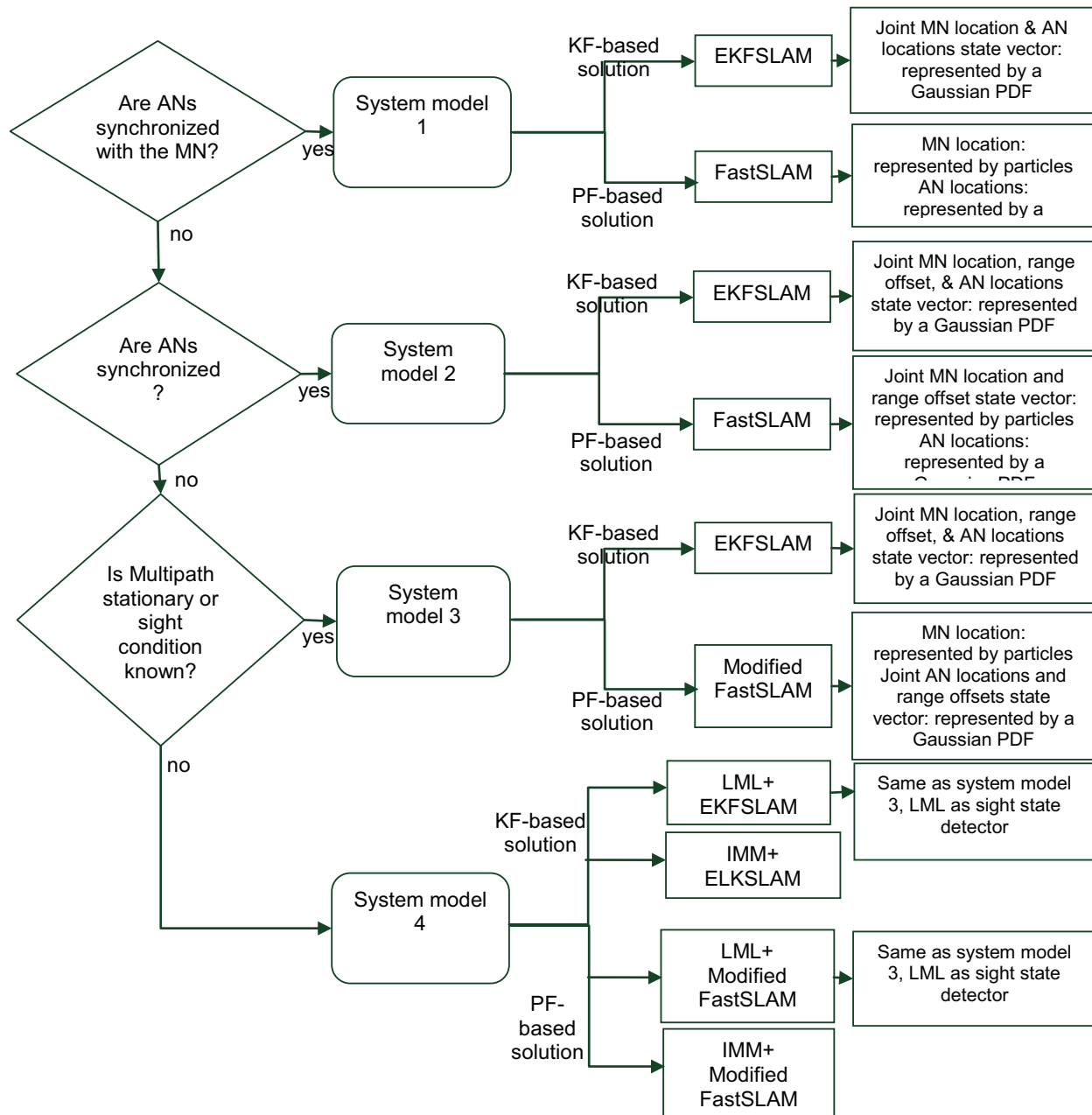


**Figure 0-25 Flowchart of OWLS algorithms according to system models**

based and PF-based solutions for an arbitrary trajectory of a single MN in a rectangular room.

*Figure 0-26* illustrates the Matlab-based user interface to simulate an OWLS scenario. Initially, an arbitrary MN trajectory is generated by choosing the spline points shown by yellow squares in *Figure 0-26*. The MN trajectory is depicted by blue line and the MN locations where it receives

new measurements and updates its position is shown by red dots. The number and the location of FPs (shown by a red square box) and APs (shown by a green square box) can be chosen by user visually over the trajectory plot. To generate both NLOS and LOS conditions along the simulated trajectory, a wall is simulated which can be created and moved by user, depicted green rectangular in *Figure 0-26*
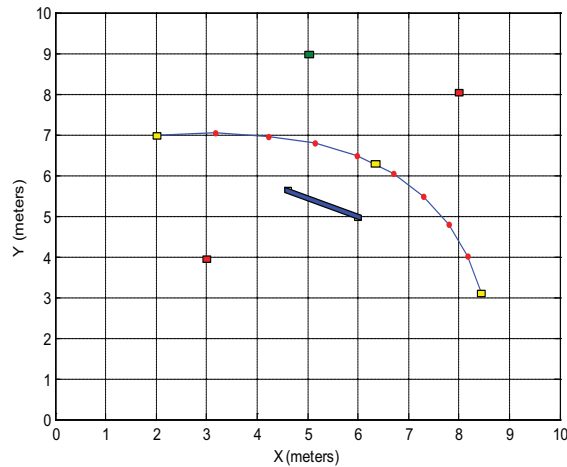


**Figure 0-26 User interface to simulate MN trajectory and locations of FPs and APs**

In next stage, the toolbox generates measurements according to the selected system model and simulates EKF-based and PF-based solutions simultaneously as illustrated in Figure 0-25. The 95% confidence regions obtained by approximated posterior PDF by tracking algorithm and BFIM formulation from Chapter 3 are generated; where the former is shown by ellipsoids with solid line (red for FP location estimate and blue for the MN location estimate), and the latter is shown by ellipses with dashed line. The figure also compares the true MN trajectory with the estimated MN trajectory, shown by black thick line with yellow dots representing the MN location estimates, and FP location estimates trajectory are illustrated by green dots. The MN localization errors can be appreciated by looking at the black lines that connect the true and the estimated MN positions. The final estimates of MN location and FP locations are shown by purple donuts where the initial estimates are shown by black stars. The

start point of the MN trajectory can be detected in EKF-based results as the red point which is

centered by two blue solid ellipsoids where the larger one represents the 95% confidence region

obtained from initial conditions. A listing of figure legend descriptions is summarized in Table

0-2.



**EKFSLAM**

**FastSLAM**

a)

b)
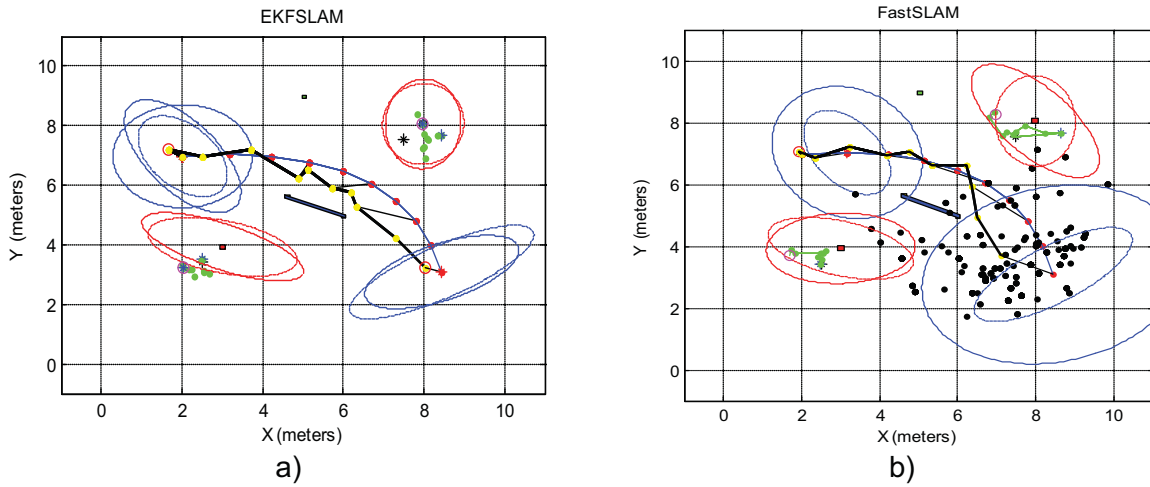
*Figure 0-27 Example of EKFSLAM/FastSLAM tracking results*

**Table 0-2 Figures' legend guideline**

| Legend | Description |
|---|---|
| Blue line | The MN true trajectory |
| Red dots on blue line | MN estimate update |
| Yellow square | Spline points for simulating the MN trajectory |
| Green box | AP location |
| Red box | FP location |
| Green/blue rectangular | Wall |
| Black star | Initial estimate |
| Purple donut | Final estimate |
| Green dot | FP estimate |
| Yellow dots | MN location estimates |
| Red dots | Particle-conditioned FP estimates |
| Black dots | MN location particles |
| Red ellipse with solid line | 95% confidence region from posterior PDF for the FP estimates |
| Blue ellipse with solid line | 95% confidence region from posterior PDF for the MN estimates |
| Red ellipse with dashed line | 95% confidence region from BFIM for the FP estimates |
| Blue ellipse with dashed line | 95% confidence region from BFIM for the MN estimates |

*System model 1: synchronized ANs, MN synchronized with ANs, known sight conditions*

In the first case, the MN receives signal from an arbitrary number of stationary and synchronized ANs including both FPs and APs. The MN clock drift from ANs clock is not an issue since the MN is synchronized with ANs initially in calibration stage and then via a global reference clock such as GPS clock as the MN moves. As earlier described in Section 0 , the location state MN $\mathbf{p}_t = \left[ x_t, y_t \right]^T$ is modeled as a first-order Markov process ruled by

$\mathbf{p}_t = \mathbf{p}_{t-1} + \mathbf{v}_t$, where the $\mathbf{v}_t \sim N(0, Q_p)$ . Covariance matrix of motion process, $Q_p$ , can be chosen commensurate with the velocity variance of the mobile user. However, a more

informative motion model can be replaced from output CV or IMU sensors, whenever available.

The current state vector of unknown variables is denoted by $\mathbf{q}_t = \begin{bmatrix} \mathbf{p}_t & \mathbf{m}_{fp} \end{bmatrix}^T$, where $\mathbf{m}_{fp}$ is the

stacked vector of the FP locations, defined by $\begin{bmatrix} m_{N_{AP+1},x} & m_{N_{AP+1},y} & \cdots & m_{N_{AN},x} & m_{N_{AN},y} \end{bmatrix}^T$. The

estimate of $\mathbf{q}_t$ must be extracted from the history of measurements by the time step $t$,

$\mathbf{z}_{1:t} \square \{ \mathbf{z}_1 \quad \mathbf{z}_2 \quad \cdots \quad \mathbf{z}_t \}$. $\mathbf{z}_k = \{ z_{1,k} \quad z_{2,k} \quad \cdots \quad z_{N_{AN},k} \}, k = 1,...,t$, denotes range measurements

at the time step $k$ from all ANs in line of sight with the MN. It is assumed that the ANs provides

LOS measurements or if not, the sight condition are known to the MN and NLOS measurements

are discarded from the measurement set. The suboptimal estimate of $\mathbf{q}_t$ is obtained by

evaluation of the posterior PDF, $p(\mathbf{q}_t \mid \mathbf{z}_{1:t})$, using EKFSLAM and FastSLAM.

## EKFSLAM solution for case 1

Based on system model 1 outlined in Section 0, EKFSLAM for this case approximates

the posterior PDF, $p(\mathbf{q}_t \mid \mathbf{z}_{1:t}) = p(\mathbf{p}_t, \mathbf{m}_{fp} \mid \mathbf{z}_{1:t})$, by a joint Gaussian PDF whose the mean vector

and the covariance matrix are given by

$$\hat{\mathbf{q}}_{t|t=} \begin{bmatrix} \hat{\mathbf{p}}_{t|t} \\ \hat{\mathbf{m}}_{fp,t} \end{bmatrix} = \begin{bmatrix} \hat{\mathbf{p}}_{t|t-1} \\ \hat{\mathbf{m}}_{fp,t-1} \end{bmatrix} + \mathbf{K}_t \left[ \mathbf{z}_t - \mathbf{h}(\hat{\mathbf{p}}_{t|t-1}, \hat{\mathbf{m}}_{fp,t-1}) \right] \qquad \textit{0-136}$$

$$\Sigma_{t|t} = \Sigma_{t|t-1} + \mathbf{K}_t \mathbf{D}_t \mathbf{K}_t^T$$

where $\hat{\mathbf{q}}_{t|t-1} = \begin{bmatrix} \hat{\mathbf{p}}_{t|t-1} & \hat{\mathbf{m}}_{fp,t-1} \end{bmatrix}$ and $\Sigma_{t|t-1}$ are the mean and covariance matrix of apriori PDF,

stated by

$$\hat{\mathbf{q}}_{t|t-1} = \begin{bmatrix} \hat{\mathbf{p}}_{t|t-1} \\ \hat{\mathbf{b}}_{t|t-1} \\ \hat{\mathbf{m}}_{fp,t-1} \end{bmatrix} = \begin{bmatrix} \hat{\mathbf{p}}_{t-1|t-1} \\ \hat{\mathbf{b}}_{t-1|t-1} \\ \hat{\mathbf{m}}_{fp,t-1} \end{bmatrix}$$

$$\Sigma_{t|t-1} = \Sigma_{t-1|t-1} + F^T Q_{p,t} F$$

and

$$F = \begin{bmatrix} 1 & 0 & 0 & 0 & \cdots & 0 \\ 0 & 1 & 0 & 0 & \cdots & 0 \end{bmatrix}$$
$$\underbrace{\qquad\qquad\qquad\qquad}_{2+2N_{FP}}$$

$$\mathbf{D}_t = H \sum{}_{t|t-1} H^T + R_t$$

$$\mathbf{K}_t = \sum{}_{t|t-1} H^T \mathbf{D}_t^{-1}$$

where $H$ is the Jacobian of range measurement function, evaluated at $\hat{\mathbf{q}}_{t|t-1} = [\hat{\mathbf{p}}_{t|t-1}, \hat{\mathbf{m}}_{t-1}]^T$,

previously defined in Eq. (0-92)-(0-93).

**FastSLAM solution for case 1**

The FastSLAM solution is based on the Rao-Blackwellization theorem where the joint

posterior PDF can be factored into the MN location components and a conditional ANs location

component as described in Eq. (0-27). It approximates the posterior PDF by set of particles

where each particle of posterior PDF represents the history of MN locations which additionally

contains the Gaussian parameters (i.e. the mean and covariance matrix) of FP locations

estimates. The FastSLAM for system model 1 adopts the same procedure explained previously,

Eq. (0-27)-(0-31) where the measurement function $h_i(.,.)$ is described by the range

measurement function stated in Eq. (0-66).

The performance of the SLAM algorithms is assessed by a simulated localization

scenario shown in Figure 0-28. The MN, while moving within a environment of 10m by 10m ,

localizes itself and maps FPs using the range measurement obtained from all ANs in the LOS

condition. A smooth MN trajectory $\{\mathbf{p}_t\}_{t=1}^{L}$ is simulated within the allowed 2-D space (walls and

the AN locations are not permitted). Sight conditions are generated by accessing the

LOS/NLOS map, as shown in Figure 0-28 for four ANs, according to the simulated MN

trajectory. It can be noticed that most of the area is always covered by at least 2 ANs which their

locations are not necessary known to the MN. This makes the localization task particularly

complicated and requires MN tracking in order to avoid large errors due to poor network

cooperation. Nevertheless, it will be shown that the Bayesian-based SLAM algorithms will

provide good localization performances.

a) AN 01 sight condition                                              b) AN 02 sight condition

c) AN 03 sight condition                                              d) AN 04 sight condition
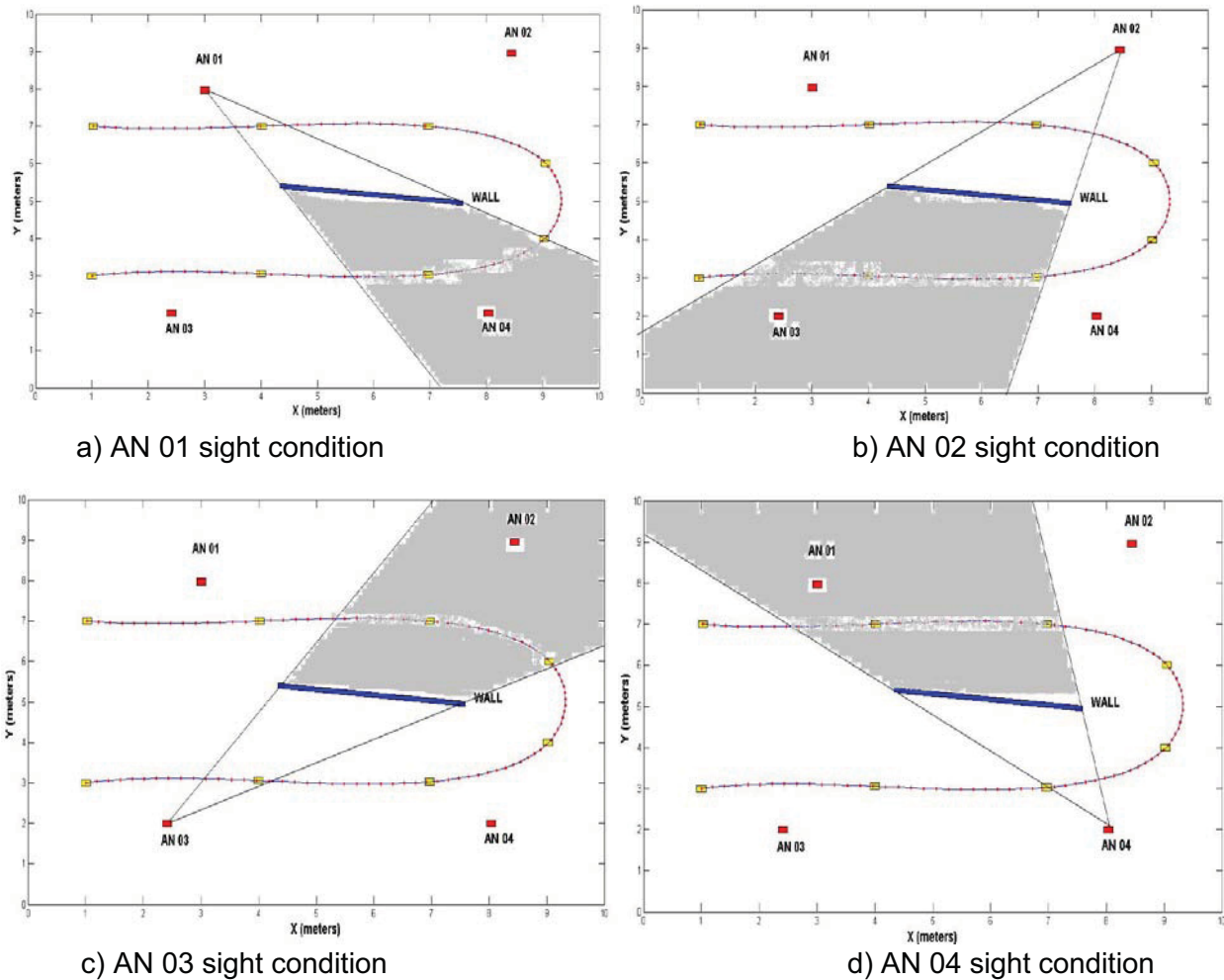
*Figure 0-28 Sight condition map for 4 ANs along with the MN trajectory in a 2D 10m by 10m room: NLOS propagation area for every AN is illustrated by gray color*

Measurements are simulated according to Eq. (0-66) and EKF-SLAM and FastSLAM algorithm are implemented for different scenarios: 4 APs, 3 FPs-1 AP, and 4 FPs to investigate the effect of knowledge of the AN location(s) over localization accuracy.

A single Monte Carlo simulation is carried out for the tracking example illustrated in Figure 0-29 based on system model 1, referred as case 1. For better visual purposes, the MN path has been generated smoother and shorter for only 100 points and the two sided 95% confidence region ellipse for the MN location estimate is plotted for every 10 time step. This figure compares the true trajectory (blue line with red square representing the sampled actual

MN location) with the estimated one (black thick line with yellow dots representing the MN location estimates) obtained by EKF-SLAM in left side and FastSLAM in right side. The MN localization errors can be appreciated by looking at the lines that connect the true and the estimated MN positions in Figure 0-29(a)–(e). It must be noted in all simulations the true MN location is inserted as initial condition of MN trajectory which can fix the origin of coordinate system; however, the coordinate system still has rotational DOF unless another known-located point fixes the coordinate system such an AP or a FP can be located with good approximation before the algorithm diverges. The number of ANs in NLOS conditions are plotted in Figure 0-30 for each position of the MN along the path. It can be seen that for time interval $[22,31]$, half of ANs are blocked by the wall and FP locations estimates still have high uncertainty, leading to large MN localization errors.
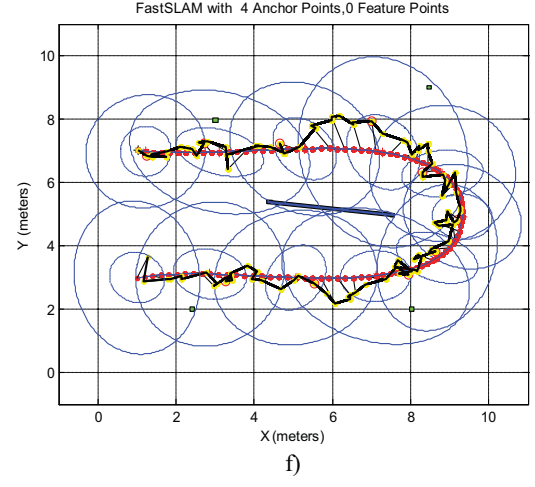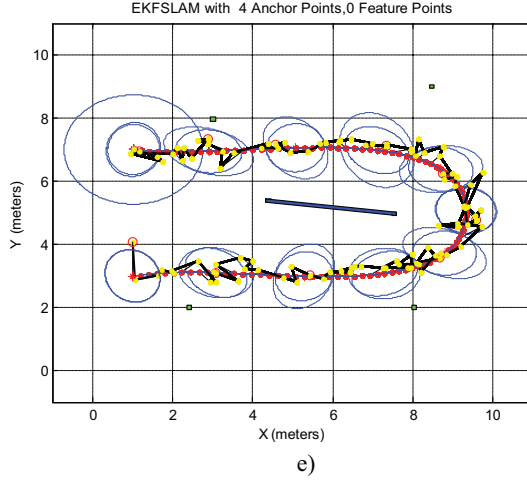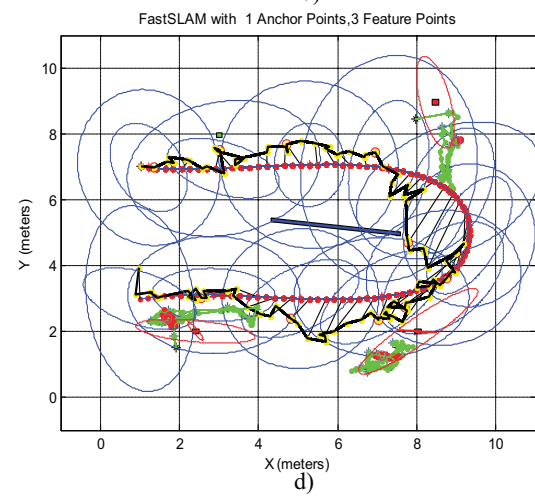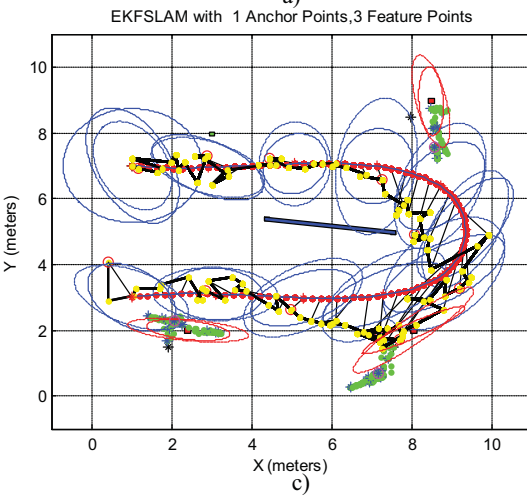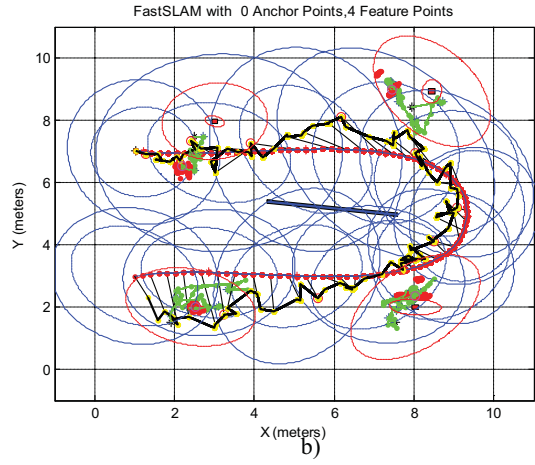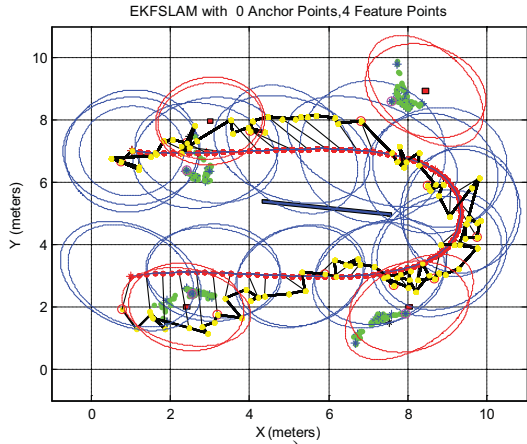
**Figure 0-29 Example of MN tracking and ANs mapping for system model 1**

a) 4 FPs                    b) 3 FPs- 1 AP
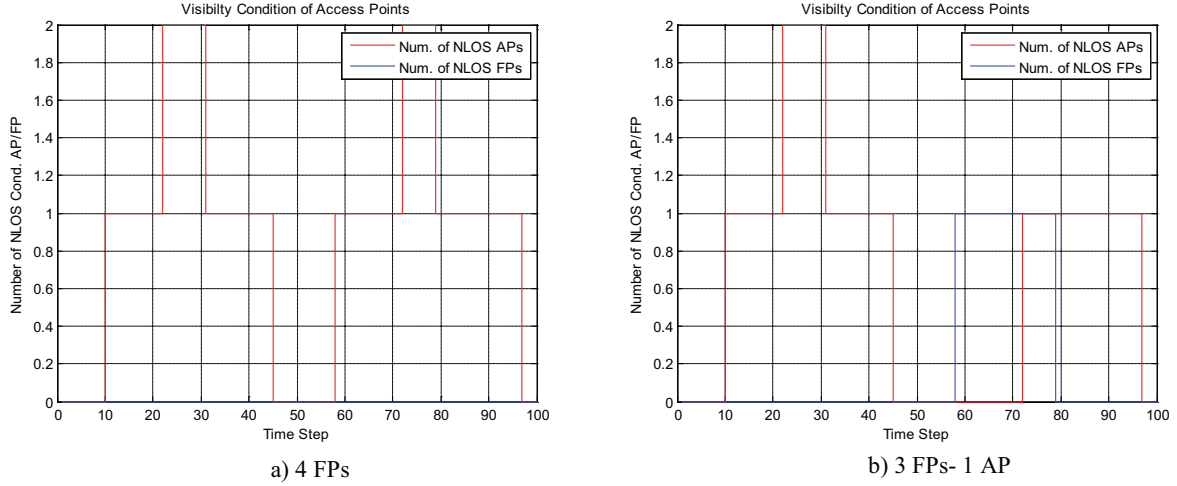
**Figure 0-30 Number of ANs (APs/FPs) in NLOS condition**

The 95% confidence region for the MN location and FP locations calculated based on corresponding submatrixes of $\left[ J_{tot}\left(\mathbf{q}_{1:t}\right)\right]^{-1}$ to their state variables. The semiaxes of the confidence region ellipse is $g$ times of square roots of the Eigen values of this corresponding submatrix. For example, the ellipse formula for the MN location estimate is calculated as

$$\left(\mathbf{p}_t - \hat{\mathbf{p}}_t\right)^T J_{to}\left(\mathbf{p}_{tt}\right)\left(\mathbf{p}_t - \hat{\mathbf{p}}_t\right) = g^2 \qquad \textit{0-138}$$

where $J_{tot}\left(\mathbf{p}_t\right) = \left[\left[J_{tot}\left(\mathbf{q}_{1:t}\right)^{-1}\right]^{MN}_{2\times2}\right]^{-1}$ and $\left[J_{tot}\left(\mathbf{q}_{1:t}\right)^{-1}\right]^{MN}_{2\times2}$ is the corresponding submatrix of

$\left[J_{tot}\left(\mathbf{q}_{1:t}\right)\right]^{-1}$ to the MN location variables. For a single run MC and 2D location variable

$g = F_{\chi 2}^{-1}(0.95) = 2.447$, where $F_{\chi 2}^{-1}$ is the inverse function of second order chi-square CDF. The confidence region obtained by the BFIM is also compared with the confidence region provided by the covariance matrix of the approximated posterior PDF from EKFSLAM or FastSLAM. For FastSLAM, the posterior PDF covariance matrix of the MN location estimate is approximated from distribution of particles, and for the AN location estimate, is approximated by spread of $N_p$ FP estimates obtained in each EKF run.

For a single MC run, it can be seen that FastSLAM and EKFSLAM performance in terms of MN/FP location estimates are comparable for 4-FP scenario. However, the concentrated estimates of FP locations in red dots illustrates that FastSLAM becomes overconfident. This is also observed from the large difference between the confidence region obtained from BFIM and estimated FP covariance matrix. This is due to inability of FastSLAM to maintain particle diversity over long periods of time. The effect of single AN location knowledge over EKFSLAM and FastSLAM performance can be observed by comparing Figure 0-29 (a)-(b) to Figure 0-29 (c)-(d). Finally, in Figure 0-29 (e)-(f) where it is assumed that there is no ambiguity about FP location, the EKF performed far superior regarding uncertainty estimation; however, in FastSLAM, uncertainty estimation degrades as a function of trajectory length.

For all ANs, Figure 0-31 shows the actual MN-AN distance and the corresponding estimates by EKFSLAM and FastSLAM. For the NLOS area, the distance is estimated based on the last FP location estimate and current MN location estimate. It can be seen that however the MN localization error can reach to 2 meters, the ranging error remains lower than 1 meter, except NLOS areas of AN 03 and AN 04 where the FP is occluded while its uncertainty is moderate. EKFSLAM and FastSLAM have almost similar ranging accuracy; however, EKF have slightly better performance in NLOS areas. EKFSLAM allows FP locations' uncertainty to be remembered as it saves and keeps the track of their information in terms of the covariance matrix. Moreover, the correlation between states in the covariance matrix allows the FP location estimate to be updated in its NLOS area. Whenever they reappear, this information is re-called and the estimate can also be highly improved due to its correlation with MN location and other FP estimates specially if other FP locations' estimates have obtained good accuracy. However, in the FastSLAM method, whenever a FP goes out of sight, the resampling may discard most of the particles relating to that FP, so eventually the entire FP location history map is lost and cannot be recovered if the FP reappears.

a) AN 01        b) AN 02

c) AN 03        d) AN 04
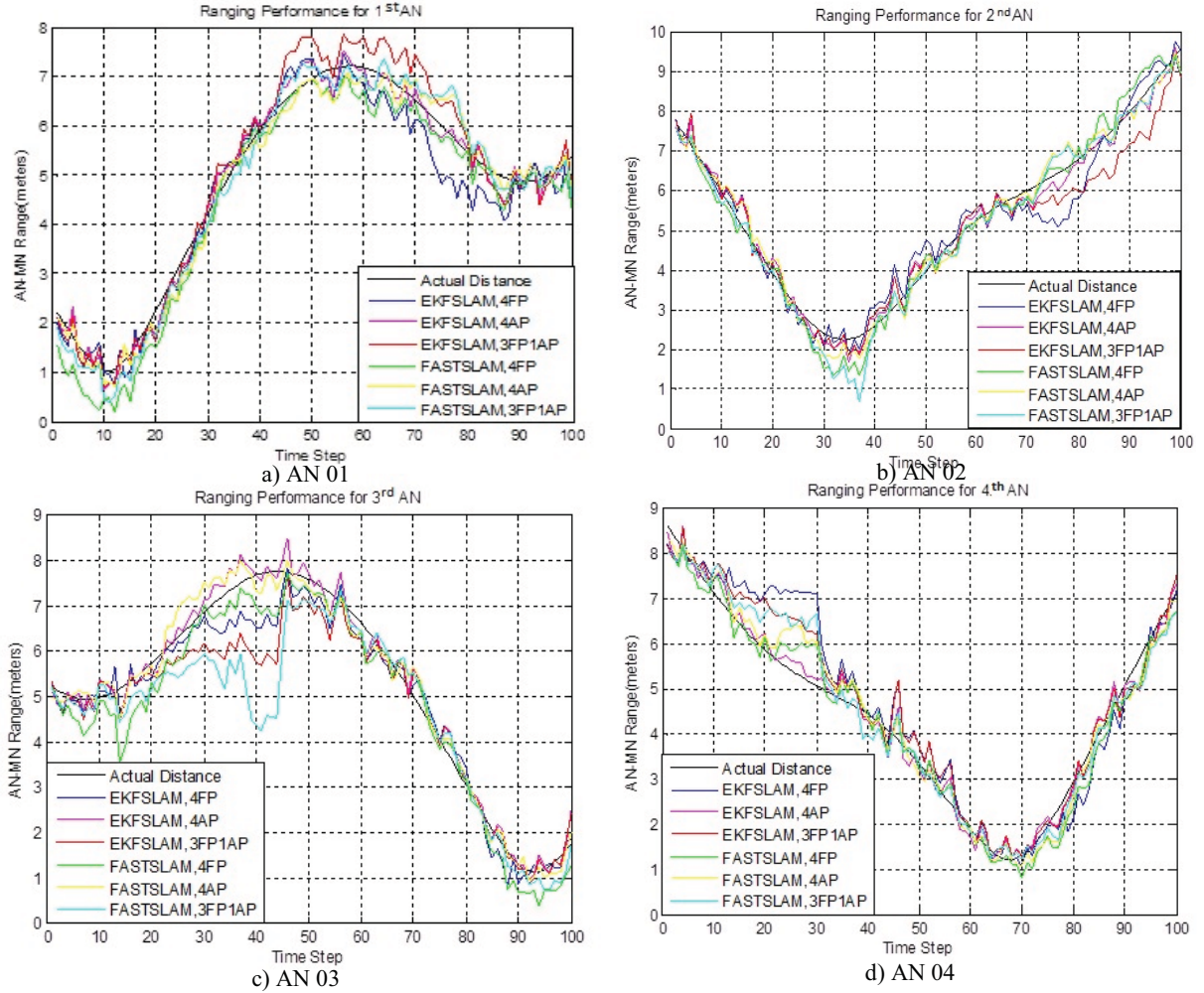
*Figure 0-31 MN-ANs actual and estimated distances for case 1*

The position error bound (PEB), obtained by trace of the corresponding submatrix of the BFIM can be utilized to evaluate the localization result error instead of the whole BFIM which also includes nuisance parameters information. As an extension of Eq. (0-113) for OWLS, we modified this bound for both the MN location estimate and FP locations estimates, given by

$$E\left\{\left(x_t - \hat{x}_t\right)^2 + \left(y_t - \hat{y}_t\right)^2\right\} \geq tr\left\{\left[J\left(\mathbf{q}_{1:t}\right)^{-1}\right]_{2\times2}^{MN}\right\}$$   *0-139*

$$E\left\{\left(m_{i,x} - \hat{m}_{i,x,t}\right)^2 + \left(m_{i,y} - \hat{m}_{i,y,t}\right)^2\right\} \geq tr\left\{\left[J\left(\mathbf{q}_{1:t}\right)^{-1}\right]_{2\times2}^{FP,i}\right\}$$

where $\left[J_{tot}\left(\mathbf{q}_{1:t}\right)^{-1}\right]_{2\times2}^{MN}$ and $\left[J_{tot}\left(\mathbf{q}_{1:t}\right)^{-1}\right]_{2\times2}^{FP,i}$ are the $2\times2$ submatrixes of inverse FIM corresponding to the MN location and $i^{th}$ FP location variables, respectively. Since the true joint

probability density function is not available; to calculate the left side, the expectation is approximated by averaging over N=50 Monte Carlo simulation runs,

$$E\left\{\left(x_t - \hat{x}_t\right)^2 + \left(y_t - \hat{y}_t\right)^2\right\} \approx \frac{1}{N}\sum_{n=1}^{N}\left(\left(x_t - \hat{x}_t\right)^2 + \left(y_t - \hat{y}_t\right)^2\right)_n \qquad \textbf{0-140}$$

The 50-run average position error plots for the MN location and FP locations are shown in Figure 0-30 for both EKF-SLAM and FastSLAM estimates. It can be seen that FastSLAM, unlike its overconfident uncertainty, outperforms EKFSLAM in terms of MN location error, except in interval [80,100] when the information from re-seen AN01 and AN02 must be restored. In loop closure, when the MN moves through unknown trajectory, and at some points encounters FPs which are not seen for a long time, maintaining the correlation between estimates is very essential in a SLAM algorithm. In EKFSLAM, it is maintained directly in the covariance matrix while in FastSLAM, it is maintained through particles diversity. Unfortunately, in FastSLAM, new observations cannot improve the FP location estimates observed prior to this point, thus their correlation to the particles degrades and corresponding particles are discarded eventually through resampling. Moreover, PEB plots can reveal how much new information can improve the localization accuracy and if it worth to use it. Comparing PEB results for 4-FP and 3 FP- 1 AP scenarios in Figure 0-32, it can be inferred that for the given example, the knowledge of a single FP location improves position error MN location estimate approx. by 0.2 meters.
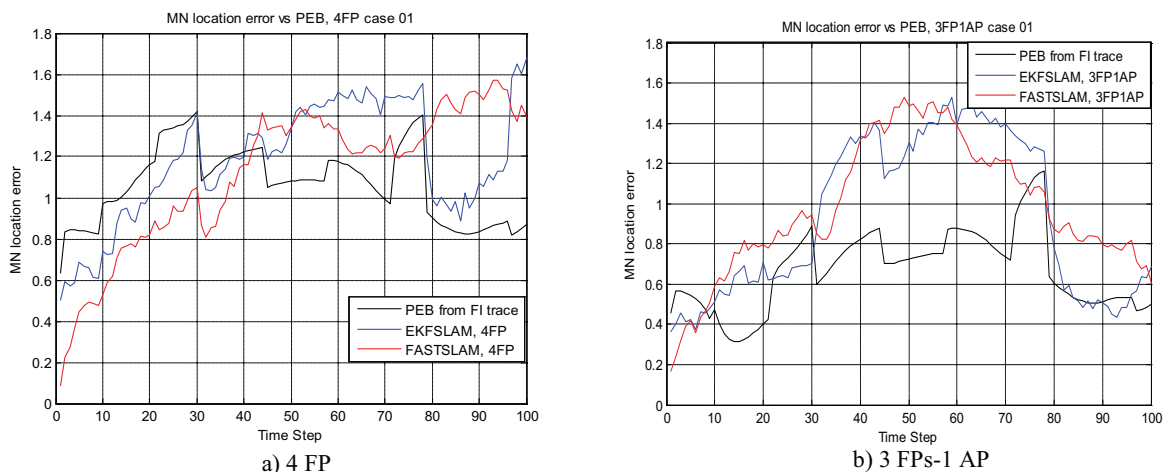


*Figure 0-32 MN position error in meters for case 1*

Figure 0-33 shows the FP04 position error and PEB obtained from the BFIM. It is illustrated that in a Gaussian linear system, FP PEB will converge to zero; however, as FastSLAM or EKFSLAM cannot guarantee this convergence due to system nonlinearity. Another interesting observation from comparison between Figure 0-33 and Figure 0-32, both EKFSLAM and FastSLAM can achieve PEB for the MN location with good approximation but not for the FP location estimates. Therefore, the total Euclidian distance between true state vector and estimated state vector is dominated by the FP location error as shown in Figure 0-31. It must be mentioned that effect of initial conditions is not considered in MC simulation and the results is averaged for 50 realizations of measurement model with constant initial condition for MN/FP locations.
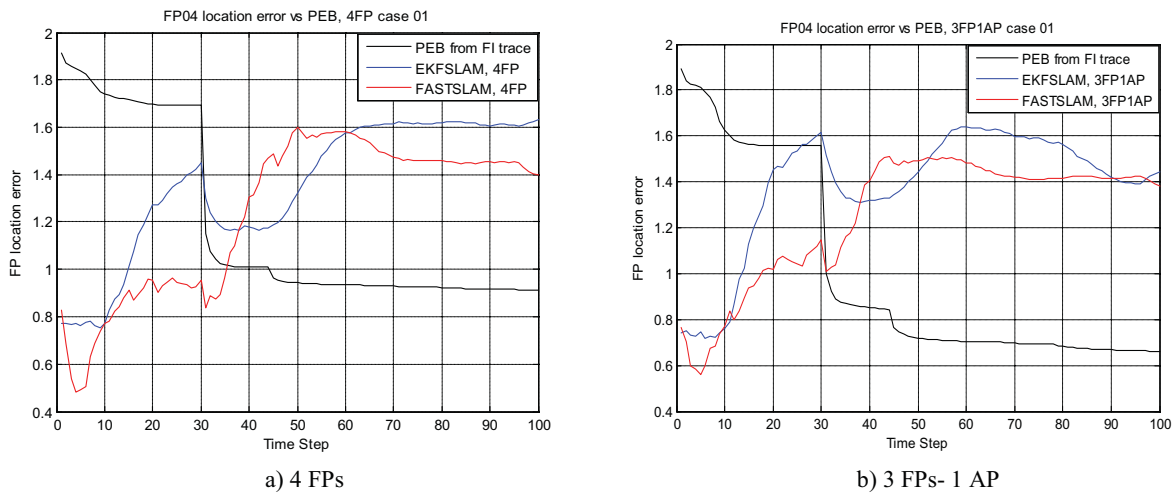


a) 4 FPs                                    b) 3 FPs- 1 AP

**Figure 0-33 FP04 position error in meters for case 1**

a) 4 FPs                    b) 3 FPs- 1AP
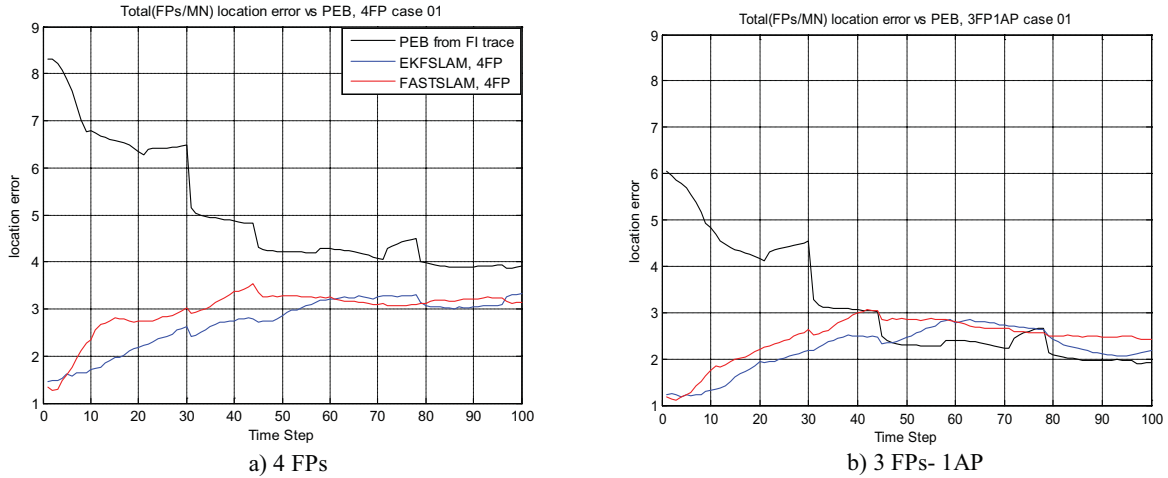
**Figure 0-34 Total MN/FPs location error in meters for case 1**

Another measure to characterize the SLAM performances is known by NEES $\varepsilon_q$ , earlier outlined in Eq. (0-114). Nonlinearity nature of SLAM prevents it to find an efficient solution by FastSLAM or EKFSLAM. However, averaged NEES, $\overline{\varepsilon}_q$, as defined in Eq. (0-115) over N runs can still be used to evaluate the SLAM performance for inconsistency. It is due to the fact that since the error sequence is correlated, a single run NEES cannot follow the chi-square distribution. Given N=50 runs, the consistency of both solutions are evaluated by averaged NEES as given in Eq. (0-114) and (0-115) for the MN location, ANs location, and the whole state vector. Given the hypothesis of a consistent linear-Gaussian filter, averaged NEES has a chi-squared density with $N \dim(\mathbf{q}_t)$ degrees of freedom

Thus, with N =50, the two sided 95% probability confidence region for the 2-dimensional location (for the MN or any FP), is bounded by the interval [1.48,2.59], for the $2 + 2N_{fp}$ - dimensional state vector is bound by the interval [6.93,9.15]. If $\overline{\varepsilon}_q$ rises significantly higher than the upper bound, the filter is optimistic, if it tends below the lower bound, the filter is conservative. As shown in Figure 0-35 and Figure 0-36, there is a discernible difference between EKFSLAM and FastSLAM in terms of NEES. The measure of performance obtained by

EKFSLAM for MN location and FP locations, corresponding marginal posterior PDF covariance matrix, is far superior since the calculated NEES stays within consistency bounds and close to the dimensionality of state space (2, here for the FP location or MN location). NEES statistics indicated that FastSLAM underestimates the covariance matrix due to loss of particles diversity. However, EKFSLAM performance is consistent in state space of MN location and FP location separately; it underestimates the posterior covariance matrix for overall state space as shown in Figure 0-37.
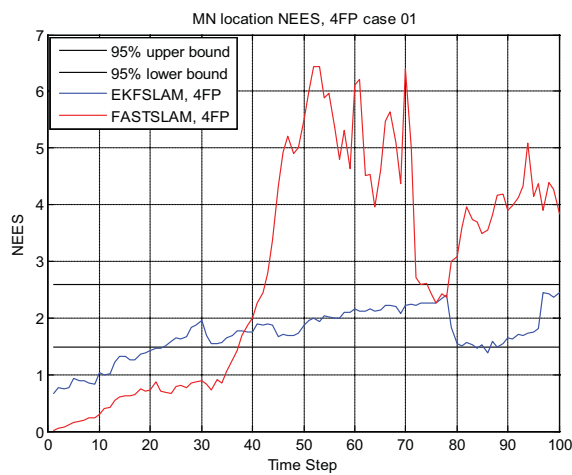


**Figure 0-35 MN location averaged NEES from EKFSLAM and FastSLAM for case 1**
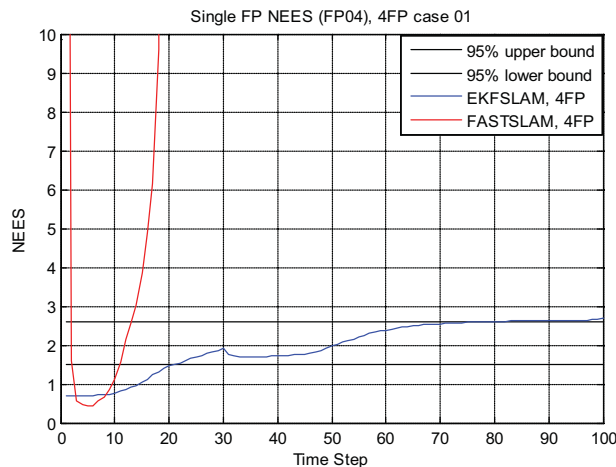


**Figure 0-36 FP04 location NEES from EKFSLAM and FastSLAM for case 1**
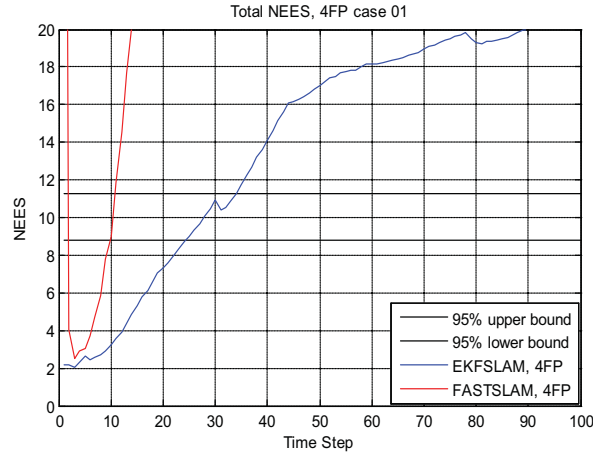
*Figure 0-37 Total state NEES from EKFSLAM and FastSLAM for case 1*

**System model 2: synchronized ANs, MN not synchronized with ANs, known sight conditions**

The previous case modeled an idealistic SLAM problem where the MN-ANs links are synchronized. In practical situation, the MN clock is subject to drift, leading to bias error in TOA or range measurements. As earlier explained in chapter 03, the random effect of MN clock drift is modeled as a random walk process which can be estimated to mitigate its effect on the MN location estimate and FP mapping. The effect of new augmented nuisance variable is investigated and the result is compared with the case where it is ignored.

**EKFSLAM solution for case 2**

For the expanded state vector, $\mathbf{q}_t = [\mathbf{p}_t \quad \mathbf{b}_t \quad \mathbf{m}_{fp}]^T$, the Gaussian posterior PDF is approximated by

$$\begin{bmatrix} \hat{\mathbf{p}}_{t|t} \\ \hat{b}_{t|t} \\ \hat{\mathbf{m}}_{fp,t} \end{bmatrix} = \begin{bmatrix} \hat{\mathbf{p}}_{t|t-1} \\ \hat{b}_{t|t-1} \\ \hat{\mathbf{m}}_{fp,t-1} \end{bmatrix} + \mathbf{K}_t \left[ z_t - h(\hat{\mathbf{p}}_{t|t-1}, \hat{b}_{t|t-1}, \hat{\mathbf{m}}_{fp,t-1}) \right] \tag{0-141}$$

$$\Sigma_{t|t} = \Sigma_{t|t-1} + \mathbf{K}_t \mathbf{D}_t \mathbf{K}_t^T$$

where $\hat{\mathbf{p}}_{t|t-1}$ and $\Sigma_{pp,t|t-1}$ are the mean and covariance matrix of apriori PDF, stated by

$$\begin{bmatrix} \hat{\mathbf{p}}_{t|t-1} \\ \hat{b}_{t|t-1} \\ \hat{\mathbf{m}}_{fp,t-1} \end{bmatrix} = \begin{bmatrix} \hat{\mathbf{p}}_{t-1|t-1} \\ \hat{b}_{t-1|t-1} \\ \hat{\mathbf{m}}_{fp,t-1} \end{bmatrix}$$

$$\Sigma_{t|t-1} = \Sigma_{t-1|t-1} + F^T Q F$$

and

$$F = \begin{bmatrix} 1 & 0 & 0 & 0 & \cdots & 0 \\ 0 & 1 & 0 & 0 & \cdots & 0 \\ 0 & 0 & 1 & 0 & \cdots & 0 \end{bmatrix}$$

$$\underbrace{\qquad\qquad\qquad}_{3+2N_{fp}}$$

*0-142*

$$\mathbf{D}_t = H \Sigma_{t|t-1} H^T + R_t$$

$$\mathbf{K}_t = \Sigma_{t|t-1} H^T \mathbf{D}_t^{-1}$$

$H$ is the Jacobian matrix of range measurement function, evaluated at

$\hat{\mathbf{q}}_{t|t-1} = [\hat{\mathbf{p}}_{t|t-1} \quad \hat{\mathbf{b}}_{t|t-1} \quad \hat{\mathbf{m}}_{fp,t-1}]^T$, where the elements are defined in Eq. (0-100) and (0-101).

**FastSLAM solution for case 2**

Since the range offset is common between all ANs measurement, the joint posterior PDF is factorized based on Rao-Blackwellizied theorem for case 2 as follows

$$p(\mathbf{p}_{1:t}, b_{1:t}, \mathbf{m}_{fp} \mid \mathbf{z}_{1:t}) = p(\mathbf{p}_{1:t}, b_{1:t} \mid \mathbf{z}_{1:t}) \prod_{i=1}^{N_{FP}} p(\mathbf{m}_{fp,i} \mid \mathbf{p}_{1:t}, b_{1:t}, \mathbf{z}_{1:t})$$

*0-143*

The trajectory of MN locations and range offsets is represented by weightening samples and the map is computed analytically using the EKF algorithm. The $m^{th}$ particle of the posterior PDF, at time step $t$, represents not only the history of MN locations but also the history on range offsets.

The apriori PDF is approximated by $N_p$ independent and identically distributed (i.i.d) samples (particles),

$$p(\mathbf{p}_{1:t}, b_{1:t} \mid \mathbf{z}_{1:t-1}) \approx \frac{1}{N_p} \sum_{m=1}^{N_p} \delta\left(\mathbf{p}_{1:t} - \mathbf{p}^{[m]}_{1:t}\right) \delta\left(b_{1:t} - b^{[m]}_{1:t}\right)$$

*0-144*

which is drawn from proposal distribution, $p(\mathbf{p}_t, b_t \mid \mathbf{p}_{t-1}^{[m]}, b_{t-1}^{[m]}, \mathbf{m}_{fp}^{[m]})$. Then similar to previous case, for each particle, an EKF update is performed over the observed ANs as a simple mapping operation under the known MN location and range offset assumption.

For the same trajectory used for case 1, the proposed EKFSLAM and FastSLAM solution are applied for a single Monte Carlo simulation run of system model 1. The initial conditions, measurement noise, and process noise parameters have kept the same as the ones used in case 01 for comparison purposes, except the measurement with range offset model according to Eq. (0-67) is used for generating range measurement data.

Figure 0-38 (a)-(d) compare the EKFSLAM and FastSLAM performance in a single run MC for 4 FPs and 3 FPs-1 AP scenarios where the range offset is tracked along with other location parameters, and Figure 0-38 (e)-(f) illustrates their performance where the range offset effect is not ignored. For the 4 FPs scenario, the FastSLAM shows a slightly better performance than the EKFSLAM, as shown in Figure 0-38 (a)-(b), while their performance is comparable in the 3 FPs- 1 AP scenario, as shown in Figure 0-38(c)-(d). Since the FastSLAM tracks its solutions in a wide area of room through particles, it shows higher robustness to ambiguous and uncertain situation in comparison to the EKFSLAM such as 4 FPs case when there is no knowledge about source locations. The effect of range offset is observed in Figure 0-38(e)-(f), where MN localization error is increased to more than 1 meter for most of the MN trajectory while it is less than 1 meter in average when the range offset is modeled, as illustrated Figure 0-38(a)-(b). The range offset estimates along trajectory for both EKFSLAM and FastSLAM are shown in Figure 0-37.
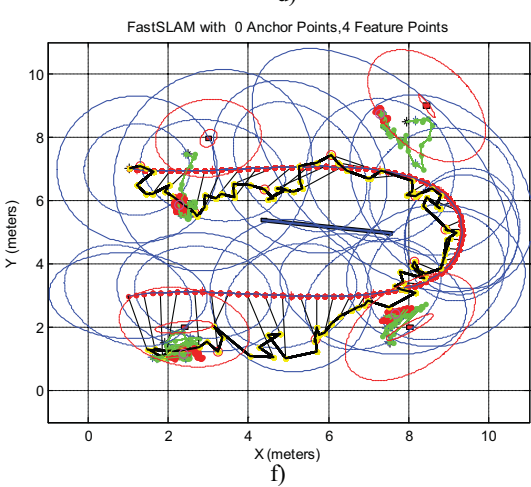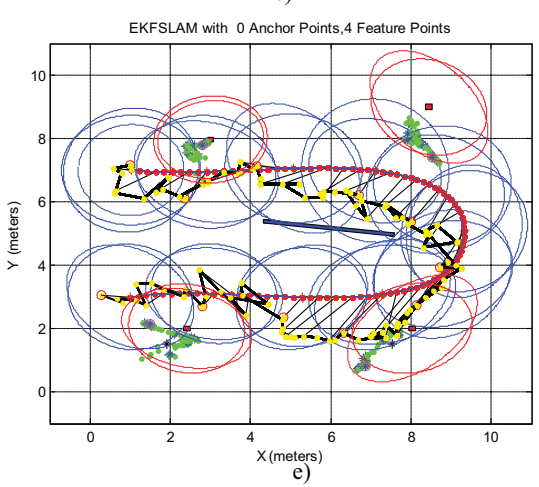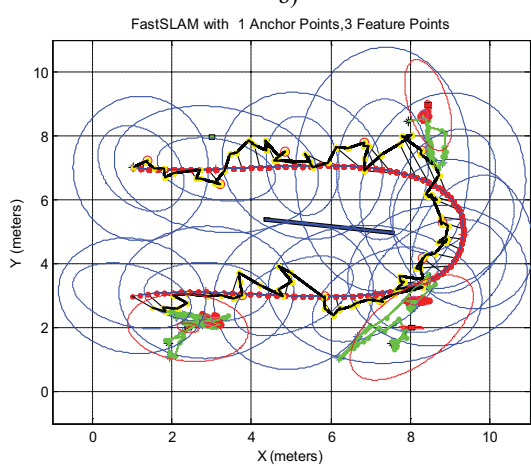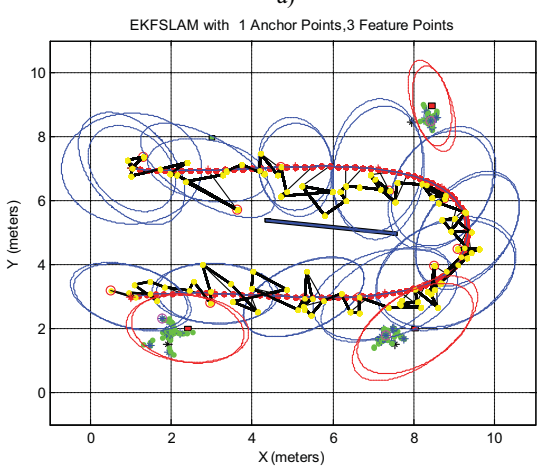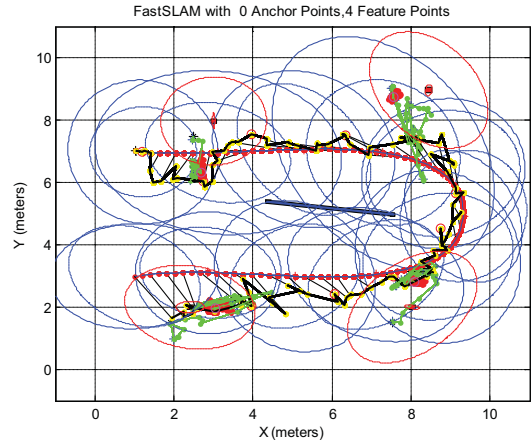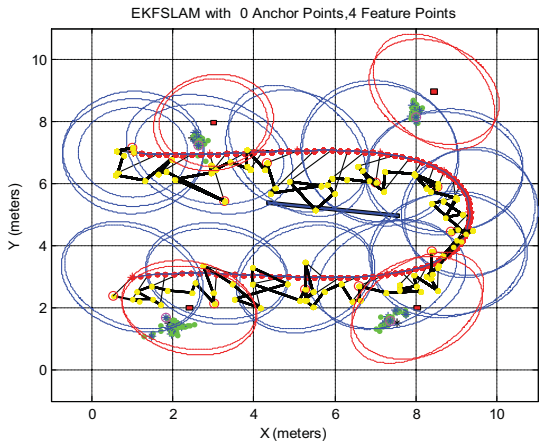
**Figure 0-38 Example of MN tracking and ANs mapping for system model 2**
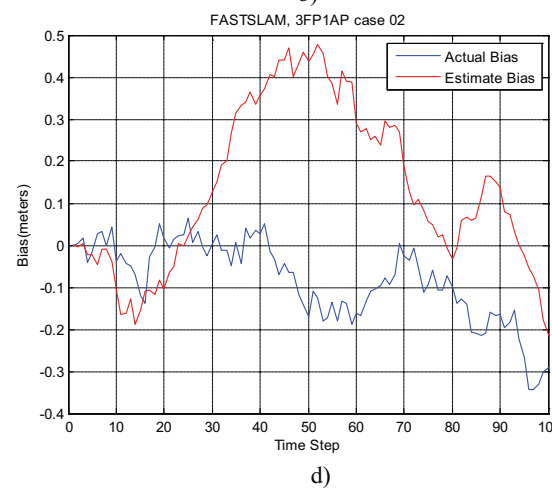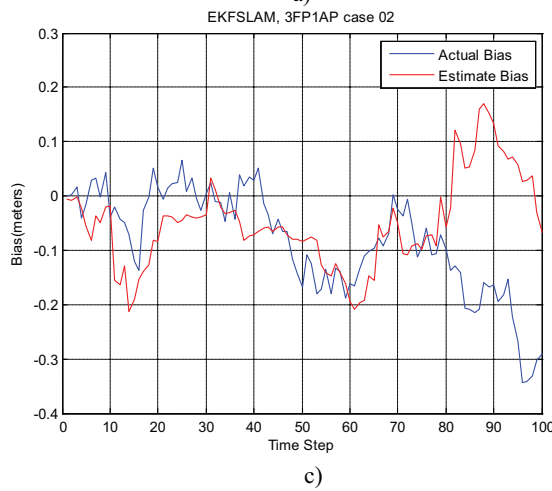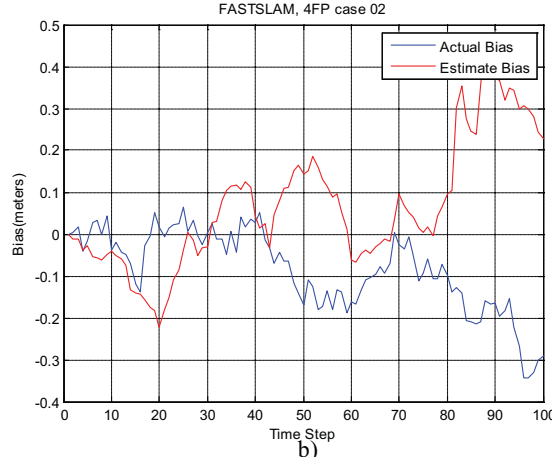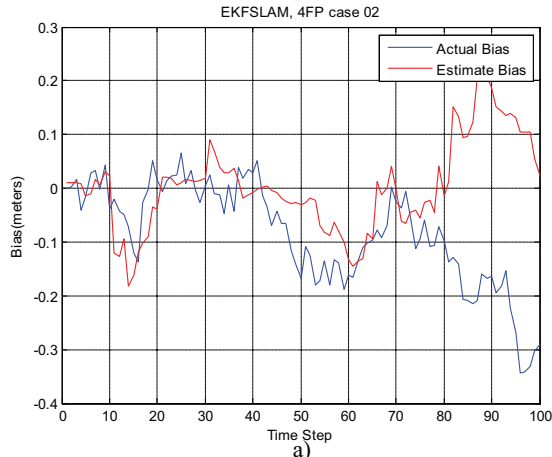
**Figure 0-39 Bias tracking for case 2**

For case model 2, Figure 0-40 shows the actual MN-ANs distances and the corresponding estimates obtained by EKFSLAM and FastSLAM. For the NLOS area, the ranging information is blocked with a grey rectangular. It is shown range estimation is exact (with error less than 0.5 meter) for all methods even when bias effect is ignored, while the MN localization error reaches to 2 meters.
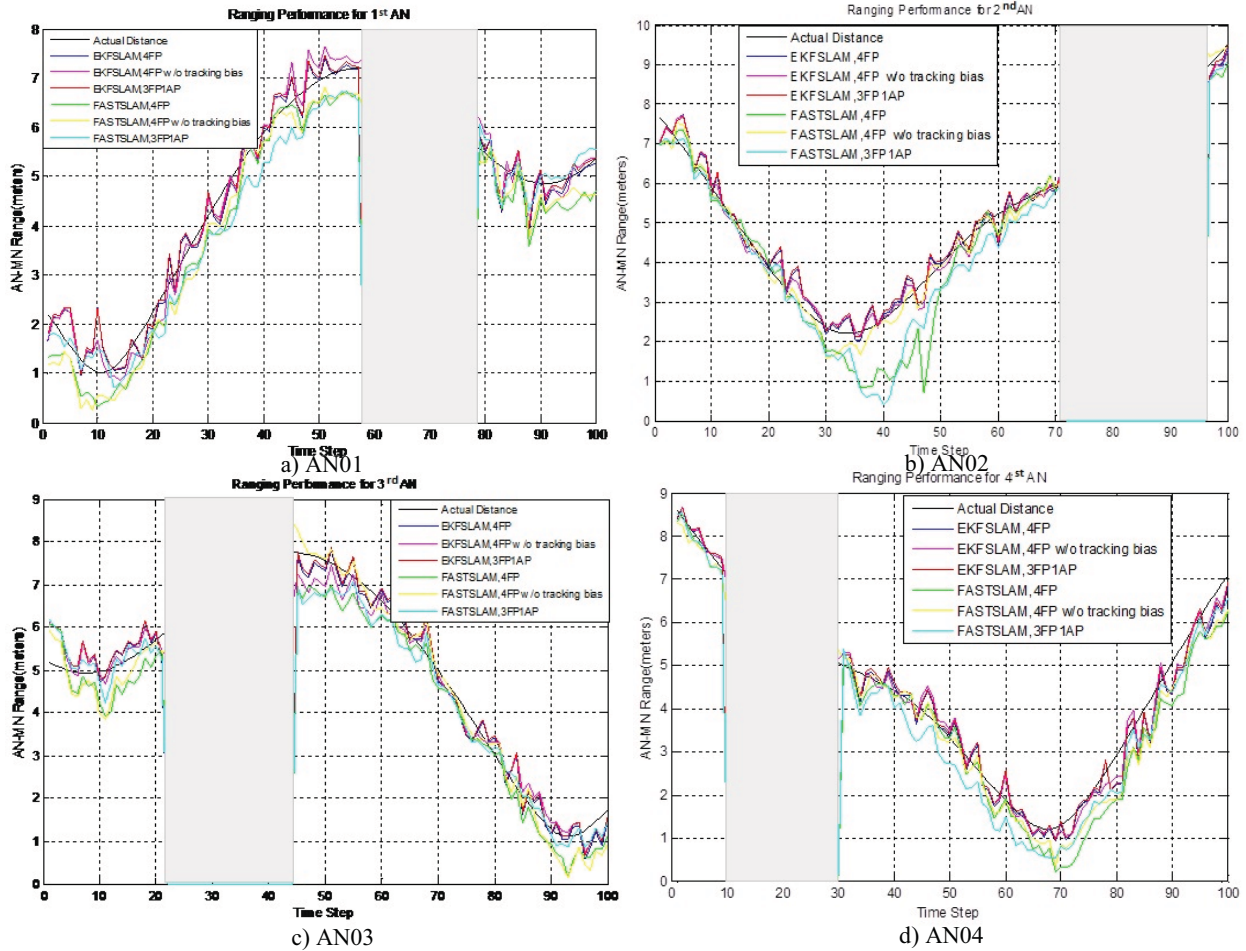
**Figure 0-40 MN-ANs actual and estimated distances for case 2**

The 50-run average position errors for the MN location, FP 04 location and total state is shown in Figure 0-41, Figure 0-42, Figure 0-43, for both EKF-SLAM and FastSLAM estimates. Unlike the expectation from single MC run results, MN position error obtained by FastSLAM is higher than position error obtained by EKFSLAM. This is because FastSLAM performance is not consistent, as also observed in case 1, due to particle diversity loss. FastSLAM particles does not represent a momentary MN location and/or range offset; they represent the entire MN trajectory and range offset history. The dimension of state space increases with time while the number of particles representing this large state-space dimension become insufficient. This is observed as the degradation of FastSLAM performance in the case 2 in comparison with its performance in the case 1 where it outperformed EKFSLAM in term of MN location error

(excluding loop closure areas). The results comply with consistency test obtained by NEES test shown in Figure 0-44, Figure 0-45, and Figure 0-46.
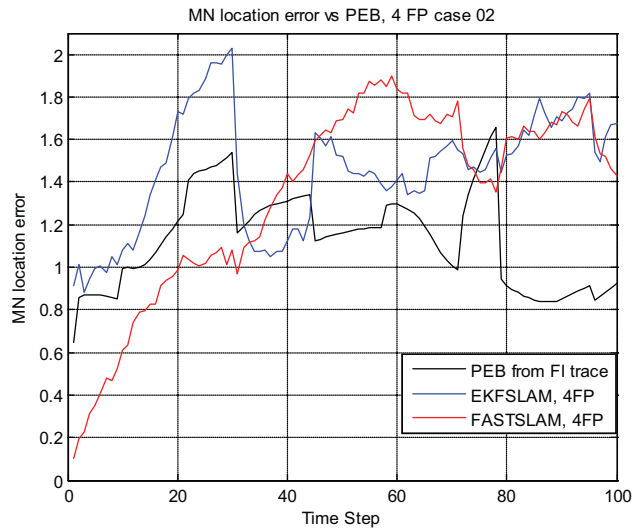


**Figure 0-41 MN position error in meters for case 2**
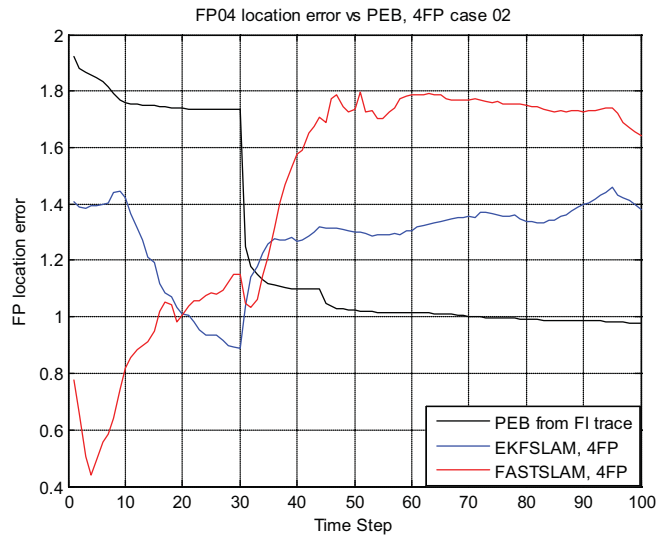


**Figure 0-42 FP04 position error in meters for case 2**
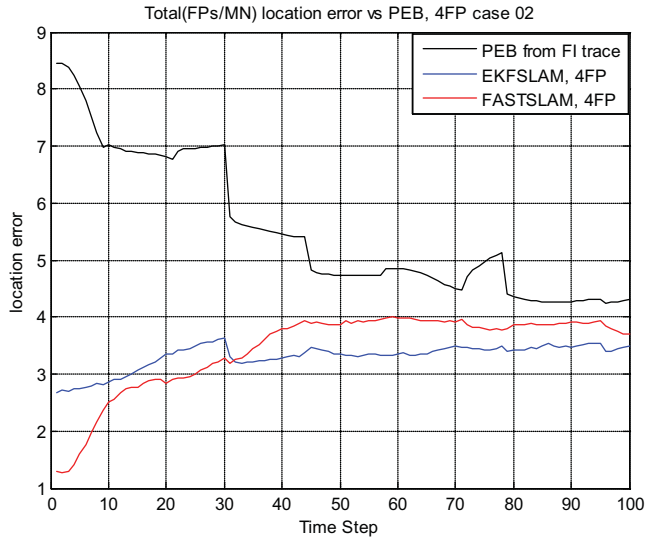
**Figure 0-43 Total state error in meters for case 2**
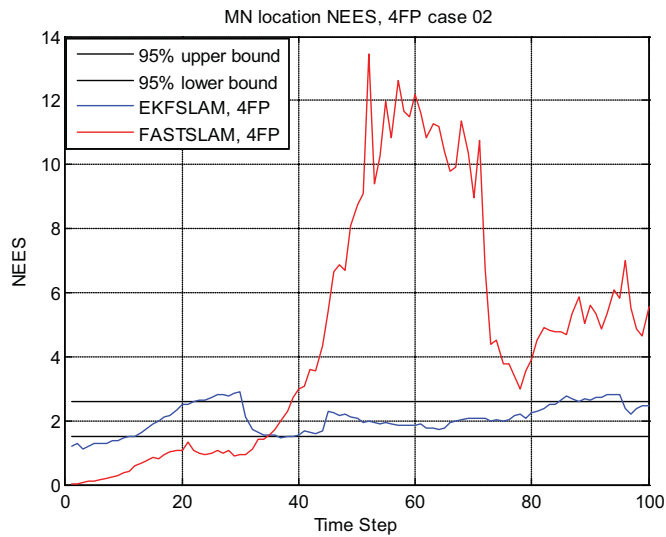


**Figure 0-44 MN location averaged NEES from EKFSLAM and FastSLAM for case 02**
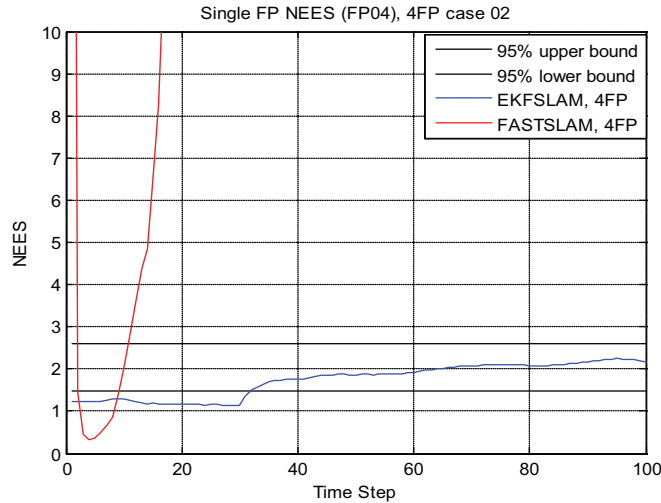
*Figure 0-45 FP04 location NEES from EKFSLAM and FastSLAM for case 02*
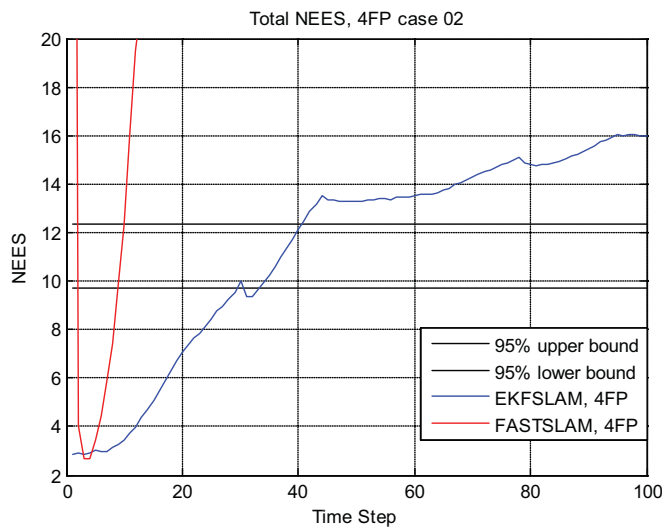


*Figure 0-46 Total state NEES from EKFSLAM and FastSLAM*

**System model 3: unsynchronized ANs, MN not synchronized with ANs, known sight condition**

In the third case, the system model is extended to when the MN free running clock is not synchronized with ANs, and ANs are not time synchronized with each other. To model the range measurement data, a single bias for each MN-AN link can model both MN and ANs clock drifts. As earlier described in Section 0, the MN location state $\mathbf{p}_t$ is modeled as a first-order Markov process ruled by $\mathbf{p}_t = \mathbf{p}_{t-1} + \mathbf{v}_t$, where the $\mathbf{v}_t \sim N(0, Q_p)$. Based on smooth trajectory

assumption, the range offset vector, $\mathbf{b}_t = \begin{bmatrix} b_{1,t} & \cdots & b_{N_{AN},t} \end{bmatrix}^T$ can also be modeled as $N_{AN}$

independent first-order Markov processes, given by $\mathbf{b}_t = \mathbf{b}_{t-1} + \mathbf{v}_{b,t}$, where $\mathbf{v}_{b,t} \sim N(0, Q_b)$ and

$Q_b = diag \left\{ \sigma_{1,b}^2 \quad \cdots \quad \sigma_{N_{AN},b}^2 \right\}$. The range offset evolves independently from MN location states.

The current state vector of unknown variables is denoted by $\mathbf{q}_t = \begin{bmatrix} \mathbf{p}_t & \mathbf{b}_t & \mathbf{m}_{fp} \end{bmatrix}^T$, where $\mathbf{m}_{fp}$

is the stacked vector of the FP locations, defined by $\begin{bmatrix} m_{N_{AP+1},x} & m_{N_{AP+1},y} & \cdots & m_{N_{AN},x} & m_{N_{AN},y} \end{bmatrix}^T$.

Modified version of EKF-SLAM and FastSLAM as suboptimal solutions for this system model

are proposed based on reasonable assumptions that allow the evaluation of posterior PDF with

efficient computation.

**EKF-SLAM solution for case 3**

For the defined state vector, $\mathbf{q}_t = [\mathbf{p}_t \quad \mathbf{b}_t \quad \mathbf{m}_{fp}]^T$, the EKFSLAM approximates the

posterior PDF by multivariate Gaussian PDF where it means and covariance are given by

$$\hat{\mathbf{q}}_{t|t=} \begin{bmatrix} \hat{\mathbf{p}}_{t|t} \\ \hat{\mathbf{b}}_{t|t} \\ \hat{\mathbf{m}}_{fp,t} \end{bmatrix} = \begin{bmatrix} \hat{\mathbf{p}}_{t|t-1} \\ \hat{\mathbf{b}}_{t|t-1} \\ \hat{\mathbf{m}}_{fp,t-1} \end{bmatrix} + \mathbf{K}_t \left[ z_t - h(\hat{\mathbf{p}}_{t|t-1}, \hat{\mathbf{b}}_{t|t-1}, \hat{\mathbf{m}}_{fp,t-1}) \right]$$

$$\Sigma_{t|t} = \Sigma_{t|t-1} + \mathbf{K}_t \mathbf{D}_t \mathbf{K}_t^T$$

*0-145*

where $\hat{\mathbf{q}}_{t|t-1} = \begin{bmatrix} \hat{\mathbf{p}}_{t|t-1} & \hat{\mathbf{b}}_{t|t-1} & \hat{\mathbf{m}}_{fp,t-1} \end{bmatrix}$ and $\Sigma_{t|t-1}$ are the mean and covariance matrix of apriori

PDF, stated by

$$\hat{\mathbf{q}}_{t|t-1} = \begin{bmatrix} \hat{\mathbf{p}}_{t|t-1} \\ \hat{\mathbf{b}}_{t|t-1} \\ \hat{\mathbf{m}}_{fp,t-1} \end{bmatrix} = \begin{bmatrix} \hat{\mathbf{p}}_{t-1|t-1} \\ \hat{\mathbf{b}}_{t-1|t-1} \\ \hat{\mathbf{m}}_{fp,t-1} \end{bmatrix}$$

$$\Sigma_{t|t-1} = \Sigma_{t-1|t-1} + F^T Q F$$

*0-146*

and

$$F = \begin{bmatrix} 1 & 0 & 0 & 0 & \cdots & 0 \\ 0 & \ddots & 0 & 0 & \cdots & 0 \\ 0 & 0 & 1 & 0 & \cdots & 0 \end{bmatrix}$$

$$\underbrace{\qquad\qquad\qquad}_{2+N_{AN}+2N_{FP}}$$

$$Q = diag\left\{ Q_p \quad Q_b \right\}$$

$$\mathbf{D}_t = H \sum_{t|t-1} H^T + R_t$$

$$\mathbf{K}_t = \sum_{t|t-1} H^T \mathbf{D}_t^{-1}$$

$H$ is the Jacobian of range measurement function, evaluated at $\hat{\mathbf{q}}_{t|t-1} = [\hat{\mathbf{p}}_{t|t-1} \quad \hat{\mathbf{b}}_{t|t-1} \quad \hat{\mathbf{m}}_{fp,t-1}]^T$,

previously defined in Eq. (0-103) and (0-104).

**FastSLAM solution for case 3**

The traditional FastSLAM method is based RB factorization where the EKFs used for

FPs location is only conditioned on MN trajectory which is represented by particles. The

simulation results from case 02 showed that FastSLAM performance is very sensitive to the

dimension of state space which is represented by particles. The FastSLAM degradation due to

loss of particle diversity is observed for case 3 where the particle space's dimension is

increased to $N_{AN} \times t + 2 \times t$ where is the dimension of range offset sequence $\mathbf{b}_{1:t}$ and $2 \times t$ is

the dimension MN trajectory $\mathbf{p}_{1:t}$. In this regard, we have modified the assumption of FastSLAM

in such a way that the particle dimension can stays the same as original version (as in case 1),

$2 \times t$, but the conditioned EKF part of FastSLAM is modified to jointly estimates the low

dimension FP location and its range offset recursively. Therefore, The Rao-Blackwellization

factorization for joint posterior PDF is modified as

$$p(\mathbf{p}_{1:t}, \mathbf{b}_{1:t}, \mathbf{m}_{fp} \mid \mathbf{z}_{1:t}) = p(\mathbf{p}_{1:t} \mid \mathbf{z}_{1:t}) \prod_{i=N_{AP+1}}^{N_{AN}} p(\mathbf{m}_{fp,i}, b_{i,1:t} \mid \mathbf{p}_{1:t}, \mathbf{z}_{1:t})$$

The $m^{th}$ particle of posterior PDF, at time $t$, represents the history of MN locations

denoted as $\mathbf{p}_{1:t}^{[m]}$, which additionally contains the Gaussian parameters (the mean and

covariance matrix) of $\left\{ \mu_{1,t}^{[m]} \Sigma_{1,t}^{[m]}, ..., \mu_{N_{FP},t}^{[m]} \Sigma_{N_{FP},t}^{[m]} \right\}$ of jointly FPs location and its range offset $\left\{ w_k^i, \mathbf{p}_{1:t}^i \right\}$.

First, the FastSLAM extend the MN trajectory by drawing new sample according to the motion statistics as

$$\mathbf{p}_t^{[m]} \square\ p(\mathbf{p}_t \mid \mathbf{p}_{t-1}^{[m]}) \tag{0-149}$$

Next, for each particle, an EKF is implemented to update FP estimates and range offsets. The output of this stage is $\left\{ \mu_{i,t}^{[m]}, \Sigma_{i,t}^{[m]} \right\}$, defined by

$$\mu_{i,t}^{[m]} = \mu_{i,t|t-1}^{[m]} + K_t^{[m]}(z_t - h_i(\mu_{i,t-1}^{[m]}, p_t^{[m]})) \tag{0-150}$$
$$\Sigma_{i,t}^{[m]} = \Sigma_{i,t|t-1}^{[m]} + K_t^{[m]} D_t^{[m]} K_t^{[m],T}$$

where, for observed FPs, $i = N_{AP+1}, ..., N_{AN}$,

$$\mu_{i,t|t-1}^{[m]} = \mu_{i,t-1}^{[m]} \tag{0-151}$$
$$\Sigma_{i,t|t-1}^{[m]} = \Sigma_{i,t-1}^{[m]} + \sigma_{i,b}^2 . e_{3\times3}^3$$

for observed APs, $i = 1, ..., N_{AP}$

$$\mu_{i,t}^{[m]} = \mu_{i,t-1}^{[m]} \tag{0-152}$$
$$\Sigma_{i,t}^{[m]} = \Sigma_{i,t-1}^{[m]} + \sigma_{i,b}^2$$

and

$$D_t^{[m]} = H_t^{[m]} \Sigma_{t|t-1}^{[m]} H_t^{[m],T} + \sigma_{i,z}^2 \tag{0-153}$$
$$K_t^{[m]} = \Sigma_{t|t-1}^{[m]} H_t^{[m],T} \left[ D_t^{[m]} \right]^{-1}$$

Next, the samples weights $w_t^{[m]}$ are calculated according to importance function which is based on the conditional probability of $p\left( \mathbf{z}_t \mid \mathbf{p}_t^{[m]} \right)$. Finally, resampling is accomplished with replacement from the set $\left\{ \mathbf{p}_{0:t}^{[m]} \right\}_{m=1}^{N_P}$, including their associated AN locations' and range offsets' estimates considering each particle has probability proportional to $w_t^{[m]}$.

For the same trajectory used for case 1 and 2, the proposed EKFSLAM and FastSLAM solutions are applied for a single Monte Carlo simulation run of system model 03. The initial conditions, measurement noise, and process noise are similar to case 01 for comparison purposes, except the measurement data is generated based on the system model 3.

Figure 0-45 (a)-(d) compare the EKFSLAM and FastSLAM performance for a single run MC for 4 FPs, and 3 FPs-1 AP scenarios where the range offsets are tracked along with other location parameters; whereas Figure 0-47 (e)-(f) illustrates their performance where the range offset effect is ignored. For 4 FPs scenario, modified FastSLAM and EKFSLAM shows a similar performance, as shown in Figure 0-47 (a)-(b), while the EKFSLAM have slightly better performance for 3 FPs- 1AP , as shown in Figure 0-47 (c)-(d). The effect of range offset is observed in Figure 0-47 (e)-(f); MN localization error increases to 4 meters, EKFSLAM and modified FastSLAM which model and track range offsets provide less than 1 meter localization error. The range offset estimates within trajectory for both EKFSLAM and FastSLAM is shown in Figure 0-48.
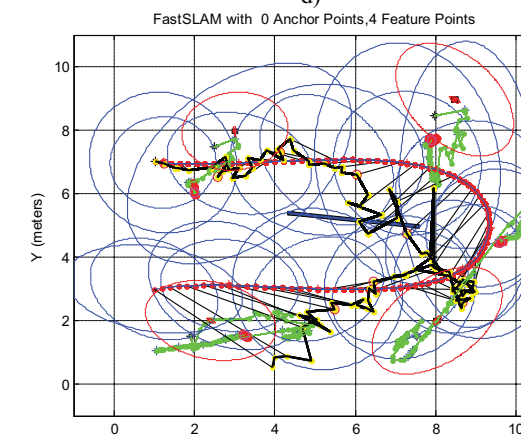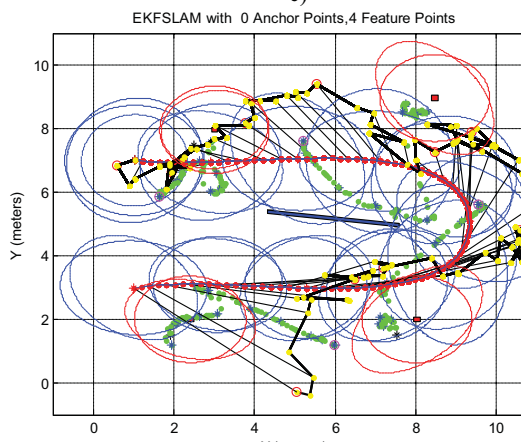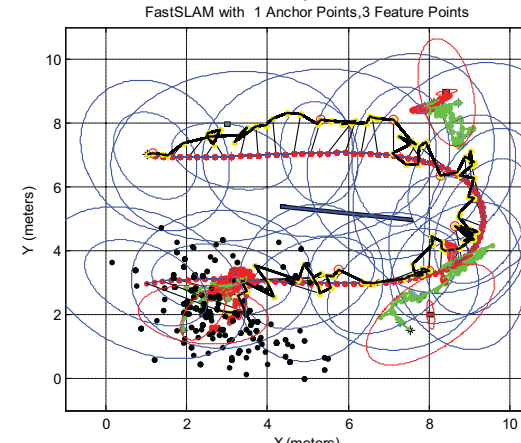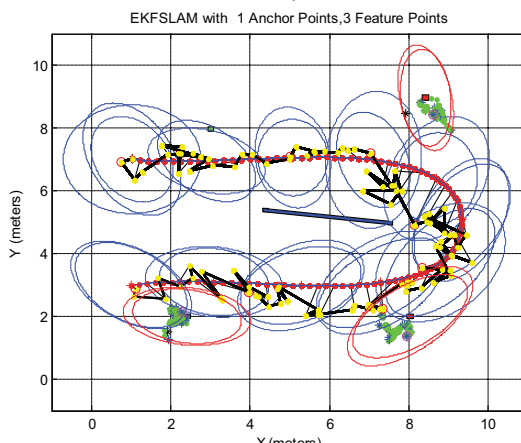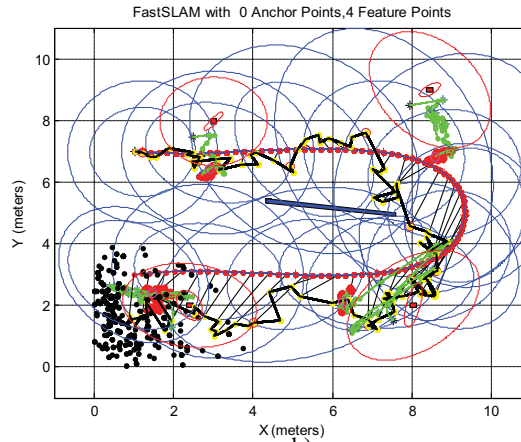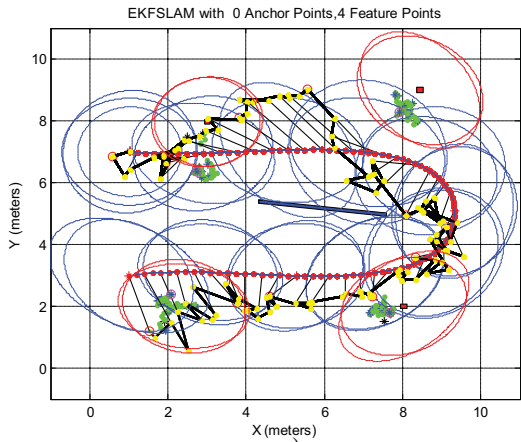
**Figure 0-47 Example of MN tracking and ANs mapping for system model 3**

a) EKFSLAM, 4 FPs

b) Modified FastSLAM, 4 FPs

c) EKFSLAM, 3 FPs- 1AP

d) FastSLAM, 3 FPs- 1AP
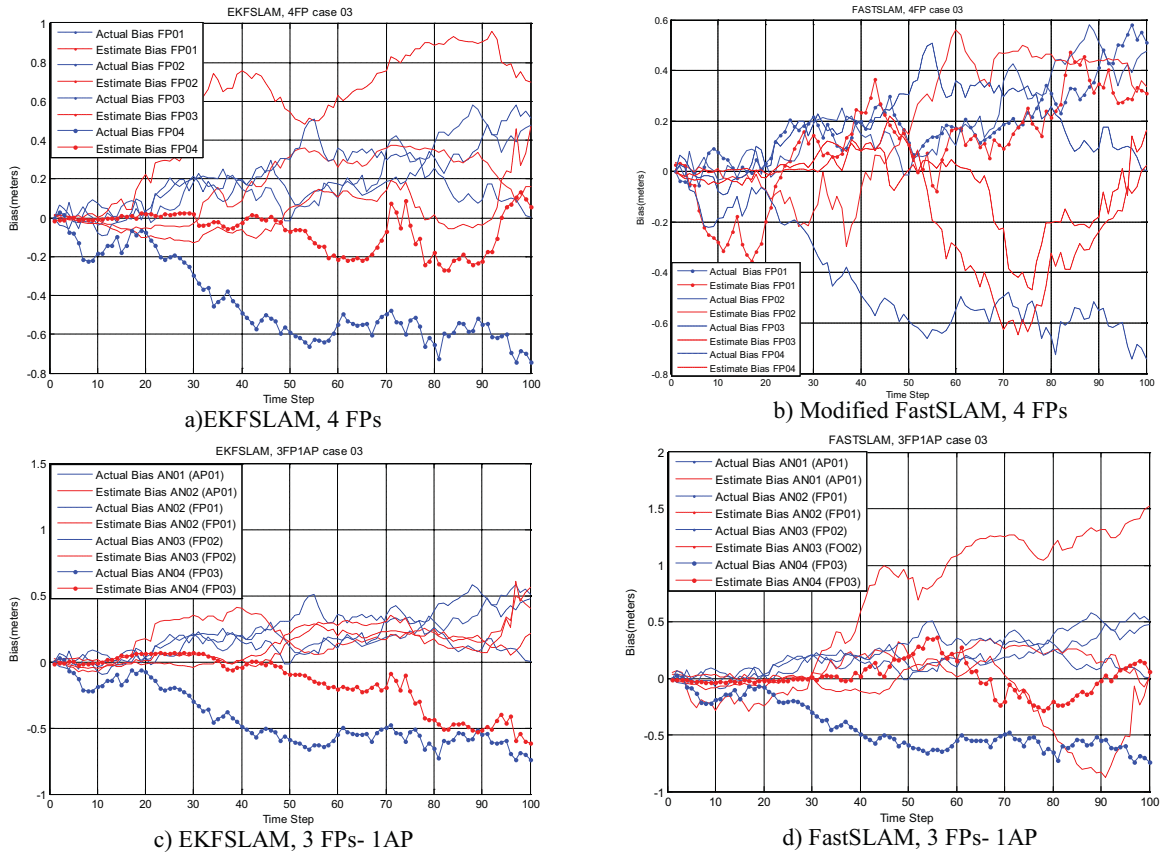
*Figure 0-48 Bias tracking for case 3*

For case 3, Figure 0-49 shows the actual MN-ANs distances and the corresponding estimates obtained by EKFSLAM and FastSLAM. It is shown range estimation is exact (with error less than 0.5 meter) for all methods even when range offset is ignored. Both EKFSLAM and FastSLAM have comparable performance in ranging accuracy.

The 50-run average position error results for the MN location, FP 04 location and total state vectors are shown in Figure 0-50, Figure 0-51, and Figure 0-52, for both EKF-SLAM and FastSLAM estimates. MN position errors obtained by both the FastSLAM and EKFSLAM are comparable and approximately near the optimal PEB bound obtained by BFIM, except loop closure area where the FastSLAM fails. In terms of FP position error, the EKFSLAM not only outperforms FastSLAM but also can reach the PEB. NEES results obtained for the modified

FastSLAM and EKFSLAM shown in Figure 0-53,Figure 0-54,Figure 0-55 evaluates the consistency of both methods.



*a) AN01*  *b) AN02*
*c) AN03*  *d) AN04*
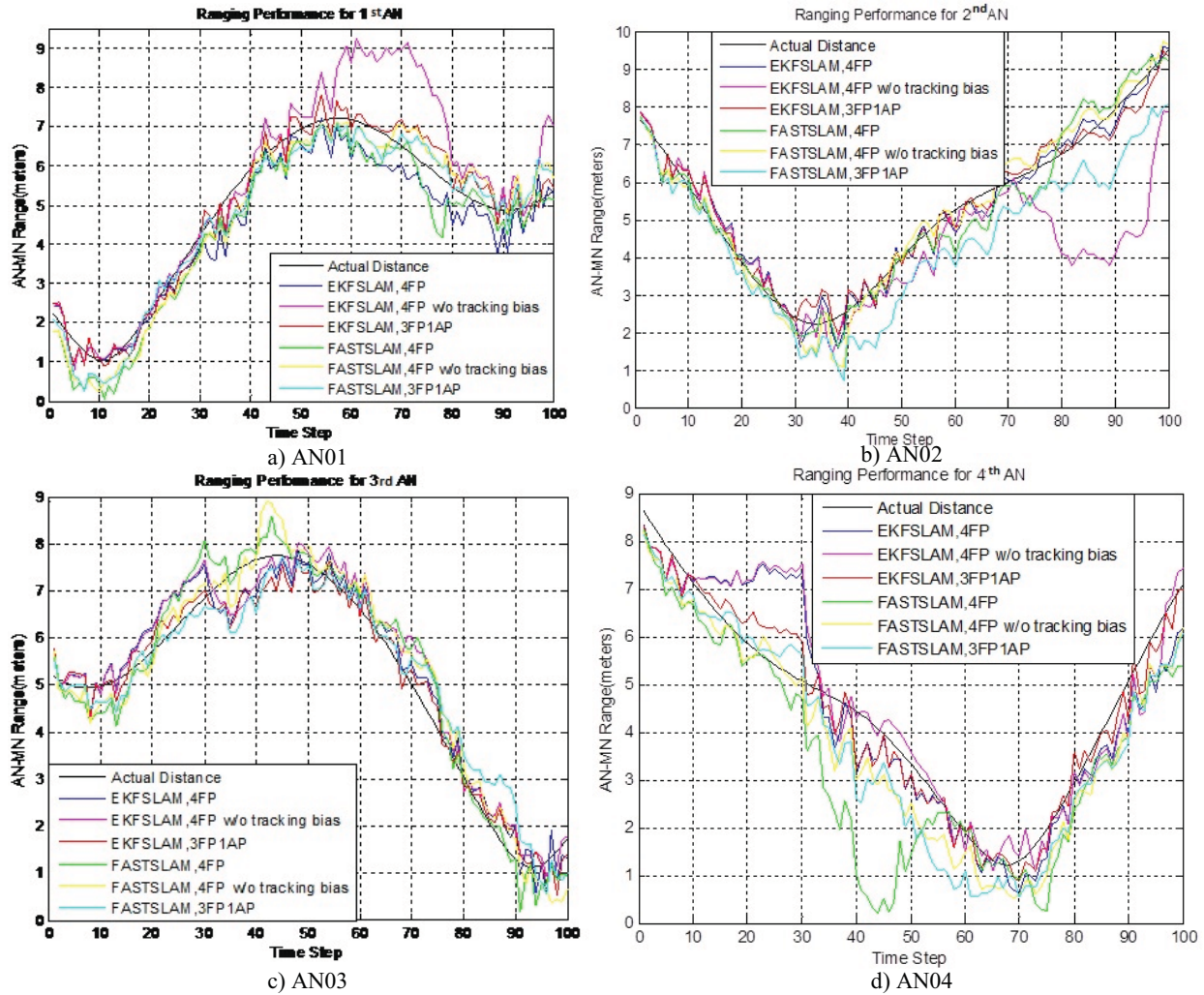
**Figure 0-49 MN-ANs actual and estimated distances for case 3**

The FastSLAM performance is not consistent because of the same reasons already explained for case 1 and 2. On the other hand, EKFSLAM consistency is degraded due to expansion of state space in comparison with previous cases, where the multivariate Gaussian PDF will no longer can represent joint MN location, FP location and AN range offsets state space. The uncertainty obtained from EKFSLAM is underestimated since the NEES is near the lower bound for FP 04 location and completely under lower bound for overall state space.
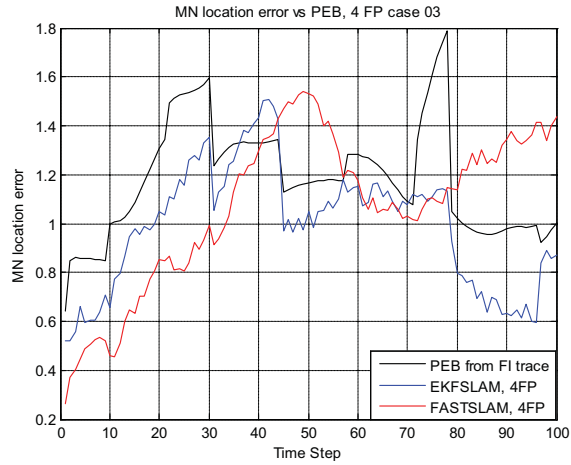
**Figure 0-50 MN position error in meters for case 3**
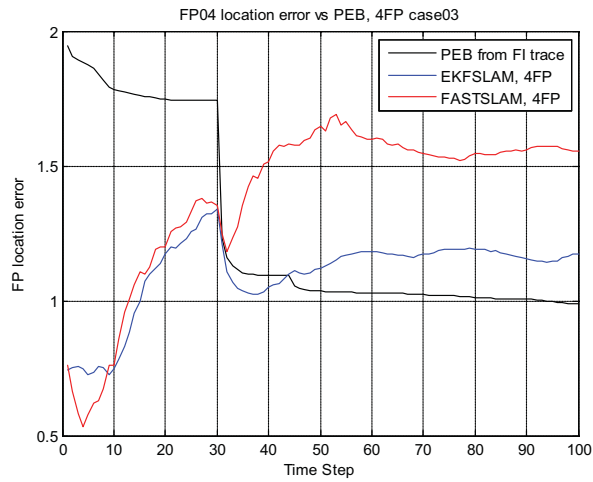


**Figure 0-51 FP04 position error in meters for case 3**
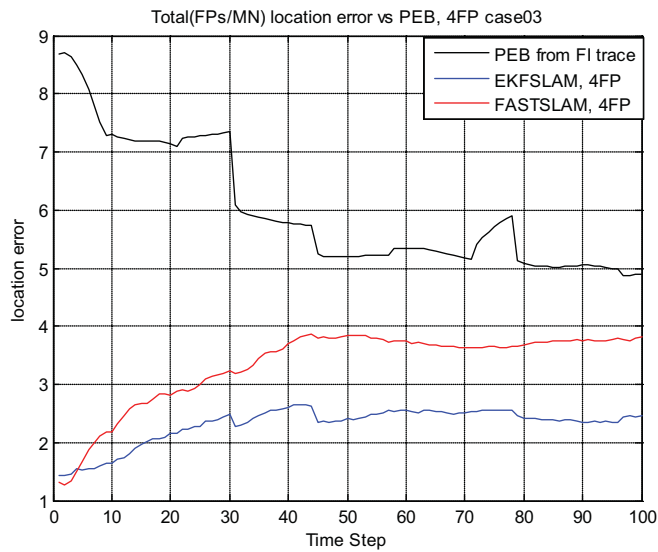


**Figure 0-52 Total state error in meters for case 3**
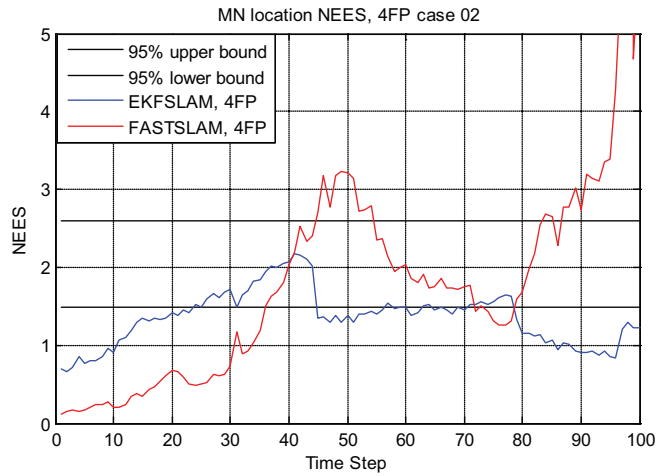
**Figure 0-53 MN location NEES from EKFSLAM and modified FastSLAM for case 3**
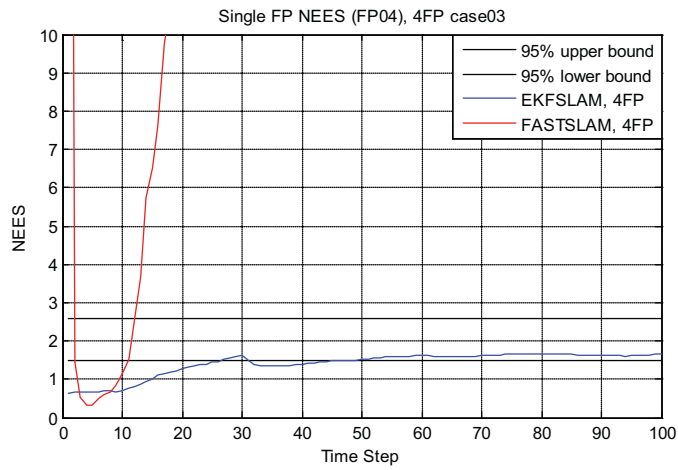


**Figure 0-54 FP04 NEES from EKFSLAM and modified FastSLAM for case 3**
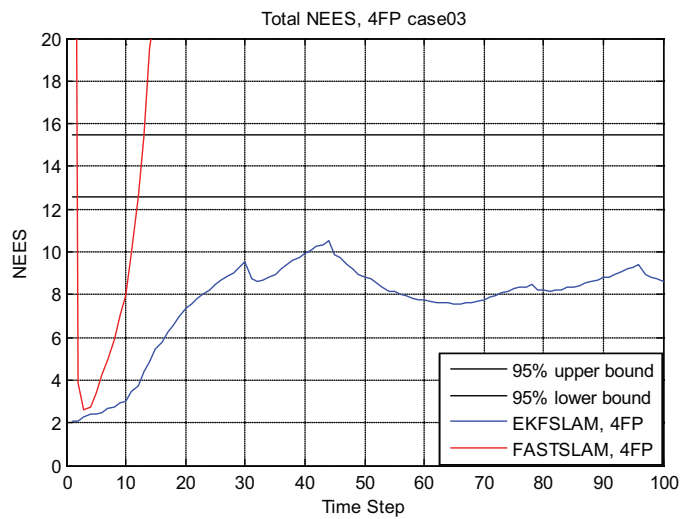


**Figure 0-55 Total state NEES from EKFSLAM and modified FastSLAM for case 3**

**System model 4: unsynchronized ANs, MN not synchronized with ANs, unknown sight conditions**

In the system model 4, it is assumed that the MN receives signal of opportunity from unsynchronized network in a non-stationary mixed LOS/NLOS propagation. The statistic of the observables $\mathbf{z}_t$ changes over the time due to random variation of clock drift and the AN sight conditions. In such a scenario, optimal tracking algorithm requires the definition of additional dynamic models that describe the evolution of range bias as well as ANs sight state. This leads to a composite dynamic model where the state is composed of the *joint* MN position, AN location , range bias and sight state variables $\mathbf{q}_t = \begin{bmatrix} \mathbf{p}_t & \mathbf{b}_t & \mathbf{s}_t & \mathbf{m} \end{bmatrix}^T$ where

$\mathbf{s}_t = \begin{bmatrix} s_{1,t} & s_{2,t} & \cdots & s_{N_{AN},t} \end{bmatrix}^T$ is the vector of ANs' sight states at time step $t$.

This composite localization system is described by a nonlinear jump Markov system where the state and/or the measurement model depend on a driving Markov chain. Following our assumptions, in the particular case herein considered, only the range measurement model $\mathbf{z}_t$ depends on the jumping feature $\mathbf{s}_t$. In fact, the PDF of measurement $\mathbf{z}_t$ is driven by a the discrete process $\mathbf{s}_t$, while the state $\mathbf{p}_t$ is assumed to be independent of $\mathbf{s}_t$. Once the JMS is defined, the evolution of joint state $\mathbf{q}_t$ can be tracked by a Bayesian filter.

As outlined in Section 0 for the system model 4, the MN location $\mathbf{p}_t$ is modeled as a first-order Markov process ruled by $\mathbf{p}_t = \mathbf{p}_{t-1} + \mathbf{v}_t$, where $\mathbf{v}_t \sim N(0, Q_p)$. Based on the smooth trajectory assumption, the range offset vector, $\mathbf{b}_t = \begin{bmatrix} b_{1,t} & \cdots & b_{N_{AN},t} \end{bmatrix}^T$ is described by $N_{AN}$ independent first-order Markov processes, given by $\mathbf{b}_t = \mathbf{b}_{t-1} + \mathbf{v}_{b,t}$, where $\mathbf{v}_{b,t} \sim N(0, Q_b)$ and $Q_b = diag\left\{ \sigma_{1,b}^2 \quad \cdots \quad \sigma_{N_{AN},b}^2 \right\}$. The range offset evolves independently from MN location states.

In the same manner, each AN sight state variable $s_{i,t}$ is modeled as a binary Markov chain. The Markov chain process is described by a $2 \times 2$ transition probability matrix $\Pi$ which is completely defined by the transition probabilities $P(s_{i,t} = 0 \mid s_{i,t-1} = 0) = p_0$ and $P(s_{i,t} = 1 \mid s_{i,t-1} = 1) = p_1$. Under the independence assumption between the MN–AN links, the whole sight state vector $\mathbf{s}_t$ is determined by a first-order Markov chain with transition probabilities $P(\mathbf{s}_t = \mathbf{c} \mid \mathbf{s}_{t-1} = \mathbf{d}) = \prod_{i=1}^{N_{AN}} P(s_{i,t} = c_i \mid s_{i,t-1} = d_i)$ for $\mathbf{c} = \begin{bmatrix} c_1 & \cdots & c_{N_{AN}} \end{bmatrix}$,

$\mathbf{d} = \begin{bmatrix} d_1 & \cdots & d_{N_{AN}} \end{bmatrix}$ where $d_i, c_i \subset \{0,1\}$.

The overall state vector of unknown variables is denoted by $\mathbf{q}_t = \begin{bmatrix} \mathbf{p}_t & \mathbf{b}_t & \mathbf{s}_t & \mathbf{m}_{fp} \end{bmatrix}^T$, where $\mathbf{m}_{fp}$ is the stacked vector of the FP locations, defined by

$\begin{bmatrix} m_{N_{AP+1},x} & m_{N_{AP+1},y} & \cdots & m_{N_{AN},x} & m_{N_{AN},y} \end{bmatrix}^T$. The transition PDF from previous state

$\mathbf{q}_{t-1} = \begin{bmatrix} \mathbf{p}_{t-1} & \mathbf{b}_{t-1} & \mathbf{s}_{t-1} & \mathbf{m} \end{bmatrix}^T$ to the next one $\mathbf{q}_t = \begin{bmatrix} \mathbf{p}_t & \mathbf{b}_t & \mathbf{s}_t & \mathbf{m} \end{bmatrix}^T$ is given by

$p(\mathbf{q}_t \mid \mathbf{q}_{t-1}) = p(\mathbf{p}_t \mid \mathbf{p}_{t-1}) p(\mathbf{b}_t \mid \mathbf{b}_{t-1}) p(\mathbf{s}_t \mid \mathbf{s}_{t-1})$ under the assumption that MN trajectory evolves independently from both clock drift and ANs' sight state processes. The JMS state $\mathbf{q}_t$ is hidden into the $N_{AN}$-link observation vector $\mathbf{z}_t$ composed by the conditionally independent measurements $p(\mathbf{z}_t \mid \mathbf{q}_t) = \prod_{i=1}^{N_{AN}} p(z_{i,t} \mid \mathbf{q}_t)$ where each $p(z_{i,t} \mid \mathbf{q}_t)$ has to be evaluated according to the observation model defined in Eq. (0-70) and (0-71)

An optimal estimate of $\mathbf{q}_t$ can be extracted from the whole set of available measurement by time $t$, $\mathbf{z}_{1:t} \square \{\mathbf{z}_1 \quad \mathbf{z}_2 \quad \ldots \quad \mathbf{z}_t\}$ where $\mathbf{z}_k = \{z_{1,k} \quad z_{2,k} \quad \ldots \quad z_{N_{AN},k}\}$ denotes range measurements at time step $k$ from all ANs in NLOS or LOS with the MN, where the AN sight

conditions are unknown to the MN. The estimate is obtained by evaluating the a posterior pdf

$p(\mathbf{q}_t \mid \mathbf{z}_{1:t})$ which can be expressed as a

$$p(\mathbf{p}_t, \mathbf{m}_{fp} \mid \mathbf{z}_{1:t}) = \sum_{l=1}^{t^{N_s}} p(\mathbf{p}_t, \mathbf{m}_{fp} \mid \mathbf{s}_{1:t}^l, \mathbf{z}_{1:t}) p(\mathbf{s}_{1:t}^l \mid \mathbf{z}_{1:t})$$

where $p(\mathbf{s}_{1:t}^l \mid \mathbf{z}_{1:t})$ is the probability of a particular sight state sequence, $\mathbf{s}_{1:t}^l$, given the

measurement. $N_s = 2^{N_{AN}}$ is the total number of all possible ANs sight state combinations at each

time step. Each possible ANs sight state combination is also referred as sight mode. As earlier

discussed, the optimal solution for $p(\mathbf{p}_t, \mathbf{m}_{fp} \mid \mathbf{z}_{1:t})$ cannot be found analytically in a closed form

due to nonlinear feature of measurements. Moreover, the number of mixture components in the

PDF sum of Eq. (0-153) grows exponentially with time. Hence, a practical solution has to be

suboptimal. Following, two solutions for this jump Markov SLAM problem based on EKF and PF

are proposed.

**IMM-EKFSLAM**

A practical implementation of JMS solution is to limit the growth of number of mixture

components by merging of the sight state mixture components. This type of algorithm is

generally known as interactive multiple model (IMM) estimator. The proposed IMM-EKFSLAM

algorithm employs the EKF to linearize the nonlinear system and filter every mode and then

uses the nonlinear IMM algorithm to fuse the estimated state of the filtering for each mode, and

finally to get an overall estimated state. We define the state vector for each sight mode as

$\mathbf{q}_{s,t} = \begin{bmatrix} \mathbf{p}_t & \mathbf{b}_t & \mathbf{m} \end{bmatrix}^T$. Before filtering for each sight mode, the IMM obtains a hybrid prior

estimate by mixing of modes where the mean and covariance of Gaussian posterior PDF at time

step $t-1$ for sight mode $j$ are defined by

$$\hat{\mathbf{q}}_{s,t-1|t-1}^{(j)} = \sum_{i=1}^{N_s} \mu_{t-1|t-1}^{(i,j)} \hat{\mathbf{q}}_{s,t-1|t-1}^{(i)}$$

$$\hat{\Sigma}_{s,t-1|t-1}^{(j)} = \sum_{i=1}^{N_s} \mu_{t-1|t-1}^{(i,j)} \left[ \Sigma_{s,t-1|t-1}^{(i)} + (\hat{\mathbf{q}}_{s,t-1|t-1}^{(i)} - \hat{\mathbf{q}}_{s,t-1|t-1}^{(j)})(\hat{\mathbf{q}}_{s,t-1|t-1}^{(i)} - \hat{\mathbf{q}}_{s,t-1|t-1}^{(j)})^T \right]$$

It is easier to address sight modes by an integer number instead of a binary vector. In this

regard, we define $r_t \subset \{1,...,N_s\}$ as an integer index for the binary vector of ANs' sight state $\mathbf{s}_t$.

With this definition, the weights $\mu_{t-1|t-1}^{(i,j)}$ as the mixing probabilities are given by

$$\mu_{t-1|t-1}^{(i,j)} \ \square \ p(r_{t-1} = i \mid r_{t-1} = j, \mathbf{z}_{1:t}) = \frac{\Pi_{i,j} \mu_{t-1}^{(j)}}{\sum_{i=1}^{N_s} \Pi_{i,j} \mu_{t-1}^{(i)}}$$

where $\Pi = \Pi^1 \otimes ... \otimes \Pi^{N_{AN}}$ and $\mu_{t-1}^{(j)}$ is the $j$-th mode probability which obtained after filtering at

previous time step. The next phase is extended Kalman filtering based on each sight mode,

where the prediction and update stages are stated as

*Filter predict stage:*

$$\hat{\mathbf{q}}_{t|t-1}^{(i)} = \begin{bmatrix} \hat{\mathbf{p}}_{t|t-1} \\ \hat{\mathbf{b}}_{t|t-1} \\ \hat{\mathbf{m}}_{fp,t-1} \end{bmatrix}^{(i)} = \begin{bmatrix} \hat{\hat{\mathbf{p}}}_{t-1|t-1} \\ \hat{\hat{\mathbf{b}}}_{t-1|t-1} \\ \hat{\hat{\mathbf{m}}}_{fp,t-1} \end{bmatrix}$$

$$\Sigma_{t|t-1}^{(i)} = \hat{\Sigma}_{t-1|t-1}^{(i)} + F^T Q F$$

*Filter update stage:*

$$\mathbf{D}_t^{(i)} = H^{(i)} \Sigma_{t|t-1}^{(i)} (H^{(i)})^T + R_t^{(i)}$$

$$\mathbf{K}_t^{(i)} = \Sigma_{t|t-1}^{(i)} (H^{(i)})^T \left[ \mathbf{D}_t^{(i)} \right]^{-1}$$

$$\hat{\mathbf{q}}_{s,t|t=}^{(i)} \begin{bmatrix} \hat{\mathbf{p}}_{t|t} \\ \hat{\mathbf{b}}_{t|t} \\ \hat{\mathbf{m}}_{fp,t} \end{bmatrix}^{(i)} = \begin{bmatrix} \hat{\mathbf{p}}_{t|t-1} \\ \hat{\mathbf{b}}_{t|t-1} \\ \hat{\mathbf{m}}_{fp,t-1} \end{bmatrix}^{(i)} + \mathbf{K}_t^{(i)} \left[ (\mathbf{z}_t - h(\hat{\mathbf{q}}_{s,t|t-1}^{(i)})) \right]$$

$$\Sigma_{t|t}^{(i)} = \Sigma_{t|t-1}^{(i)} + \mathbf{K}_t^{(i)} \mathbf{D}_t^{(i)} (\mathbf{K}_t^{(i)})^T$$

Finally, the output of IMM-EKFSLAM filter is calculated as the mean and the covariance

of the Gaussian mixture of a mode-based posterior PDF as follows

$$\hat{\mathbf{q}}_{s,t|t} = \sum_{i=1}^{N_s} \mu_t^{(i)} \hat{\mathbf{q}}_{s,t|t}^i$$

<div align="right">*0-158*</div>

$$\Sigma_{t|t} = \sum_{i=1}^{N_s} \mu_t^{(i)} \left[ \Sigma^{(i)}_{t|t} + (\hat{\mathbf{q}}_{s,t|t}^i - \hat{\mathbf{q}}_{s,t|t})(\hat{\mathbf{q}}_{s,t|t}^i - \hat{\mathbf{q}}_{s,t|t})^T \right]$$

where the mode probabilities are calculate using the Bayes rule as

<div align="right">*0-159*</div>

$$\mu_t^{(j)} \square \frac{\Lambda_t^j \sum_{i=1}^{N_s} \Pi_{i,j} \mu_{t-1}^{(i)}}{\sum_{j=1}^{N_s} \Lambda_t^j \sum_{i=1}^{N_s} \Pi_{i,j} \mu_{t-1}^{(i)}}$$

where $\Lambda_t^i = p(\mathbf{z}_t \mid \mathbf{z}_{1:t}, r_t = i) \square N((\mathbf{z}_t - h(\hat{\mathbf{q}}_{s,t|t-1}^{(i)})), \mathbf{D}_t^{(i)})$. Moreover, the sight mode is estimated by

<div align="right">*0-160*</div>

$$\hat{r}_t = \arg\max_i \left\{ \mu_t^{(i)}, i = 1, ..., N_s \right\}$$

**IMM-FASTSLAM**

The IMM-FastSLAM is proposed as an extension of jump Markov PF (also known as MM-PF) for SLAM problem with switching dynamic models. However, the RB factorization for posterior PDF is modified by

<div align="right">*0-161*</div>

$$p(\mathbf{p}_{0:t}, \mathbf{s}_{0:t}, \mathbf{b}_{0:t}, \mathbf{m}_{fp} \mid \mathbf{z}_{1:t}) = p(\mathbf{p}_{0:t}, \mathbf{s}_{0:t} \mid \mathbf{z}_{1:t}) \prod_{i=N_{AP+1}}^{N_{AN}} p(\mathbf{m}_{fp,i}, b_{i,0:t} \mid \mathbf{p}_{0:t}, \mathbf{s}_{0:t}, \mathbf{z}_{1:t})$$

In first stage, the algorithm generates a random set $\left\{ s_t^{[m]} \right\}_{m=1}^{N_P}$ based on $\left\{ s_{t-1}^{[m]} \right\}_{m=1}^{N_P}$ and the state mode transitional probability matrix $\Pi$. Next, IMM-Fast SLAM performs a PF filtering conditioned by mode particles. For each particle, the EKF is applied to update the estimation of range offsets and FP locations. Finally, particle weights are updated based on EKF estimates and the resampling is done as before. The state vector can be calculated through the weighted means:

$$\hat{\mathbf{p}}_t = \sum_{m=1}^{N_P} w_t^{[m]} \mathbf{p}_t^{[m]}$$

$$\hat{\mathbf{s}}_t = \sum_{m=1}^{N_P} w_t^{[m]} \mathbf{s}_t^{[m]}$$

$$\hat{\mathbf{m}}_{i,t} = \sum_{m=1}^{N_P} w_t^{[m]} \hat{\mathbf{m}}_{i,t}^{[m]} , i = N_{AP}+1,...,N_{AN}$$

$$b_{i,t} = \sum_{m=1}^{N_P} w_t^{[m]} \hat{b}_{i,t}^{[m]}$$

where the FPs location estimates $\hat{\mathbf{m}}_{i,t}^{[m]}$ and range offset estimate $\hat{b}_{i,t}^{[m]}$ is obtained from the mean of the EKF solution for $m^{\text{th}}$ particle.

A similar MN trajectory and ANs map used for the previous case is considered for evaluating the proposed methods for case 4. The initial conditions, measurements and transition model parameters are kept the same as before except the measurement data is generated according to Eq. (0-70) and (0-71) where

$$w_{i,t} \square \begin{cases} N(0,0.2) & if\ s_{i,t}=0 \\ N(0,2) & if\ s_{i,t}=1 \end{cases}$$

Figure 0-56(a)-(b) compare the EKFSLAM and modified FastSLAM performance for a single run MC for 4 FPs scenario when the ANs sight mode is detected by local maximum likelihood (LML) criteria

$$\hat{r}_t = \arg\max_i \Lambda_t^i = \arg\max\ p(\mathbf{z}_t|r_t=i,\mathbf{z}_{1:t-1})$$

$$\left|2\pi\mathbf{D}_t^i\right|^{-1} ex\ \left\{-\frac{1}{2}(\mathbf{z}_t-\hat{\mathbf{z}}_t^i)^T\left[\mathbf{D}_t^i\right]^{-1}(\mathbf{z}_t-\hat{\mathbf{z}}_t^i)\right\}$$

where $\hat{\mathbf{z}}_t^i$ is range estimate obtained based on $i$-th sight mode. Then MN location and FP locations estimates are chosen based on the detected sight mode. For the same measurement data set, the proposed IMM-EKFSLAM and IMM-FastSLAM are implemented. It can be observed that localization accuracy is improved for both in comparison with LML-EKFSLAM and LML-FastSLAM. In particular, the confidence region obtained by IMM-EKFSLAM reaches the confidence region obtained by BFIM.
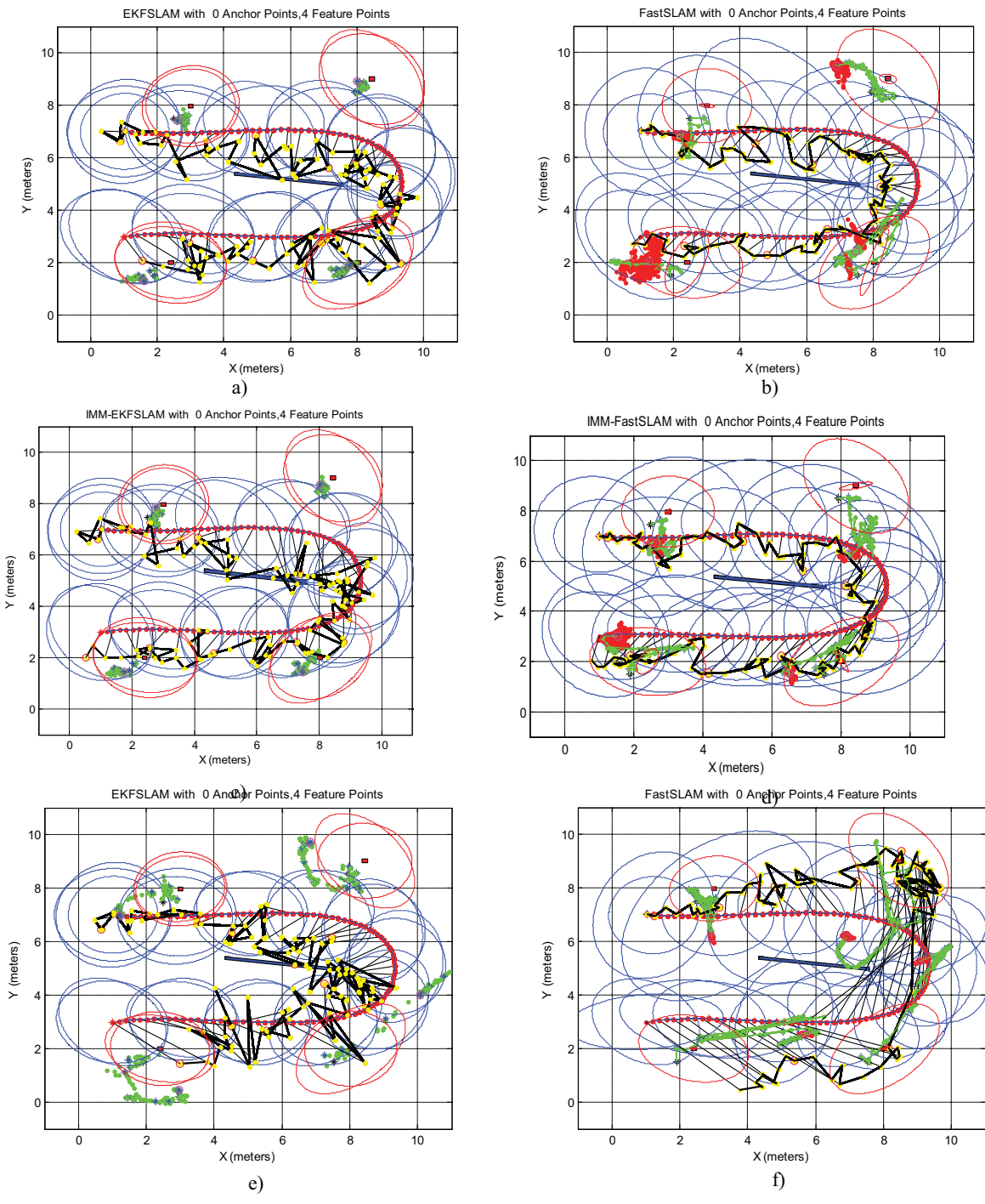
Figure 0-56 Example of MN tracking and ANs mapping for system model 4

Figure 0-54 (e)-(f) illustrates the performance of EKFSLAM and FastSLAM (as explained in case 1) where the range offset effect is not ignored and the MN has no knowledge about ANs sight conditions. It can be seen that for the area that ANs are shadowed by the wall, bias delay effect leads to large MN localization error. For this MC simulation, PF-based methods (IMM-FastSLAM and LML-FastSLAM) have better performance in terms of MN localization accuracy; however, EKFSLAM outperforms in terms of FP locations and their uncertainty estimation.

Actual ANs sight state and their estimates from LML-EKFSLAM, LML-FastSLAM, IMM-EKFSLAM, and IMM-FastSLAM are depicted in *Figure 0-57*, *Figure 0-58*, *Figure 0-59*, and *Figure 0-60*. It is shown that IMM-based methods outperform LML-based methods since they can take advantage of Markovian process between sight states to incorporate the information from previous measurements.
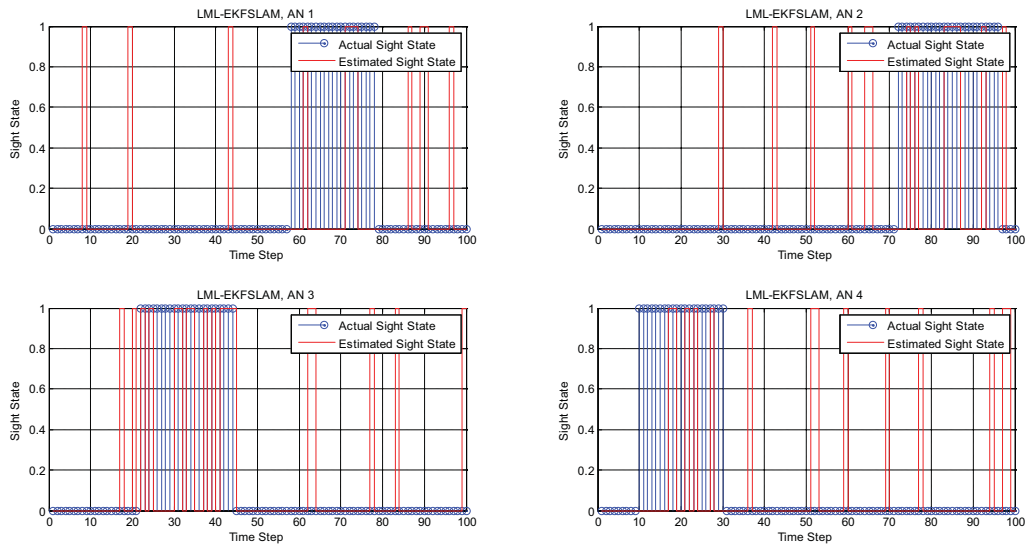


***Figure 0-57 Sight state tracking according to LML-EKFSLAM***
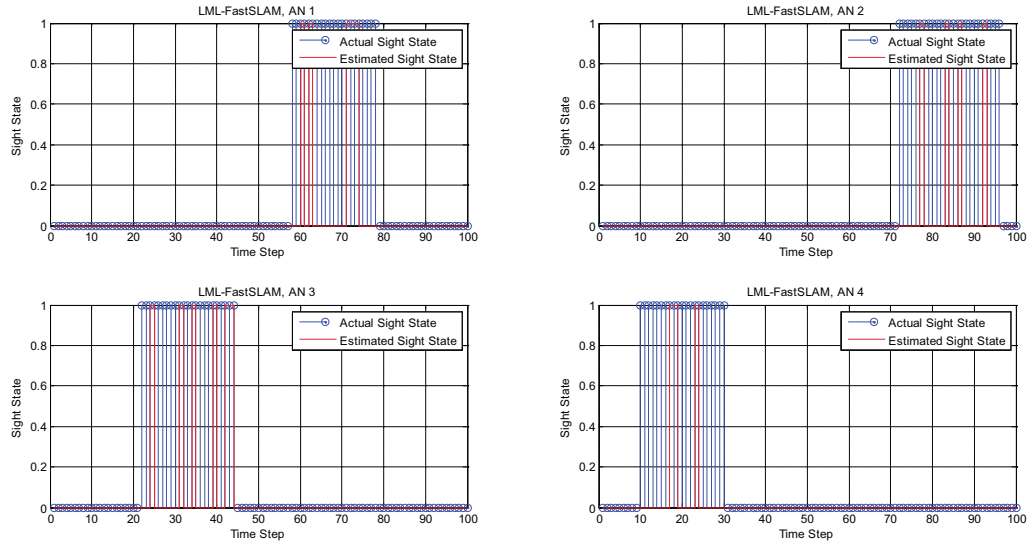
*Figure 0-58 Sight state tracking according to LML-FastSLAM*
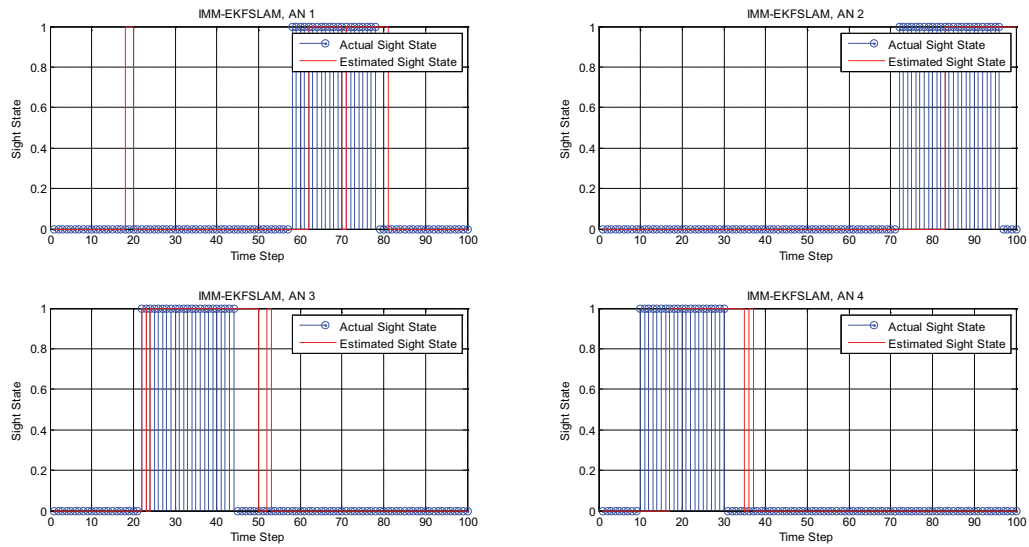


*Figure 0-59 Sight state tracking according to IMM-EKFSLAM*
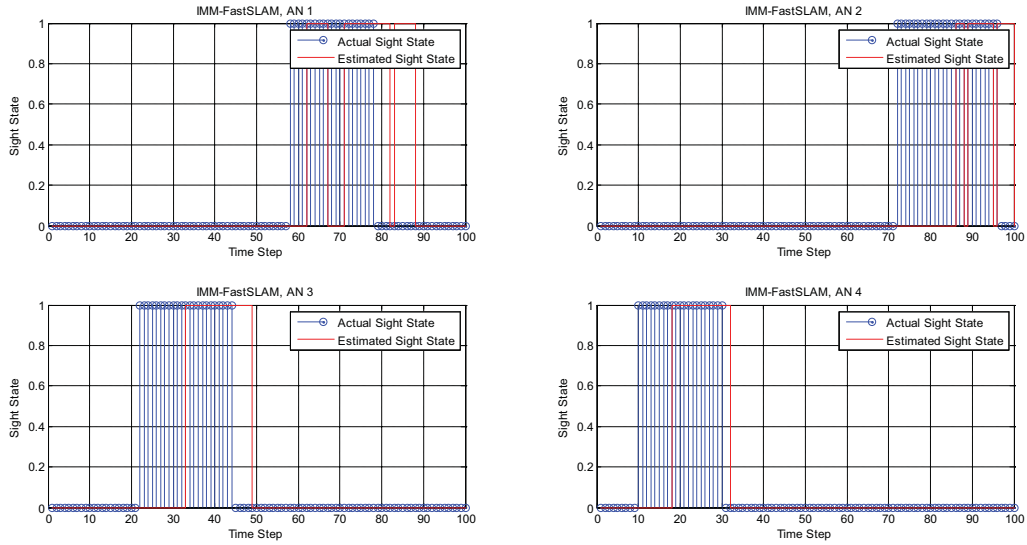
**Figure 0-60 Sight state tracking according to IMM-FastSLAM**
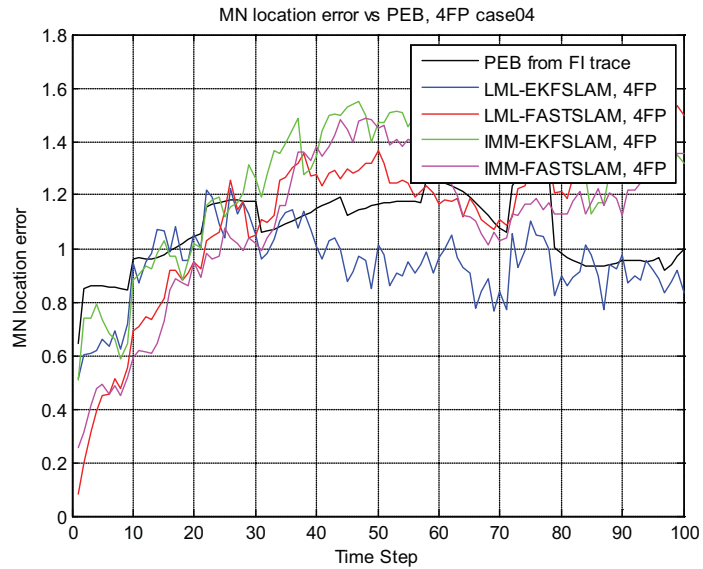


**Figure 0-61 MN position error in meters for case 4**
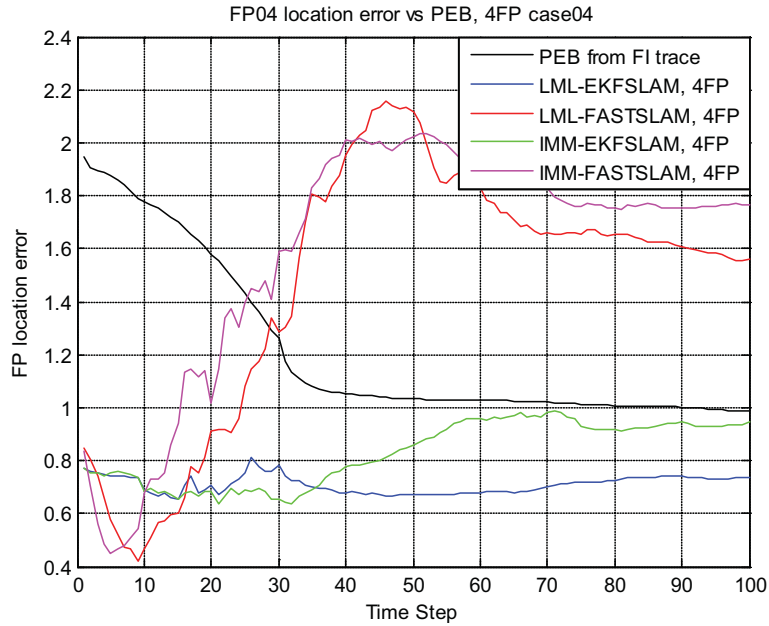
**Figure 0-62 FP04 position error in meters for case 4**
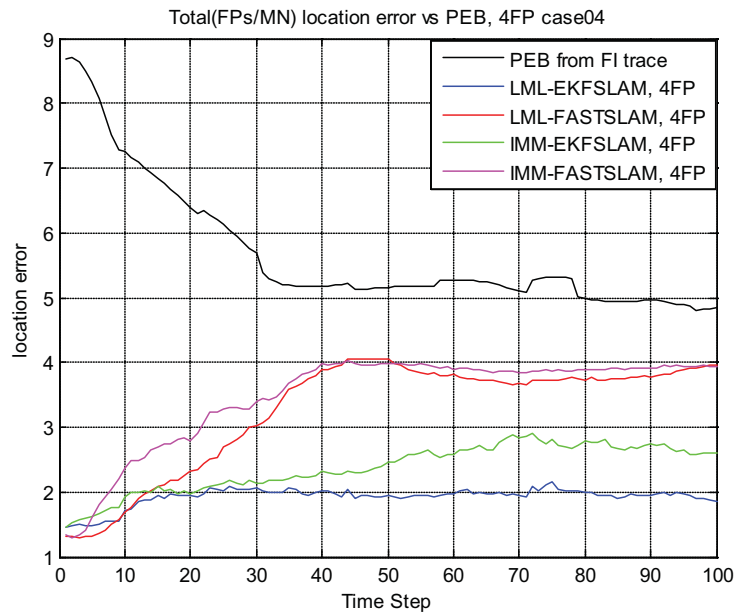


**Figure 0-63 Total state vector error in meters for case 4**

The 50-run average position errors for the MN location, FP 04 location and total state are shown in *Figure 0-61*, *Figure 0-62*, *Figure 0-63*, for LML-EKFSLAM, IMM-EKFSLAM, LML-FastSLAM and IMM-FastSLAM. It must be noted PEB is obtained from BFIM which is calculated for a deterministic mode trajectory as already outlined. Averaged MN position error obtained by

all proposed methods varies very close to this optimistic PEB. Unlike expectation from the single

MC simulation results, EKF-based methods have better performance than PF-based methods.

Specially, in terms of FP location error and overall state error, EKF-based methods are far

superior to IMM-FastSLAM and LML FastSLAM.

Figure 0-64,Figure 0-65 andFigure 0-66 illustrate averaged NEES test results obtained

for all four proposed methods to evaluate the consistency of solutions. MN location estimates

are consistent more than 60% of trajectory in PF-based methods. However, EKF –based

methods have overestimated the uncertainty while they have shown better performance in

terms of position error. In contrast, PF-based methods are, as explained earlier, underestimates

the FP locations uncertainty that has a dominant effect on overall estate uncertainty.
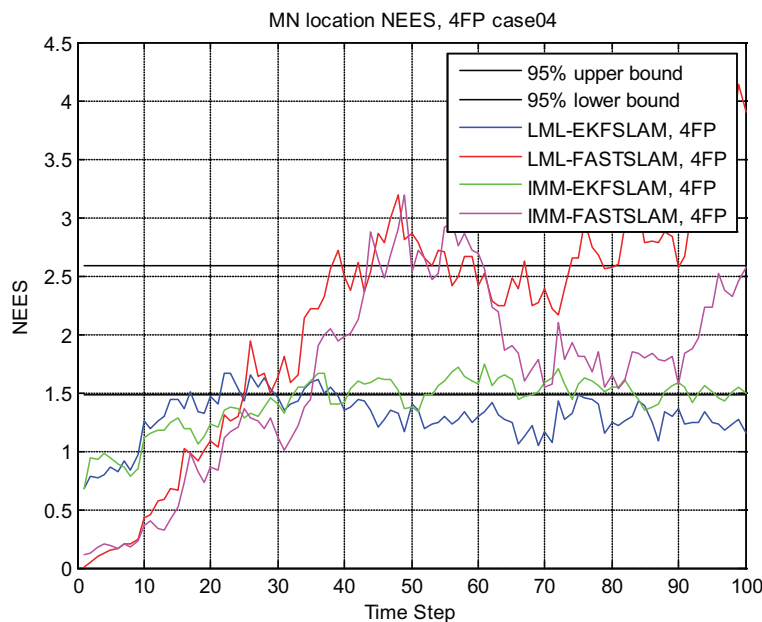


**Figure 0-64 MN location NEES for case 4**
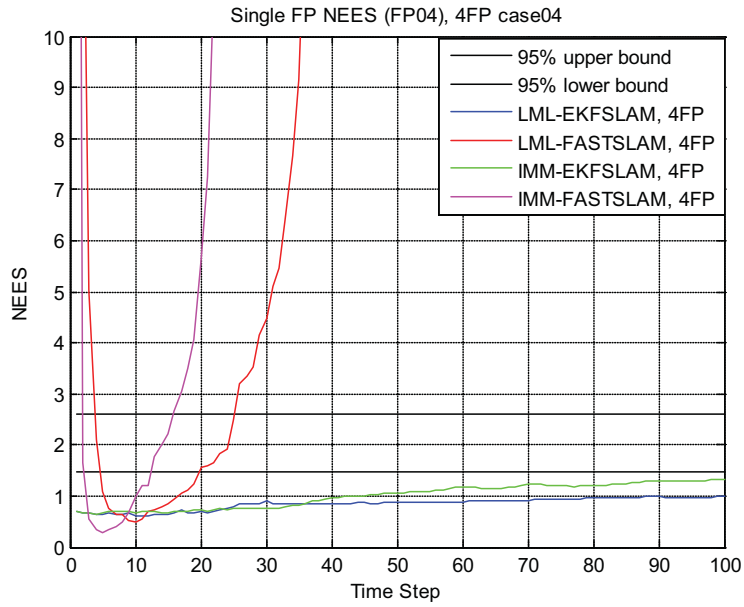
**Figure 0-65 FP04 location NEES for case 4**
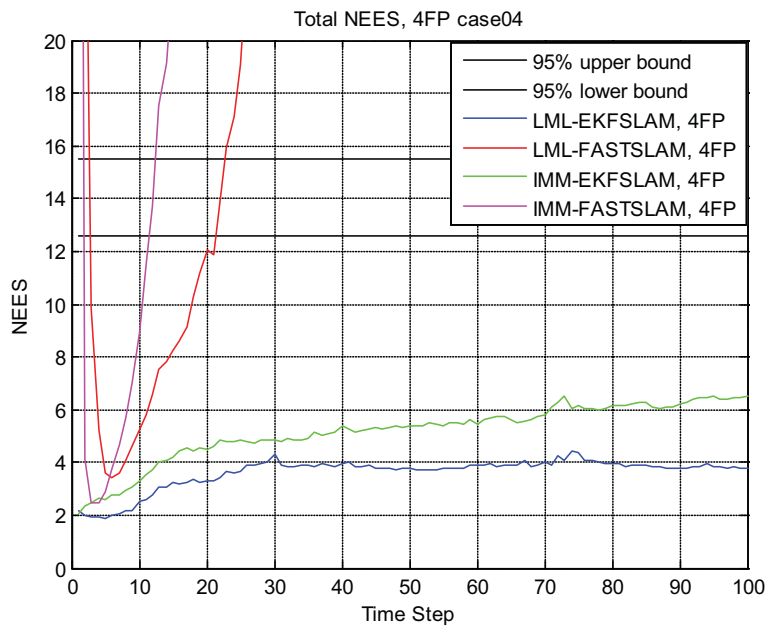


**Figure 0-66 Total state vector NEES for case 4**

**Discussion of results**

In this chapter, novel Bayesian approaches based on PF and EKF has been successfully implemented and analysed for OWLS according to four system models defined in Chapter 3. Range measurements were used by the Bayesian localization framework to jointly estimate the MN location, stationary FP locations, range bias and ANs sight conditions. The simulation results of each proposed methods were evaluated based on localization error on a single MC run , PEB obtained from the BFIM, and averaged NEES test for filter consistency and accuracy.

In the first case model, EKFSLAM and FastSLAM were applied to jointly estimate the MN locations and FP locations. EKFSLAM showed comparable localization performances to FastSLAM method in terms of MN/FP position error; however FastSLAM performance were not consistent since it underestimates the FP locations uncertainty.

In the second model, FastSLAM and EKFSLAM were extended to jointly track the MN and FPs location variables as well as single range offset. For the same number of particles as previous case, FastSLAM performance degraded in terms of consistency due to loss of particle diversity. However, both FastSLAM and EKFSLAM performances outperformed in comparison with the first case solution when the range offset is ignored.

In the third model, EKFSLAM and FastSLAM were generalized to jointly track location variables and range offsets from ANs. To limit the dimension of state space which particles represent, the range offsets were tracked jointly with FP location in the filtering stage. Unlike previous methods, EKFSLAM consistency degraded where it overestimated the FP locations and overall state uncertainty, however, its performance was still superior to modified FastSLAM.

Finally, the last system model were considered where the MN receives measurements from unknown sources in a non-stationary LOS/NLOS environment. The system model was defined by JMNLS where sight conditions were modeled by a binary state. EKFSLAM and FastSLAM were modified based on two sight state process assumptions. In first assumption, it

was considered that sight state process evolves based on Markov chain; in this case, two novel Bayesian approaches using IMM estimator were proposed: IMM-EKFSLAM and IMM-FastSLAM. In second assumption, sight states at each time step are independent where EKFSLAM and FastSLAM were modified to detect the sight state using LML criteria, called LML-EKFSLAM, LML-FastSLAM. All four algorithms showed better performance in non-stationary mixed NLOS/LOS propagation in an opportunistic unsynchronized reception in comparison with original FastSLAM and EKFSLAM. In terms of consistency and position error, proposed EKF-based methods outperforms PF-based methods. However, the LML-EKFSLAM provided better localization error in terms of FP locations and MN position error; while IMM-EKFSLAM and IMM-FastSLAM had better performance in terms of sight state tracking.

# References Used in this Document

[i] A. Howard, S. Siddiqi, and G. S. Sukhatme, "An experimental study of localization using wireless Ethernet," Proc. 4th Int. Conf. Field and Service Robotics FSR 2003, Jul. 2003.

[ii] M. Quigley, D. Stavens, A. Coates and, S. Thrun, "Sub-meter indoor localization in unmodified environments with inexpensive sensors," Proc. Int. Conf. Intell. Robots and Systems IROS, Taipai, Taiwain, 2010, pp. 2039-2046.

[iii] H. Durrant-Whyte and T. Bailey, "Simultaneous localization and mapping: part I," IEEE Robotic. Automat. Mag., vol. 13, pp. 99-110, 2006.

[iv] H. Durrant-Whyte and T. Bailey, "Simultaneous localization and mapping: part II," IEEE Robotic. Automat. Mag., vol. 13, pp. 108 – 117, 2006.

[v] M. Montemerlo, S. Thrun, D. Koller and B. Wegbreit, "FastSLAM: A factored solution to the simultaneous localization and mapping problem," Proc. AAAI Nat. Conf. Artif. Intell., 2002, pp. 593-598.

[vi] J. Wang, "Modeling and matching of landmarks for automation of Mars rover localization," Ph.D. Dissertation, Ohio State Univ., Columbus, OH, 2008.

[vii] D. Dardari, A. Conti, U. Ferner, A. Giorgetti and M. Z. Win, "Ranging With Ultrawide Bandwidth Signals in Multipath Environments," *Proc. IEEE,* vol. 97,  pp. 404-426, 2009.

[viii ] J. G. Proakis and M. Salehi, *Digital Communications.* Boston: McGraw-Hill, 2008.

[ix] B. Krach, M. Lentmaier and P. Robertson, "Bayesian detection and tracking for joint positioning and multipath mitigation in GNSS," *5th Workshop Positioning, Navigation and Communication*, pp. 173-180, 2008.

[x] Y. Shen and M. Z. Win, "Fundamental limits of wideband localization – Part I: A general framework," *IEEE Trans. Inf. Theory*, vol. 56, no. 10, pp. 4956-4980, Oct. 2010.

[xi] D. Guo, S. Shamai, and S. Verdu, "Mutual information and minimum mean-square error in Gaussian channels," *IEEE Trans. Inf. Theory,* vol. 51, pp. 1261-1282, 2005.

[xii] B. Ristic and S. Arulampalm, and N. Gordon, *Beyond the Kalman Filter: Particle Filters for Tracking Applications.* Boston: Artech House, 2004.

[xiii] J. Xiao, Z. Liu, Y. Yang, D. Liu, and X. Han, "Comparison and analysis of indoor wireless positioning techniques," *IEEE Int. Conf. Comput. Sci. and Service Syst. CSSS*, pp. 293-296, June 2011.

[xiv] J. Huang, D. Millman, M. Quigley, D. Stavens, S. Thrun, and A. Aggarwal, "Efficient, generalized indoor WiFi GraphSLAM," *2011 IEEE Int. Conf. Robotics and Automat. ICRA,* pp.1038-1043, May 2011.

[xv] S. S. Wang, M. Green, and M. Malkawi, "Mobile Positioning Technologies and Location Services," *IEEE Conf. Radio and Wireless RAWCON,* pp. 9-12, 2002.

[xvi] P. Misra and P. Enge, *Global Positioning System: Signals, Measurements, and Performance.* Lincoln, Mass.: Ganga-Jamuna Press, 2006.

[xvii] H. L. Van Trees, *Optimum Array Processing: Part IV of Detection, Estimation, and Modulation Theory*, New York: John Wiley & Sons, 2002.

[xviii] EndRun Technologies (2009, Feb.).Oscilator selection guide. [online]. Available: http://www.endruntechnologies.com/pdf/Osc-Guide.pdf

[xix] H. Hellwig, "Microwave time and frequency standards," *Radio Sci., vol. 14, no. 4, pp. 561–572, 1979.*

[xx] R. H. Jones and P.V. Tryon, "Continuous time series models for unequally spaced data applied to modeling atomic clocks," *SIAM J. Sci. Stat. Comput.,* vol.8, no. 1, pp. 71-81, 1987.

[xxi] F. Sivrikaya, B. Yener, "Time synchronization in sensor networks: a survey," *IEEE Network*, vol. 18, no.4, pp.45-50, 2004.

[xxii] B. Denis, J-B, Pierrot, C. Abou-Rjeily, "Joint distributed synchronization and positioning in UWB ad hoc networks using TOA," IEEE Trans, Microw. Theory Tech., vol. 54, no. 4, pp. 1896-1911, June 2006.

[xxiii] L. Galleani , L. Sacerdote , P. Tavella and C. Zucca, "A mathematical model for the atomic clock error", *Metrologia*, vol. 40, pp. S257-S264, 2003.

[xxiv] F. Gonzalez, P. Waller, "Short term GNSS clock characterization using One-Way carrier phase," *IEEE Int. Freq. Control Symp. Joint 21st European Frequency and Time Forum*, pp. 517-522, May 2007.

[xxv] J. R. Wright, "GPS Composite Clock Analysis," *Int. Freq. Control Symp. Joint 21st European Frequency and Time Forum*, pp. 523-528, May 2007.

[xxvi] EndRun Technologies (2011, April.).Disciplined Oscillator Options for GPS-Synchronized Time & Frequency Standards. [online]. Available: http://www.endruntechnologies.com/pdf/OscOptions.pdf

[xxvii] L. Patino-Studencka, A. Eidloth, J. Thielecke, "Modelling of free-running clocks for a virtually synchronized microwave locating system," *6th Workshop Positioning, Navigation and Commun. WPNC* , pp.151-155, *2009.*

[xxviii] R. Schmidt, "Multiple Emitter Location and Signal Parameter Estimation," *IEEE Trans. Antennas Propag.*, vol. 34, no. 3, pp. 276-280, Mar 1986.

[xxix] G. Seco, and J. A. Fernández-Rubio, "Multipath and Interference Errors Reduction in GPS /GNSS by Joint Pseudorange Measurement and Array Beamforming," *Proc, of 1$^{st}$ European Symp. Global Navigation Satellite Systems*, Munich, Germany, 1997, pp. 605-614.

[xxx] Z. Sahinoglu and I. Guvenc, "Multiuser interference mitigation in noncoherent UWB ranging via nonlinearfiltering," EURASIP J. Wireless Commun.Netw., pp. 1–10, 2006.

[xxxi] D. Dardari, A. Giorgetti, and M. Z. Win, "Time-of-arrival estimation of UWB signals in the presence of narrowband and wideband interference," *Proc. IEEE Int. Conf. Ultra-Wideband* ICUWB, Singapore, Sep. 2007, pp.71 -76.

[xxxii] J. Y. Lee and S. Yoo, "Large error performance of UWB ranging in multipath and multiuser environments," IEEE Trans. Microwave Theory Tech., vol. 54, pp. 1887–1985, Jun. 2006.

[xxxiii] S. Thrun, W. Burgard, and D. Fox. Probabilistic Robotics. Cambridge, MA: MIT Press, 2005.

[xxxiv] H. F. Durrant-Whyte, "Uncertain geometry in robotics," *IEEE Trans. Robot. Automat.,* vol. 4, no. 1, pp. 23–31, 1988.

[xxxv] N. Ayache and O. Faugeras, "Building, registrating, and fusing noisy visual maps," *Int. J. Robot. Res.,* vol. 7, no. 6, pp. 45–65, 1988.

[xxxvi] J. Crowley, "World modeling and position estimation for a mobile robot using ultrasonic ranging," *Proc. IEEE Int. Conf. Robot. Automat*., 1989, pp. 674–681.

[xxxvii] R. Chatila and J. P. Laumond, "Position referencing and consistent world modeling for mobile robots," *Proc. IEEE Int. Conf. Robot. Automat*., 1985, pp. 138–143.

[xxxviii] H. Durrant-Whyte, T. Bailey,"Simultaneous localization and mapping: part I," IEEE *Robotics Automat. Mag*., vol.13, no.2, pp. 99-110, June 2006.

[xxxix] M. Csorba, "Simultaneous Localisation and Map Building," Ph.D. dissertation, Univ. Oxford, 1997.

[xl] S. Thrun, D. Fox, and W. Burgard, "A probabilistic approach to concurrent mapping and localization for mobile robots," *Mach. Learning*, vol. 31, no. 1, pp. 29–53, 1998.

[xli] G. Castella and C. P Robert, "Rao-Blackwellization of the sampling schemes," *Biometrica,* vol. 83, pp. 81-94, 1996.

[xlii] S. J. Julier and J.K. Uhlmann, "A counter example to the theory of simultaneous localization and map building," *Proc. IEEE Int. Conf. Robot. Automat.*, pp. 4238–4243, 2001.

[xliii] T. Bailey, J. Nieto, J. Guivant, M. Stevens, E. Nebot, "Consistency of the EKF-SLAM Algorithm," IEEE Int. Conf. Intell. Robots and Systems, pp. 3562-3568, Oct. 2006.

[xliv] S. M. Kay, Fundamentals of Statistical Signal Processing: Estimation Theory, vol. 1, Upper Saddle River, N.J.: Prentice-Hall PTR, 1998.

[xlv] Y. Bar-Shalom, X. Li and T. Kirubarajan, "Estimation with Applications to Tracking and Navigation." New York ; Toronto: John Wiley & Sons, 2001.

[xlvi] H. L. Van Trees, "Detection, Estimation and Modulation Theory", vol. 1, New York, NY: Wiley, 1968.

[xlvii] R. D. Gill and B. Y. Levit, "Application of the Van Trees Inequality: a Bayesian Cramér-Rao bound," *Bernoulli*, vol. 1, pp. 59-57, 1995.

[xlviii] A. Giremus, J. Y. Tourneret, and A. Doucet, "A particle filter to mitigate jamming for GPS navigation," IEEE 13th Workshop Stat. Signal Process., pp.1298-1303, July 2005.

[xlix] J.-F. Liao and B.-S. Chen, "Robust mobile location estimator with NLOS mitigation using IMM algorithm*," IEEE Trans. Wireless Commun*., vol. 5, no. 11, pp. 3002–3006, Nov. 2006.

[l] C. Fritsche, U. Hammes, A. Klein, and A. Zoubir, "Robust mobile terminal tracking in NLOS environments using interacting multiple model algorithm," *Proc. IEEE Int. Con. Acoustics*, Speech and Signal Process., 2009, pp. 3049–3052.

[li] L. Chen, S. Ali-Loytty, R. Piche, and L. Wu, "Mobile tracking in mixed line-of-sight/non-line-of-sight conditions: algorithm and theoretical lower bound," *Wireless Personal Commun*., vol. 1, pp. 1–19, 2011.

[lii] P. Tichavsky, C. H. Muravchik, and A. Nehorai, "Posterior Cramer-Rao bounds for discrete-time nonlinear filtering," *IEEE Trans. Signal Proc.*, vol.46, no.5, pp.1386,1396, May 1998.

[liii] M. L. Hernandez, B. Ristic, and A. Farina, "A performance bound for manoeuvring target tracking using best-fitting Gaussian distributions," *Proc. Int. Conf. Inform. Fusion*, pp. 1–8, 2005.

[liv] L. Svensson, "On the Bayesian Cramér-Rao bound for Markovian switching systems," *IEEE Trans. Signal Process.*, vol. 58, no. 9, pp. 4507–4516, Sep. 2010.

[lv] C. Fritsche and F. Gustafsson, "Bounds on the Optimal Performance for Jump Markov Linear Gaussian Systems," *IEEE Trans. Signal Process.,* vol. 61, pp. 92-98, 2013.

[lvi] C. Fritsche, A. Klein, and F. Gustafsson, "Bayesian Cramer-Rao Bound for Mobile Terminal Tracking in Mixed LOS/NLOS Environments," *IEEE Wireless Commun. Lett.,* vol.2, no. 3, pp. 335-338, June 2013.

[lvii] M. Briers, S. R. Maskell and R. Wright, "A rao-blackwellised unscented kalman filter," *Proc. 6th Int. Conf. Inform. Fusion Information Fusion, 2003*, pp. 55-61.

[lviii] S. Verdú, "On channel capacity per unit cost," *IEEE Trans. Inf. Theory*, vol. 36, no. 5, pp. 1019–1030, Sep. 1990.

[lix] A. Lapidoth and S. Shamai (Shitz), "Fading channels: How perfect need 'perfect side information' be?," *IEEE Trans. Inf. Theory*, vol. 48, no. 5, pp. 1118–1134, May 2002.

[lx] S. Verdú, "Spectral efficiency in the wideband regime," *IEEE Trans. Inf. Theory*, vol. 48, no. 6, pp. 1319–1343, Jun. 2002.

[lxi] N. Moazen and J. Nielsen, "Mutual Information as a Measure of Radio Tracking Performance in Indoor Environments," presented at CSSCIT'11, Banff, 2011.

[lxii] T. M. Cover and J. A. Thomas, Elements of Information Theory. New York: Wiley, 1991.